8-31-2018

Investigating The Functions of Two Transcription Factors in Vascular Development and Wall Biosynthesis in Arabidopsis thaliana

Qian Du
University of Connecticut - Storrs, qian.du@uconn.edu

Investigating The Functions of Two Transcription Factors in Vascular Development and Wall Biosynthesis in *Arabidopsis thaliana*

Qian Du, Ph.D.

University of Connecticut, 2018

Abstract

Plant vascular system is important for plant growth and development. There are three different cell types in vascular tissues, xylems, phloems and procambial or cambial. In the presence of cambium, plants continuously generate new vascular tissues. During the differentiation process, xylem fibers and tracheary elements develop lignified secondary cell walls which provide abundant resources of renewable fibers and biofuel industry. However, the underlying mechanisms of cambium development and secondary cell wall formation are still elusive. Our objectives are to identify new transcription factors function in vascular initiation and biomass deposition in *Arabidopsis*.

In this thesis, we identified two activation-tagging mutants, *hva-d* with high vascular activity and *stp-2d* showing secondary wall thickening in pith cells. A novel mutant—*hva-d*, showed more developed vascular bundles. Histochemical analysis indicated cambium and phloem development in *hva-d* were also elevated. Activation of *HVA* (*AT5G27880*) was responsible for *hva-d* phenotypes. *HVA* functions as a transcriptional repressor and interacts with TPL. Dominant-negative mutation of corepressor TPL suppressed *hva-d* vascular defects and it indicated TPL facilitated the function of HVA. We also found that auxin homeostasis was altered in *hva-d* mutant. Auxin biosynthesis gene *YUC2* was activated while

polar auxin transporter genes *PIN1* and *PIN2* were downregulated in *hva-d*. Further transcriptome analysis revealed a downstream regulator BP involved in meristem maintenance and vascular pattern. The results demonstrated HVA was an important regulator involved in vascular development and plant growth.

Another dominant mutant—*stp-2d*, showed ectopic lignification in pith cell in Arabidopsis inflorescence stems. Immunohistochemistry assays showed secondary cell wall formation in the mutant. Activation of *miR165b* was responsible for *stp-2d* phenotypes with reduced expression of *PHB, PHV* and *AtHB15*. Single mutant of *PHB* and *PHV* did not show alterations in secondary cell wall formation, while loss-of-function mutant *athb15-1* showed lignification in pith cells. MicroRNA-resistant mtAtHB15 complemented *stp-2d* defects and it indicated that repression of *AtHB15* accounted for the abnormal lignification in *stp-2d* mutant. A number of secondary cell wall biosynthesis genes and mater regulators were activated in *athb15-1* mutant. These results illustrated a *microRNA165b-AtHB15* mediated regulatory pathway functions upstream of the secondary cell wall master regulators.

Investigating The Functions of Two Transcription Factors in Vascular Development and Wall Biosynthesis in *Arabidopsis thaliana*

Qian Du

M.A., Shandong University, 2012

B.S., Shandong University, 2009

A Dissertation

Submitted in Partial Fulfillment of the

Requirements for the Degree of

Doctoral of Philosophy

at the

University of Connecticut

2018

APPROVAL PAGE

Doctor of Philosophy Dissertation

Investigating The Functions of Two Transcription Factors in Vascular Development and Wall Biosynthesis in *Arabidopsis thaliana*

Presented by

Qian Du, M.S.

Major Advisor: _____

Dr. Huanzhong Wang

Associate Advisor: _____

Dr. Gerald Berkowitz

Associate Advisor: _____

Dr. Yi Li

Associate Advisor: _____

Dr. Yaowu Yuan

University of Connecticut

2018

Acknowledgement

I would like to express my gratitude to all those people who helped me in these years.

First and foremost, I thank my advisor Dr. Huanzhong Wang for his supporting and guidance throughout my PhD study period. The most impressive moment for me is that Dr. Wang was working on my plant tissues on Saturday morning when I felt frustrated for repeated failure of RNA extraction from plant seeds. Dr. Wang was always helpful and patient to train me how to think and work as an independent scientist. His encouragement and support inspired me to understand what is science and the goal for research. I also want to thank him for his help during the time I prepared my general examination, proposal and thesis. He spent so much time reading through the draft and providing me useful suggestions, comments and help. Without his patient instruction, insightful advice and expert guidance, the completion of the thesis is impossible.

Grateful thank also dedicate to my committees, Dr. Gerald Berkowitz, Dr. Yi Li and Dr. Yaowu Yuan. They always offer me kind guidance and help with my study. I appreciated all the encouragement and suggestions to help me to be a better researcher. I also would like to thank Dr. Richard McAvoy for attending my general exam and his kindness and help.

To all members of the Wang lab, I am grateful for the enjoyable working environment and help they offered me. I would especially like to thank Ms. Liying Qi for teaching me how to do stem sectioning and grow *Arabidopsis*, and Dr. Kwang-Hee Lee for his help in *Benthamiana* infiltration and other experiment design. I also want to thank the former graduate student Jung Yang who helped me with my speaking English and many experiments. I would like to thank them all for their help.

I would like to extend a heartful thank you to Dr. Yi Ma, Dr. Min Su and Ling Wang who helped me and gave me many kind suggestions. I also want to thank our department secretary, Christine

Strand. She worked so hard for the department and spent extra efforts and patience for placing orders and other stuffs. Big thank you to our greenhouse manager, Frederick Pettit, for the growth chambers maintenance. And thank you to Lynn Grabowski and Debra Rood for their always kind help.

Finally, I would like to thank my parents, sister and younger brother. Without their support and understanding, I can not make it in a foreign country to obtain my Doctoral degree. I love them so much.

Table of Contents

List of Tables

List of Figures

Chapter 1 Characterization of *hva-d* mutant with high vascular number and enhanced (pro)cambium activity in *Arabidopsis*

Abstract

Plant vascular system connects all the plants organs in an organized manner and plays key role in plant growth and development. Vascular tissues are important for providing physical support and transporting water and nutrients throughout the plants. The primary components of vascular tissue are xylem, phloem and meristematic (pro)cambial. The formation of plant vascular tissues is a complex process integrates hormones and transcriptional regulations. Using *Arabidopsis* as a model system, efforts have been made to understand the underlying mechanisms for vascular development and secondary cell wall formation for the past several decades. But there are still many questions related to vascular initiation and patterning remained to be addressed. Here, we identified a novel dominant mutant high vascular activity mutant, *hva-d*, which showed enhanced vascular activity and developed more vascular bundles in inflorescence stem. Using different makers, we showed that the cambium and phloem development in *hva-d* mutant were enhanced compared with wild type. The mutant showed multiple morphological abnormalities manifested by curved leaves, short stems and deformed flowers. A C2H2 zinc finger transcription factor, AT5G27880, was responsible for *hva-d* phenotype. HVA functions as a repressor and interacts with TPL via a conserved EAR motif. Dominant repression by a single mutation N197H of TPL in *hva-d* background suppressed mutant defects. A connection between *HVA* and auxin had also be inspected. Auxin biosynthesis gene *YUC2* was activated and abnormal auxin accumulation in ptotoxylems were observed in *hva-d* mutant. We also found that expression level of *PIN1* and *PIN2* was decreased in *hva-d* mutant. These results indicated that auxin might be involved in *hva-d* phenotypes. We also identified *BP* was downregulated which functions as an important

transcription factor in controlling SAM maintenance and inflorescence stem architecture. These results indicate that HVA is an important transcription factor functions in vascular initiation and plant development. Further studies in the function of *AT5G27880* and investigation its downstream genes will provide insight in vascular development and secondary cell wall formation.

Introduction

The vascular system is evolutionally important for plant growth and development. With vascular system, plant's body is connected in an organized manner from the root tip to the highest top. The vascular tissues, the conduits of water, nutrients and small molecular, are crucial to provide physical support (Carlsbecker and Helariutta 2005). There are three different cell types in vascular tissue, xylem, phloem and procambial or cambial cells (MacDaniels 1947). Xylems facilitate water transportation throughout the plant, which are comprised of conductive tracheary elements, parenchyma cells and xylem fibers (Hall 2000, Ohashi-Ito and Fukuda 2014). During the differentiation process, xylem fibers and tracheary elements develop lignified secondary cell wall to provide physical support and comprise the majority of plant biomass (Zhong and Ye 2015). Phloems, composed of conductive sieve elements and connecting companion cells, parenchyma cells and fibers, transport nutrients and signal molecules to sink organs (Edith Haritatos 2000). Both xylem and phloem are initiated from procambial cells, which can divide and potentially differentiate into different vascular cell types (Elo, Immanen et al. 2009, Miyashima, Sebastian et al. 2013). Due to the vital roles of vascular tissues, efforts have been made to understand vascular development from tissue specification during embryogenesis to the differentiation of phloem and xylem tissues. The formation of plant vascular system is strictly controlled by plant hormones, peptide signaling and transcriptional regulation (Kondo, Tamaki et al. 2014, Ruzicka, Ursache et al. 2015).

The earliest indication of vascular development is the formation of procambial cells at early globular stage during embryogenesis (Mansfield and Briarty 1991). Further differentiation of procambial cells is halted during embryo maturation and resumed following germination (Cano-Delgado, Lee et al. 2010, Jouannet, Brackmann et al. 2015). In the course of embryogenesis,

initiation of vascular procambial cells is controlled by hormonal and transcriptional regulators (ten Hove, Lu et al. 2015). Auxin is essential for procambial formation during embryogenesis. Previous studies showed that indole-3-acetic acid (IAA) was sufficient to promote cambial cells proliferation and induce xylem tissue development (Zhenghua Ye 1994, Ye 2002).

During post-embryonic growth, constitutive formation of vascular tissues comes from cell division through high mitotic activity regions called meristems (Scheres 2007). Previous studies revealed the molecular mechanisms about stem cell maintenance and vascular specification in shoot apical meristem. Mutations of genes in CLV pathway result in increased *WUS* expression and enlarged meristem with extra stem cells. The *clv* mutants also lead to increased vascular bundle number in flattened stems (Ulrike Brand 2000, Jürgens 2002, Dodsworth 2009). Another important transcription factor involved in vascular development in the SAM is TOPLESS (TPL). The *tpl-1* mutant was temperature-sensitive and showed disordered apical cell fate during embryogenesis (HeidiSzemenyei 2008). TPL is a corepressor that can directly interact with IAA12/BDL to repress *MP* and control downstream auxin-response genes (Osmont and Hardtke 2008). Recent studies also showed that TPL can interact with a wide variety of transcription factor through their ERF-associated amphiphilic repression (EAR) motif to repress the downstream genes in auxin, jasmonate and BR signaling pathways (Pauwels, Barbero et al. 2010, Espinosa-Ruiz, Martinez et al. 2017).

In *Arabidopsis* stem, procambial cells initialized from SAM localized in the vascular bundles to differentiate into protoxylems and protophloems. As plants continue to grow, the clusters of vascular bundles are interconnected by interfascicular fibers. During secondary growth, fascicular cambium and interfascicular cambium start to differentiate to enhance the thickening of plant stem (MacDaniels 1947, Spicer and Groover 2010). Plant hormones play key roles in

vascular initiation and development in *Arabidopsis* inflorescence stem. Previous molecular studies revealed that auxin distribution reached a peak level in developing cambium in woody plants (Hannele Tuominen 1997). A mathematical model predicted auxin maxima controlled by polar transportation determined vascular bundle position and spacing in stem (Marta Iban˜ es 2010). An auxin-response reporter, *DR5::GUS*, was specifically expressed at vascular bundles (Norma Fàbregas 2010). Moreover, mutants of auxin efflux carrier *PIN1* showed increased number of vascular bundles in stem (Turner and Sieburth 2003). All these results indicated that auxin flow controls vascular bundle patterning. BR signaling pathway have been shown to control xylem differentiation and modulates vascular development. It has been reported that BR-deficient mutant *dwf7* and receptor mutant *bri1* showed reduced number of vascular bundles (Choe S 1999, Cano-Delgado, Yin et al. 2004). In contrast, mutations with increased BR-signaling like *bzr1-D* and *bes1-D* exhibited more vascular bundles compared with wild type. Quantification of procambial cell numbers in BR mutants reveal that BR hormone enhanced the vascular bundles numbers by promoting procambial cells formation (Marta Iban˜ es 2010).

Secondary cell wall polymers are important renewable biomass resource for sustainable biofuel industry. Secondary cell wall formation and subsequent programmed cell death are critical for maturation of xylem tracheary elements (Schuetz, Smith et al. 2013). Several groups of transcription factors, like NAC (NAM, ATAF1/2 and CUC2) master switches, MYB domain proteins and WRKY12, have been proved to control the biosynthesis of secondary cell wall. Those key regulators also form a delicate network to cooperate and regulate downstream genes involved in secondary wall synthesis (Wang, Avci et al. 2010, Zhong and Ye 2015). As discussed above, vascular development and secondary cell wall formation are controlled under a

complicated transcriptional network. To further understand these processes, we focus on identification of novel genes involved in (pro)cambial formation and xylem differentiation.

Results

Characterization of a mutant—*hva-d* (*High Vascular Activity*) showing enhanced vascular development in *Arabidopsis*

Vascular tissues, i.e. xylem and phloem, are produced from the differentiation of progeny cells derived from vascular cambium. But how vascular cells are initiated is still unknown. To identify novel regulators of vascular development, we screened an activation-tagged population in *Arabidopsis*. A semi-dominant mutant *hva-d* was identified by screening a mutant population. The *hva-d* mutant showed enhanced vascular activity and developed more vascular bundles in inflorescence stem. Provascular tissues were initiated just below the plant apical tips. In the apex region, the disconnected vascular bundles are composed of procambium, protoxylem and protophloem cells. Along the stem periphery, wild type plants developed 5 to 8 vascular clusters, which are corresponding to the vascular bundles in older stems (Figure 1A-C). As shown by examination of cross-sections from four-week old stem, the heterozygous mutants (*hva-d/+*) showed 20 protoxylem clusters (Figure 1D, E, F), while the homozygous mutants (*hva-d*) developed over 50 clusters of protoxylem cells in stem apex (Figure 1G-I). In addition, mature *hva-d/+* plants and *hva-d* plants exhibited negative effects on plant growth. The mutant lines were noticeably smaller in size and shorter in height compared with wild type. Especially for *hva-d* homozygous plants, the mutants showed more severe phenotype, with extremely short

stem and barely harbor any seeds (Figure 1K). The results indicated that *hva-d* mutant showed growth defects and the protoxylem formation was activated in inflorescence stems.

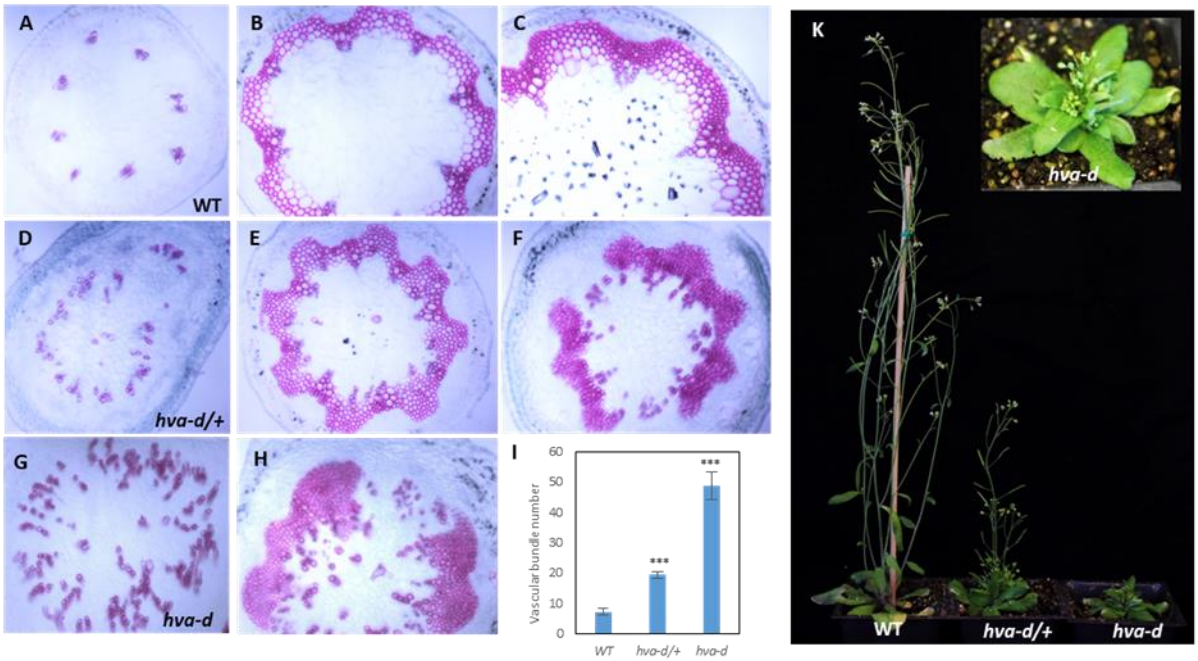

Figure 1. Characterization of the *hva-d* mutant.

(A-H) Phloroglucinol staining of transverse sections of wild type (A, B, C), *hva-d*/+ (D, E, F) and *hva-d* (G, H) plants. Sections were cut from four-week-old plants at different positions of the stem: 1cm below the shoot apical meristem (A, D, G), at one third from the SAM (B, E) and at the bottom of the stem (C, F, H). (I) Vascular bundle number of wild type, *hva*/+ and *hva-d*. Values are means for $\geqslant$ 10 plants of respective genotypes. Asterisks indicate a statistically significant difference compared with wild type by Student's t test ($P < 0.0001$). (K) Growth phenotypes of five-week old plants. From left to right, the plants are WT, *hva-d*/+ and *hva-d* mutant.

Phloem and cambium development are highly enhanced in *hva-d* mutant

In the wild type stem, the cell divisions within the pro(cambium) generally leads to formation of collateral bundles, in which xylem forms towards the pith and phloem forms towards the surface of the plant. To understand the development of cambium and phloem, we crossed *hva-d/+* mutants with two specific maker lines. In order to gain more insight about the phloem development, *hva-d/+* was crossed with *ProAPL:GUS* line. The *APL* (*Altered Phloem Development*) gene is expressed in protophloem, companion cells and metaphloem sieve elements. For cross-sectioning, we picked two different regions from the inflorescence stem, the tip region where vascular development start and the bottom part with secondary growth like woody plants. In wild type plants, GUS activity was only detected in the regions outside of the peripheral vascular bundles in the tip region (Figure 2A). In the bottom part, obvious GUS staining was also observed in the interfascicular regions which indicated secondary phloems developed from cambium (Figure 2B). In *hva-d/+* mutant background, GUS signal in the tip region turned out to be clustered instead of individually displayed (Figure 2C). In cross sections of the stem bottom region, GUS staining signals existing in the vascular bundles connected with the signals from interfascicular regions and became a ring-shape instead of well-separated organizations in wild type (Figure 2D and F). In the *hva-d* mutant, the ring-shaped GUS signal can be observed even in the tip part (Figure 2E).

Secondly, we used AtHB8 as a marker for cambial activity and crossed *hva-d/+* mutants with *ProAtHB8:GUS* plants to monitor the expression pattern of *AtHB8*. During the vascular initiation in *Arabidopsis* stems, procambium cells lies between primary xylems and primary phloems in each vascular bundles. As vascular development proceed, fascicular cambium within the bundles and interfascicular cambium between vascular bundles stay active during secondary growth. In

wild type background, GUS activity was primarily detected in the cambium of each vascular bundle (Figure 3A and B). However, in the tip part of *hva-d/+* inflorescence stem, stronger GUS activity was detected along the pericycle of the stem and ectopic signals were noticed in protoxylem regions (Figure 3C). In the basal part of *hva-d/+* stem, a continuous ring were formed after GUS staining and signals in protoxylems became more intense (Figure 3D). Moreover, in *hva-d* plants, the GUS activity was detected in the whole sections, even in the pith region (Figure 3E). These observations indicated that the development of phloem and cambium tissues were more active in *hva-d* mutant.

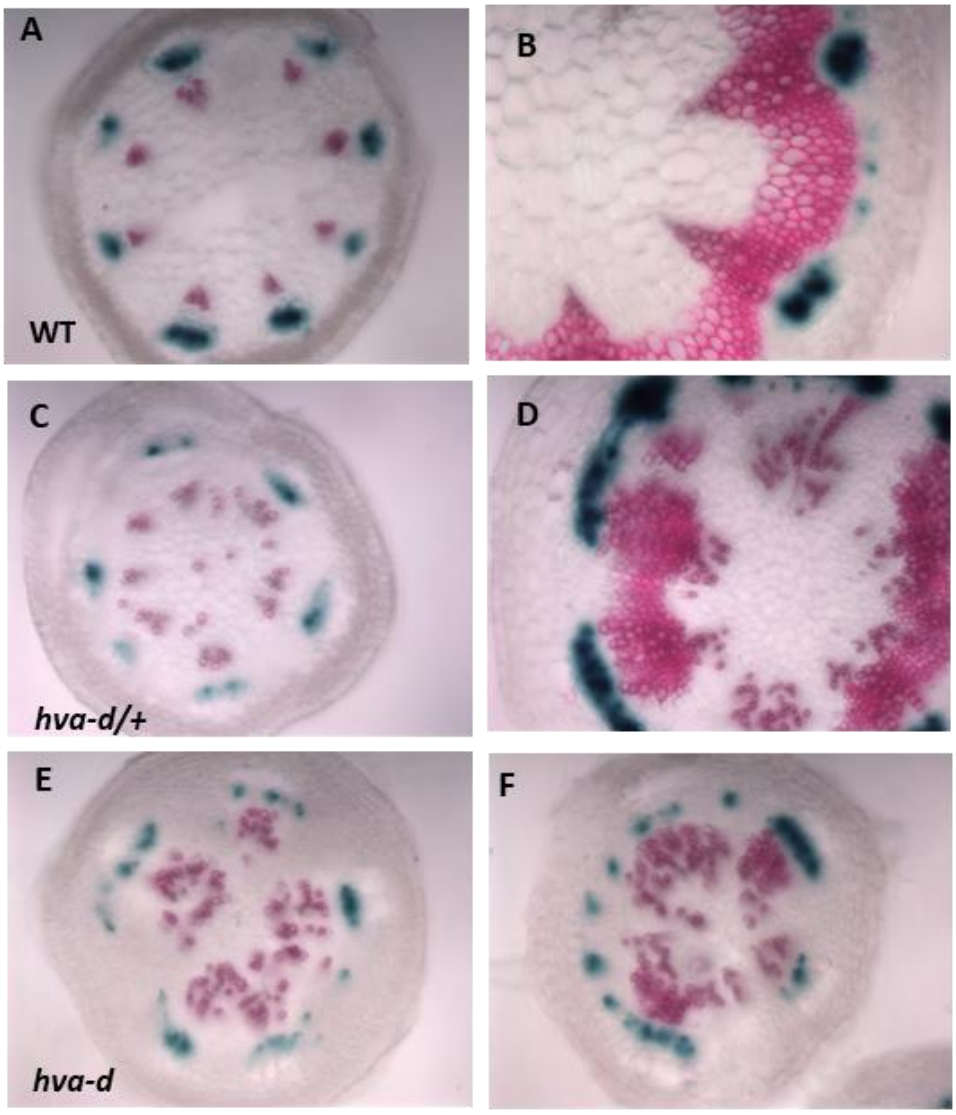

Figure 2. Histochemical analysis of phloem marker genes (*APL*) in *hva-d* mutant.

(A) and (B) Cross sections derived from the apical and basal part of the inflorescence stem in 35-day old *ProAPL:GUS* plant. (C) and (D) GUS-stained section of the apical and bottom basal of the stem of *ProAPL:GUS* plants in *hva-d/+* background. (E) and (F) Transverse section of apical and basal part of stem of *ProAPL:GUS* plants in *hva-d* background. All the samples were stained overnight and further stained with phloroglucinol-HCl to manifest lignified vessels and fiber cells. The thickness of cross-sections is 100um.

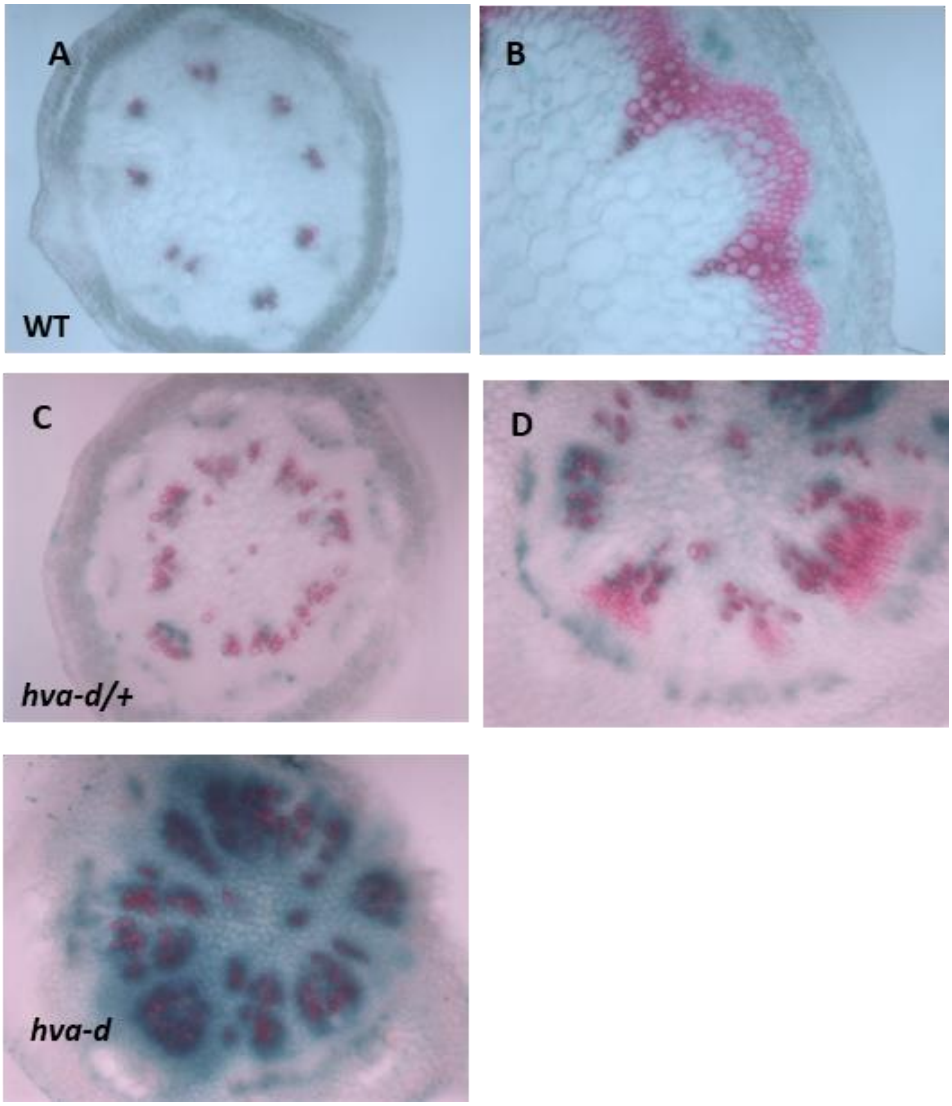

Figure 3. Histochemical analysis of cambium marker genes (*AtHB8*) in *hva-d* mutant.

(A) and (B) Cross sections derived from the upper and bottom part of the inflorescence stem in 35-day old *ProAtHB8:GUS* plant in wild type background.

(C) and (D) GUS-stained section of the apical and bottom basal of the stem of *ProAtHB8:GUS* plants in *hva-d/+* background.

(E) GUS staining in transverse section of apical part of *ProAtHB8:GUS* plants in *hva-d* background. All the samples were stained overnight and further stained with phloroglucinol-HCl to show lignin deposition in red. The thickness of cross-sections is 80um.

Activation of *AT5G27880* (*HVA*) is responsible to *hva-d* mutant phenotype

We identified the T-DNA insertion site using a plasmid rescue method. The T-DNA insertion is 2.4kb upstream of *AT5G27889* and 11.7kb downstream of *AT5G27880* on *Arabidopsis* chromosome 5 (Figure 4A). To examine whether the T-DNA insertion cosegregates with the observed phenotypes, we genotyped a segregating T3 population. Among 224 T3 plants, 55 were wild type, 47 were homozygous, and the remaining 122 were heterozygous plants. All the heterozygous and homozygous plants displayed enhanced vascular number and dwarf phenotypes compared with wild types. The segregation ratio is consistent with single gene inheritance with an expected 1:2:1 ratio ($\chi 2$=2.57, P=0.308). The results suggested that the vascular defects and dwarfism phenotypes are caused by this single T-DNA insertion.

In order to determine which gene is responsible for the phenotypes of *hva-d*, we examined expression levels of the three genes that are located in a 15kb range, upstream or downstream of the T-DNA insertion site. Quantitative RT-PCR analysis showed that expression of all the three genes was highly induced in *hva-d* mutant compared with wild type (Figure 4B). We reasoned that one of the genes must be responsible to the *hva-d* phenotype.

We overexpressed *AT5G27880* under the control of 4×35S enhancer in a construct includes a 2475bp-full-length *AT5G27880* genomic region (containing a 1038bp promoter, 837bp protein-coding sequence, and a 600bp downstream sequence). The overexpression construct was transformed into wild type plants, and 35 out of 38 transgenic plants displayed similar growth phenotypes to *hva-d* mutant. Among the 35 *hva-d*-like transgenic plants, 11 plants exhibited extremely severe growth defects with no elongated stems (Figure 5A). We selected two individual lines (*AT5G27880-OX1* and *AT5G27880-OX5*) and confirmed for the overexpression

of *AT5G27880* gene (Figure 5B). Histochemical analysis of the two overexpression lines showed more vascular bundles in the tip regions of the stems and ectopic vessels formation in pith (Figure 5C). These results demonstrated that overexpression of *AT5G27880* resulted in *hva-d* phenotypes.

To check if *AT5G27889* and *AT5G27890* were also involved in *hva-d* mutant phenotypes, we also overexpressed these two genes in wild types. Because there are only 40 nucleotides between *AT5G27889* and *AT5G27890* on the chromosome 5 and *AT5G27889* encodes a hypothetical protein with only 53 amino acids, we designed a 5.5kb construct of genomic sequence including 2.7kb promoter, *AT5G27889* and *AT5G27890* and 0.9kb downstream sequence, driven by 4×35S enhancers, and transformed to *Arabidopsis* wild type. After antibiotic screening, 72 antibiotic-resistant plants were transferred to soil, but none of them showed similar growth phenotypes like *hva-d* mutant. We randomly picked 9 plants in 72 were cross-sectioned and the vascular organizations showed similar patterns in wild type (Figure 6). So we concluded that *AT5G27889* and *AT5G27890* did not play roles in controlling the vascular phenotypes in *hva-d* mutant.

To further confirm the conclusion from earlier experiments, we also designed an RNA interference (RNAi) construct to test if repression of *AT5G27880* in *hva-d* mutant can recover the growth defects and enhanced vascular development. A microRNA construct of *AT5G27880*, driven by a cauliflower mosaic virus (CaMV) 35S promoter, was constructed and transformed into *hva-d*/+ plants. After screening, three independent transgenic lines--*microRNA-4*, *microRNA-8*, and *microRNA-10* were genotyped as *hva-d*/+ and selected for further analyses. In terms of plant height and vascular patterns of the inflorescence stems, the RNAi transgenic plants exhibited wild-type phenotypes in *hva-d*/+ background (Figure 7A and C). Quantitative RT-PCR showed decreased transcripts of *AT5G27880* in the microRNA-transgenic plants (Figure 7B).

Two approaches, overexpressing *AT5G27880* in wild type or knocking down *AT5G27880* in *hva-d* mutant, demonstrated that overexpression of *AT5G27880* resulted in the *hva-d* phenotype. We therefore renamed *AT5G27880* to *HVA*.

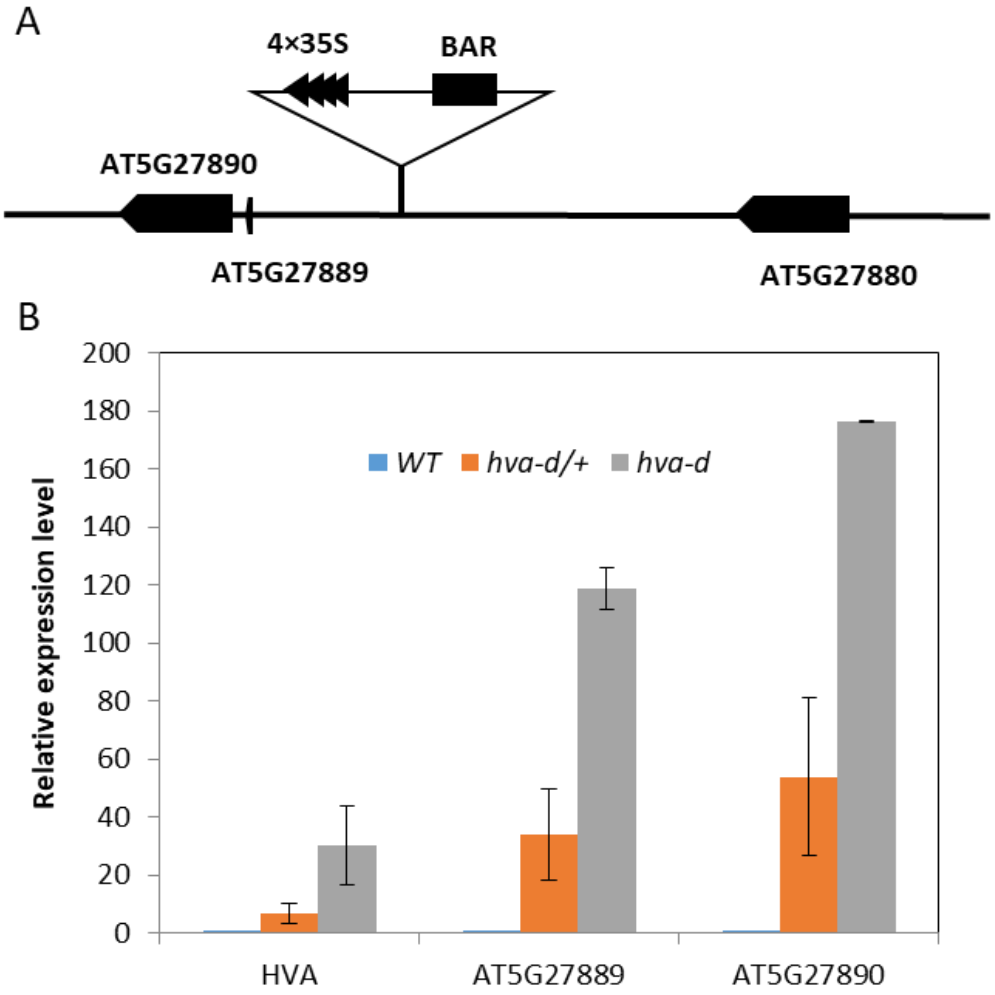

Figure 4: Activation tagging insertion caused overexpression of *AT5G27880, AT5G27889* and *AT5G27890* in *hva-d* mutant.

(A) Schematic diagram of the genomic region flanking the T-DNA insertion site in *hva-d* mutant. The arrow direction represents the transcriptional orientation of the genes. BAR indicates Basta resistant gene. The T-DNA insert position is confirmed by sequencing. (B) Expression of *AT5G27880*, *AT5G27889* and *AT5G27890* were activated in *hva-d* mutant. Values are means ±SD of three biological replicates. *UBQ5* is used as the reference gene.

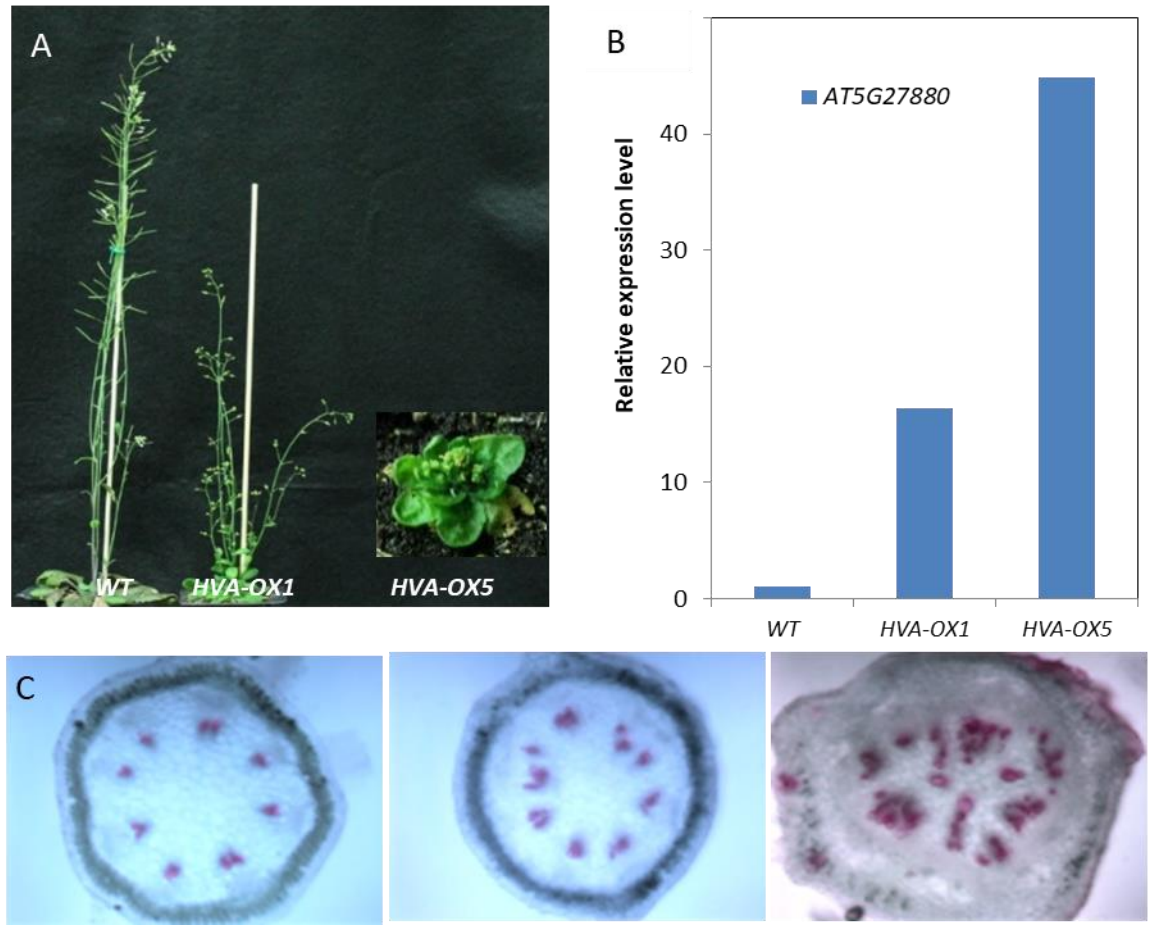

Figure 5: Activation of *AT5G27880* showed *hva-d* mutant phenotypes.

(A) Growth phenotypes of 40-day old *AT5G27880-OX1* and AT5G27880-OX5. (B) Quantitative RT-PCR analysis of two overexpression lines *AT5G27880-OX1* and *AT5G27880-OX5* showing increased expression level of *AT5G27880*. (C) The cross section of *AT5G27880-OX1* and *AT5G27880-OX5* showed more vascular bundles and ectopic xylem cells in pith similar to *hva-d* mutant.

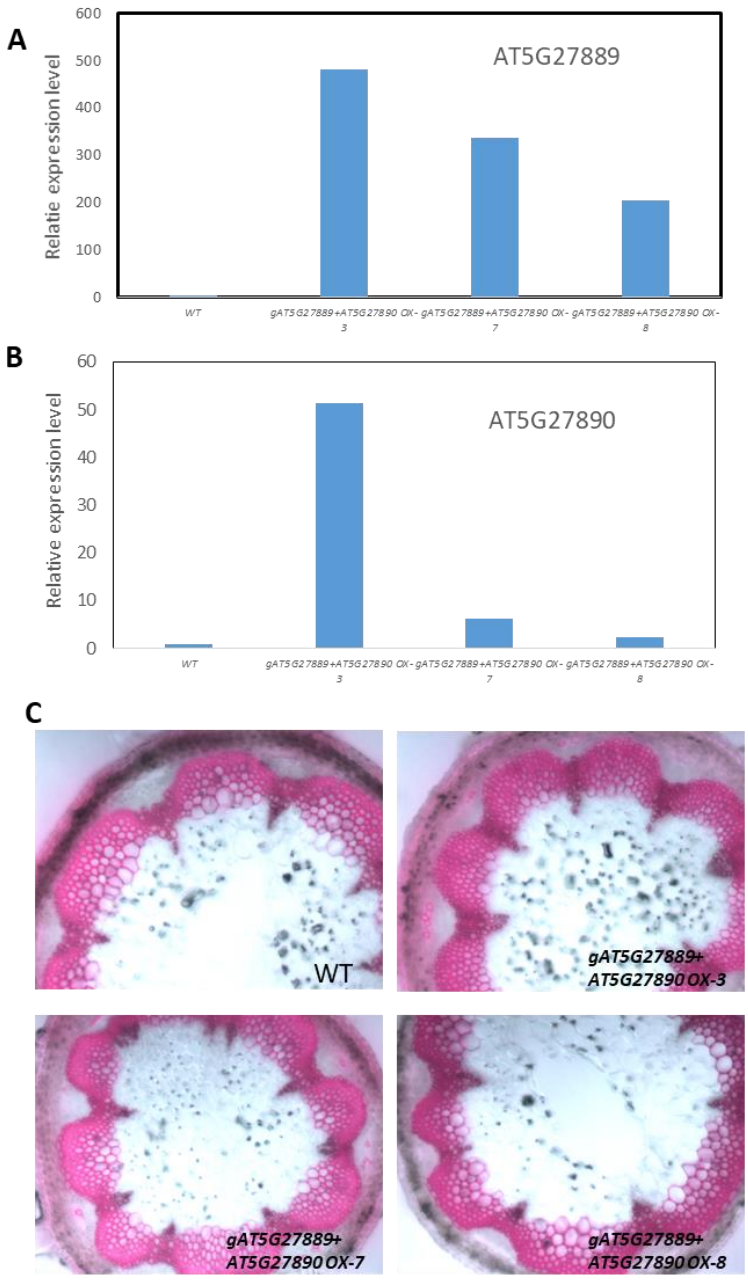

Figure 6: Overexpression of *AT5G27889* and *AT5G27890* showed normal vascular phenotype like wild type.

(A) and (B) Quantitative RT-PCR analysis showed increased expression level of *AT5G27889* and *AT5G27890* in transgenic lines. (C) Phloroglucinol staining of 35-day old overexpression line (*gAT5G27889+AT5G27890 OX-3, 7, 8*) showed similar vascular phenotype like wild type.

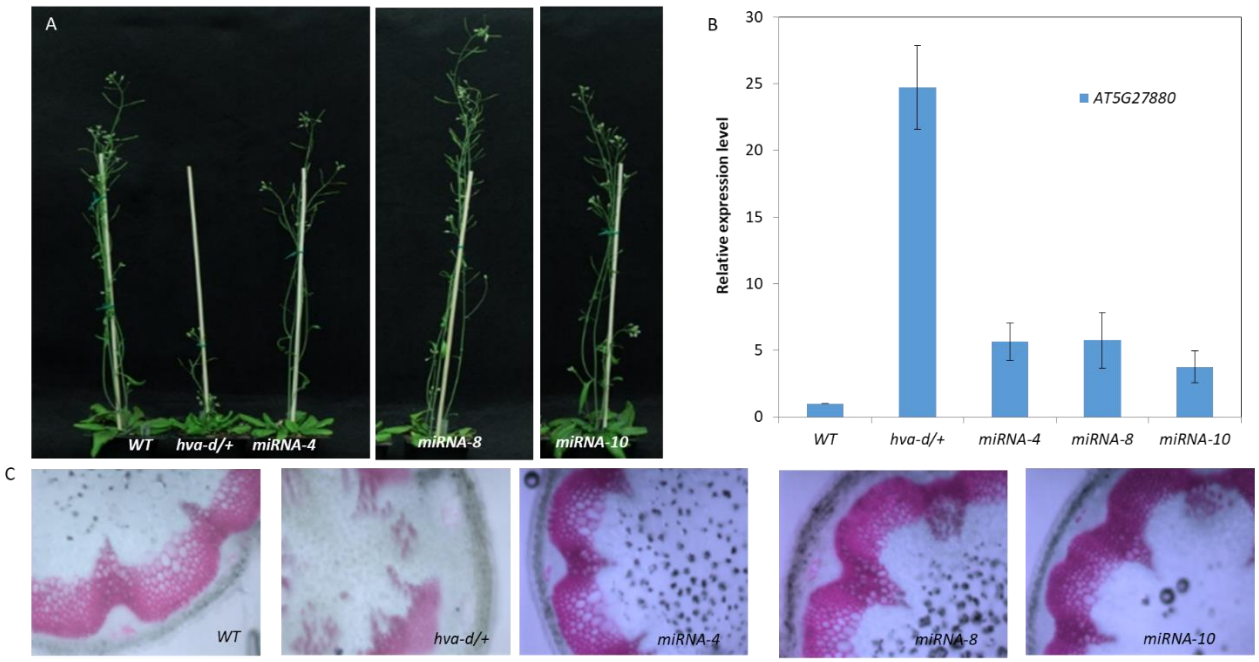

Figure 7: Repression of *AT5G27880* in *hva-d* mutant restored the mutant phenotype to wild type.

(A) 35day-old of *microRNA-4*, *microRNA-8*, *microRNA-10* in the *hva-d/+* background showed similar growth phenotype to wild type plants.

(B) Quantitative RT-PCR analysis showed that expression of *HVA* was repressed in the *35S::microRNA-HVA* transgenic plants. Values are means ±SD of three biological replicates. *UBQ5* is used as the reference gene.

(C) Phloroglucinol staining of the cross section represent that the vascular defects were recovered to wild type pattern.

HVA is a nucleus localized transcriptional reprssor

HVA gene encodes a putative transcription factor that belongs to C2H2 zinc fingers superfamily comprising 176 members in *Arabidopsis* (Englbrecht, Schoof et al. 2004). Phylogenetic classification indicated that HVA belongs to the C1-1i subfamily which includes some well-known regulators in *Arabidopsis* development, such as AT5G54360, AT5G05120, AT3G23130 (SUPERMAN), AT2G42410 (ZFP11), AT4G17810, AT2G37740 (ZFP10), AT5G06070 (RBE) and AT1G68480 (JAG) (Figure 8A). Multiple sequence alignment of the closely related proteins revealed high similarity between their conserved C2H2 domains and C-terminal ERF-associated amphiphilic repression (EAR) motif (Figure 8B). The EAR motif has been shown to have transcriptional repression activity in a broad range of developmental and physiological processes (Ohta 2001).

To investigate the subcellular localization of HVA, we made a GFP-fusion construct to verify its intracellular localization. A green fluorescent protein (GFP) was fused at the N terminus of HVA (*eGFP-HVA*), driven by a CaMV 35S promoter, was transformed to *Arabidopsis* wild type. The fluorescence pattern of eGFP in 5-day old root hair suggested that HVA is localized in the nuclei but not in the nucleolus (Figure 9), which was consistent with the role for HVA as a transcription factor.

The protein sequence of HVA has an EAR domain with LSLSL amino sequence in the C-terminus. To examine whether HVA functions as an active repressor, we performed a transient expression assay using an effector plasmid in which the coding region of HVA was fused to the yeast GAL4 DNA-binding domain (GAL4-DB) under control of 35S promoter. We co-transformed *Arabidopsis* leaf protoplasts with the effector plasmid together with a reporter

plasmid, in which a luciferase gene (*LUC*) was under the control of a minimal 35S promoter and five copies of the GAL4-binding site inserted upstream of the TATA box (5×GAL4-TATA) (Figure 10A). Bioluminescence measurements revealed that the expression level of reporter gene was reduced more than 50% in the presence of full-length HVA, while deletion or mutation of EAR motif showed no effect on the expression of the reporter gene (Figure 10B and C). The results indicated that HVA functions as a transcriptional repressor, and the repression depends on a functional EAR domain.

To further confirm the importance of the EAR motif for the functional repressive activity, we overexpressed HVA without EAR motif (*HVAΔEAR*), under the control of 4×35S enhancer in *Arabidopsis* wild type. Three transgenic plants (*HVAΔEAR-OX6, 8, 17*) showed increased expression level of truncated *HVA*, but did not show similar vascular pattern like *hva-d* mutant (Figure 11). Taking all the results together, HVA functions as a transcriptional repressor and EAR motif is responsible for the repressive activity.

A

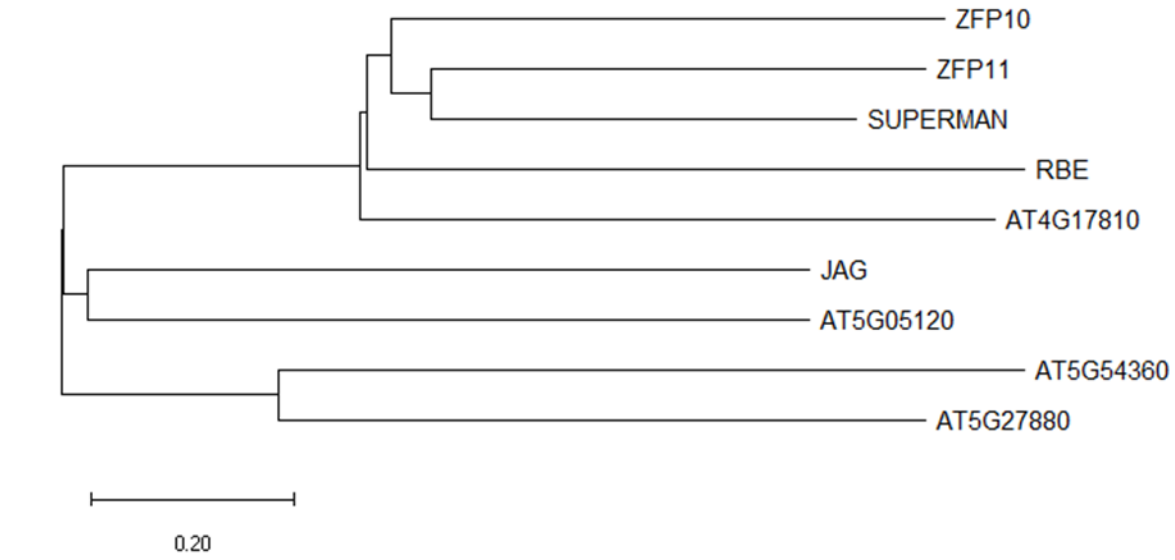
ZFP10
ZFP11
SUPERMAN
RBE
AT4G17810
JAG
AT5G05120
AT5G54360
AT5G27880
0.20

B

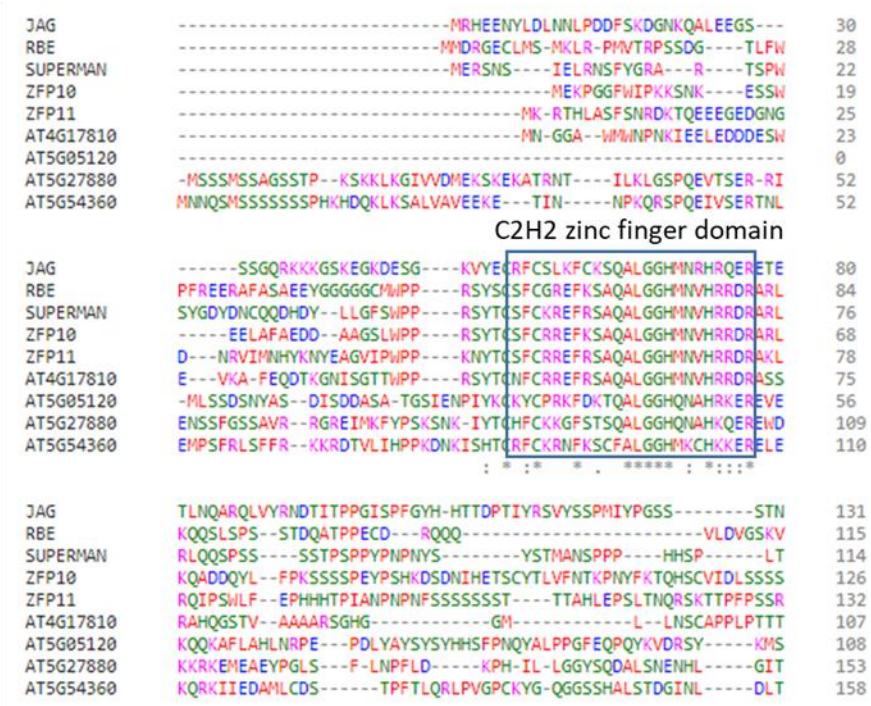
C2H2 zinc finger domain

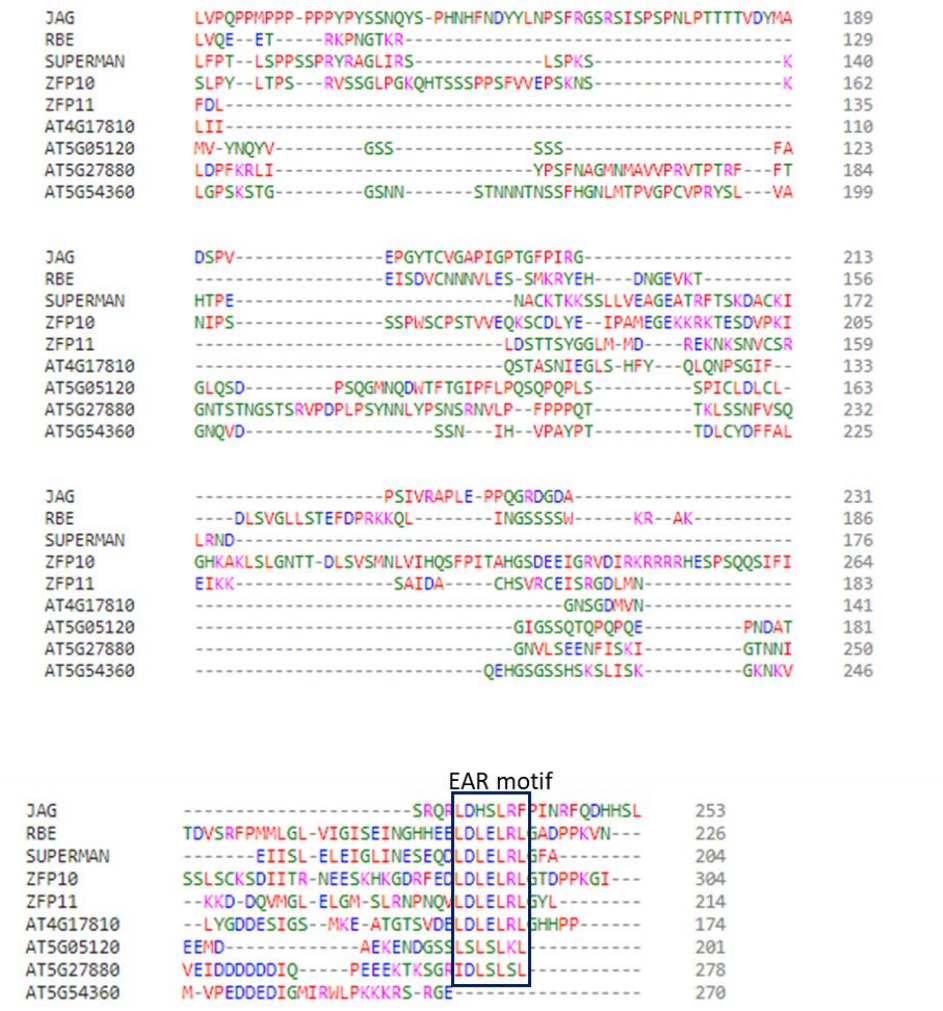

Figure 8: HVA-related C2H2 Zinc finger proteins.

(A) Phylogenetic tree of 8 C2H2 Zinc finger proteins are related to HVA protein analyzed by MEGA-X. (B) Multiple sequence alignment of the 9 closely related protein. The predicted C2H2 zinc finger domains and the conserved EAR motifs are boxed.

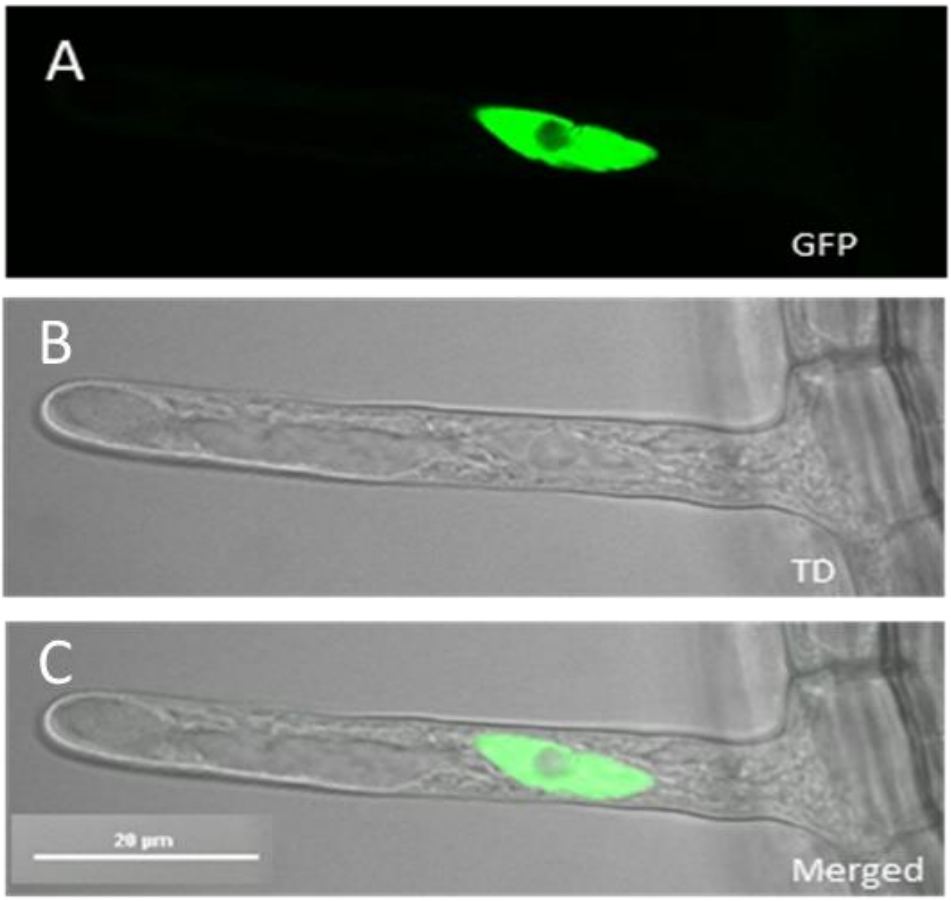

Figure 9: HVA protein is localized in the nucleus.

(A) Confocal images of nuclear localization of *eGFP-HVA* fusion proteins in *Arabidopsis* root hair of 5-day old seedling in GFP channel. (B) Confocal images of *Arabidopsis* root hair in transmitted channel (TD). (C) Confocal images of subcellular localization of *eGFP-HVA* fusion proteins in merged images. *HVA* is cloned into pK7WGF2 and transformed into wild type plants. Noting that HVA is localized in the nuclei. Bars, 20 um.

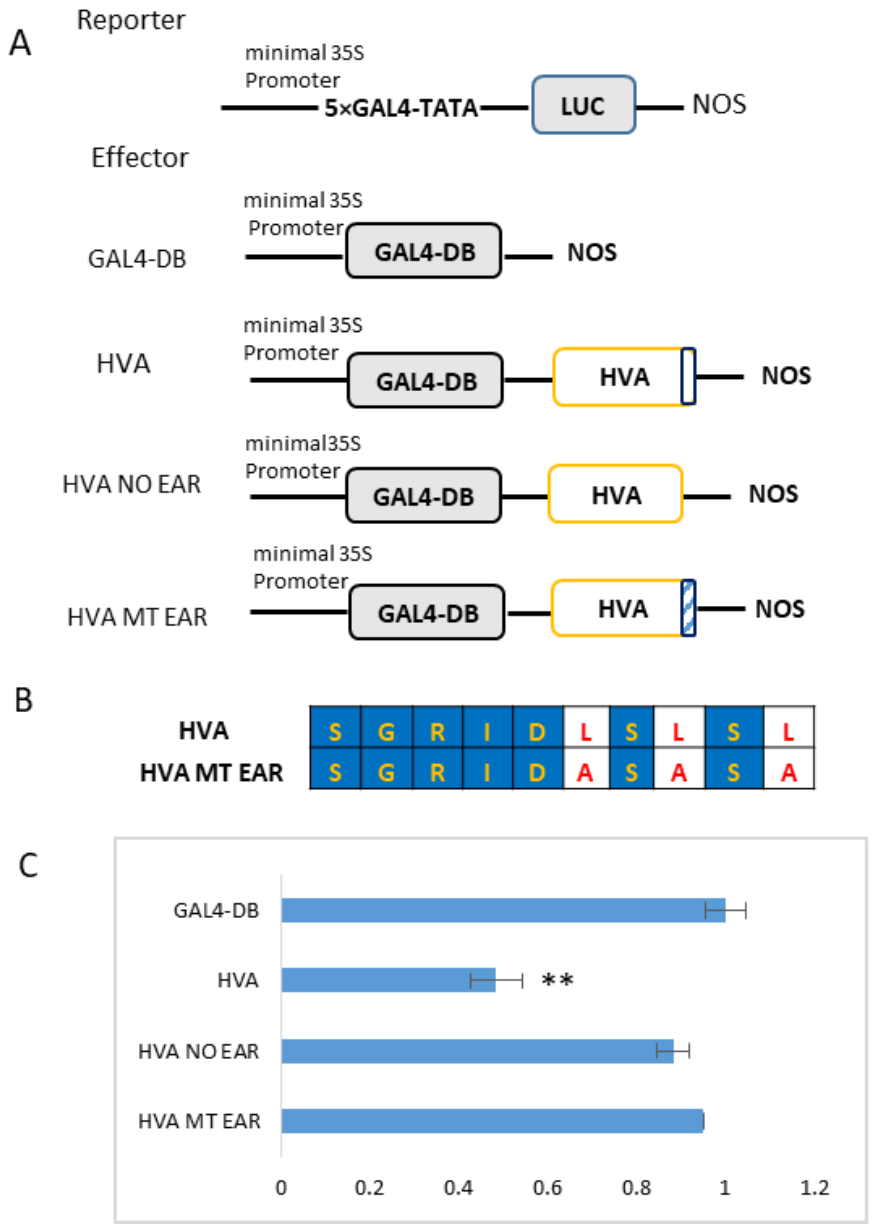

Figure 10: HVA functions as a repressor via EAR motif.

(A) Constructs used in transient expression assay. HVA has an EAR domain with (LSLSL) amino sequence in the C-terminal terminus. (B) Amino acid sequence of the EAR-domain in HVA and mutations introduced into the EAR domain (*HVA MT EAR*). The mutations were labeled in red color. (C) Relative luciferase activities using HVA or HVA mutated constructs as effector compared with GAL4-DB control. Error bars indicate SD of three biological replicates. Asterisks indicate a statistically significant difference by Student's t test (**P < 0.001).

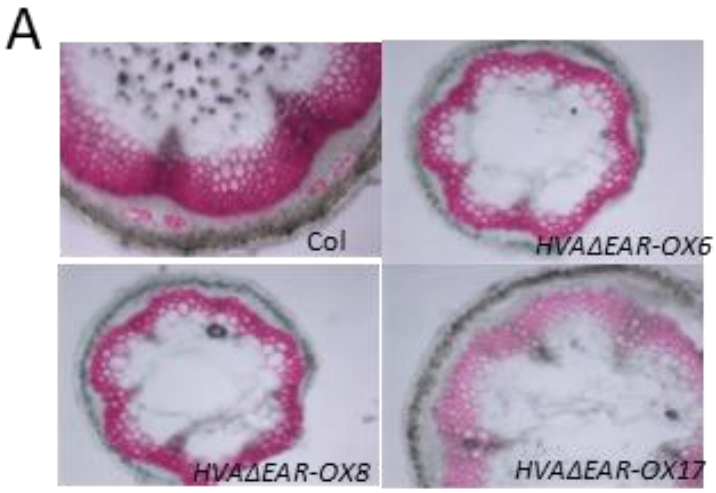

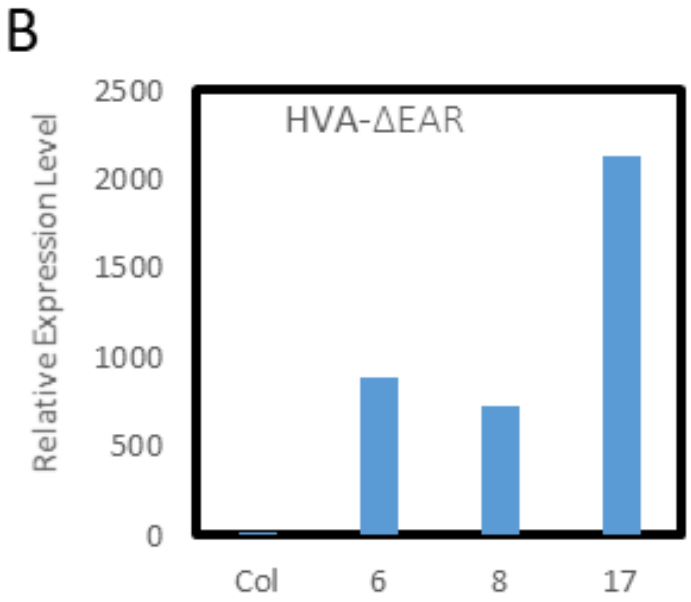

Figure 11: HVA function requires the EAR domain.

(A) Quantitative RT-PCR for 3 lines (*HVAΔEAR-OX6, 8, 17*) showed increased expression level of HVAΔEAR in the transgenic plants. An overexpressing construct was transformed into wild type with *HVAΔEAR* driven by 4×35S enhancers. (B) Cross-section of the overexpression lines showed normal vascular bundle phenotypes due to the deletion of EAR domain.

HVA interacts with corepressor TPL via EAR domain

The EAR motif has been reported play a key role in a variety of transcriptional repressors to regulate plant developmental processes. Recent studies confirmed the physical interactions between TPL and the EAR motifs in several TFs in *Arabidopsis* (HeidiSzemenyei 2008, Kagale and Rozwadowski 2014). The HVA protein has a conserved EAR motif (LSLSL) (Figure 22), which has the potential for recruiting transcriptional corepressors. To investigate whether HVA interacts with transcriptional co-repressors via its EAR motif, we performed a pairwise yeast two-hybrid assay between HVA and TPL. We found TPL interacted with HVA, but deletion of the EAR motif of HVA disrupted these protein interactions in yeast (Figure 12). To further confirm the direct interaction between HVA and TPL, we used a transient in vivo bimolecular fluorescence complementation (BiFC) in *Nicotiana benthamiana* leaves. Fluorescence of the reconstituted split YFP protein was observed in the nucleus of leaf cells co-transfected with the HVA-N-YFP and TPL-C-YFP constructs, but not in cells expressing HVAΔEAR-N-YFP and TPL-C-YFP (Figure 13). Those results demonstrated that TPL and HVA interact via the HVA EAR domain.

TPL was originally identified from a temperature-sensitive *tpl-1* mutant in the *Landsberg erecta* (*Ler*) ecotype, which shows severe polarity defects and replacement of the shoot by an apical root at higher temperature (Osmont and Hardtke 2008). The *tpl-1* has a semi-dominant character due to the dominant-negative effect of the N176H substitution. The normal function of *TPL* and its redundant *TPR* genes was interfered due to this dominant negative mutation in *tpl-1*. To further understand the biological role of HVA-TPL interaction, we transformed *hva-d/+* plants with a construct of the mutant *tpl-1* protein—mtTPL (N176H), driven by *UBQ10* promoter. We screened the transgenic plants and obtained 18 transgenic plants in *hva-d/+* background. The

growth of 9 out of 18 partially complemented the *hva-d/+* defects. Overexpression of *mtTPL* abolished the dwarfism growth and recovered the vascular organization to wild type (Figure 14). The dwarfism and enhanced protoxylem development were rescued by overexpression of *mtTPL*. Experiment analysis indicated that TPL protein is required for HVA function.

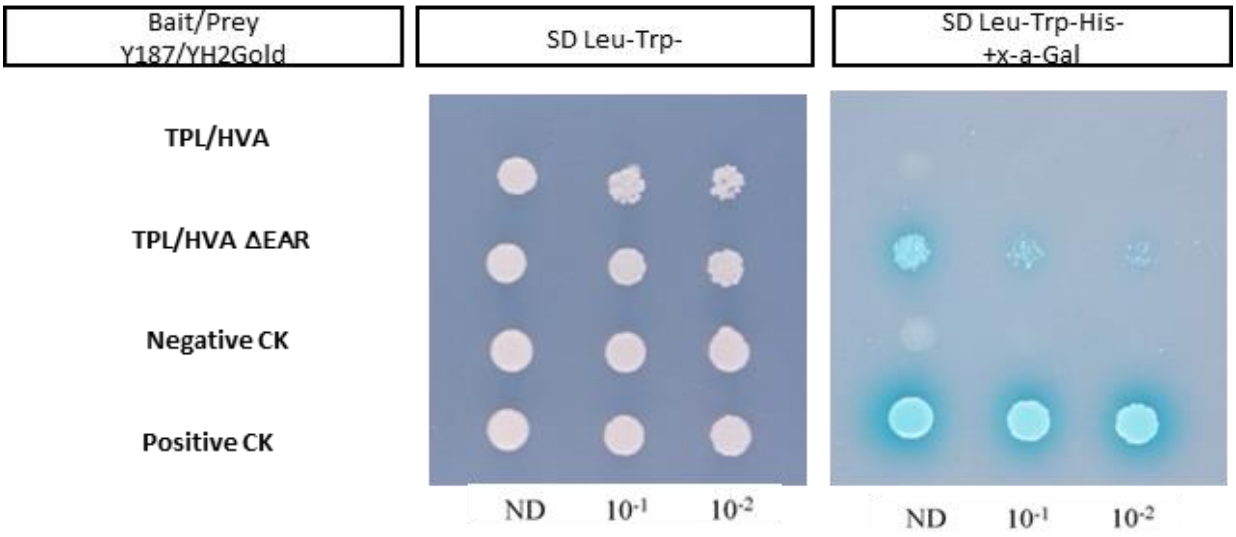

Figure 12: Interaction of HVA with TPL in yeast two-hybrid system.

For yeast two-hybrid system, 10-fold serial dilutions using distilled water of yeast cell cultures for each interaction and expressing both bait and prey constructs were spotted on selective media. Positive (p53/T-antigen) and negative (LaminC/T-antigen) controls are shown at the bottom of the figure. Baits were expressed as Gal4 DNA-BD fusion proteins in the pGBKT7 plasmid and transformed into YH2Gold yeast strain; preys were expressed as Gal4 AD fusion proteins in pGADT7 vector and transformed into the Y187 strain. (ND: non-diluted).

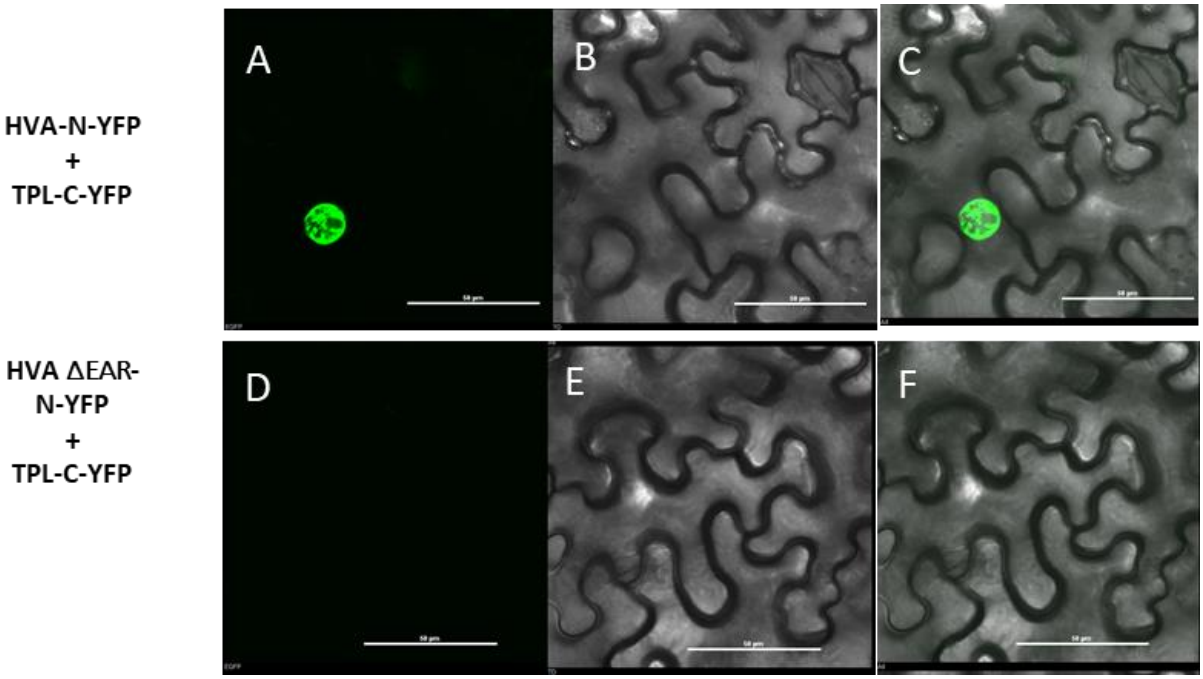

Figure 13: Bimolecular fluorescence (BiFC) analysis of interaction between HVA and TPL in Agrobacterium-infiltrated tobacco (*Nicotiana benthamiana*) leaves.

(A) Complementation analysis showed fluorescence of N-terminal part of the YFP fused with HVA and C-terminal part of the YFP fused with TPL at nucleus in GFP channel. (B) The *bethanmiana* leaf cell expressed fused proteins in transmitted light channel. (C) Confocal microscopy images showed fluorescence signal in the nucleus in the overlapped channel. (D) Confocal microscopy image showed no fluorescence when HVAΔEAR was coexpressed with TPL in GFP channel. (E) Transmitted light channel showed cotransformed *benthamiana* leaf cells. (F) Confocal microscopy image showed no fluorescence for HVAΔEAR coexpressed with TPL in overlapped channel. The scale bar is 50um.

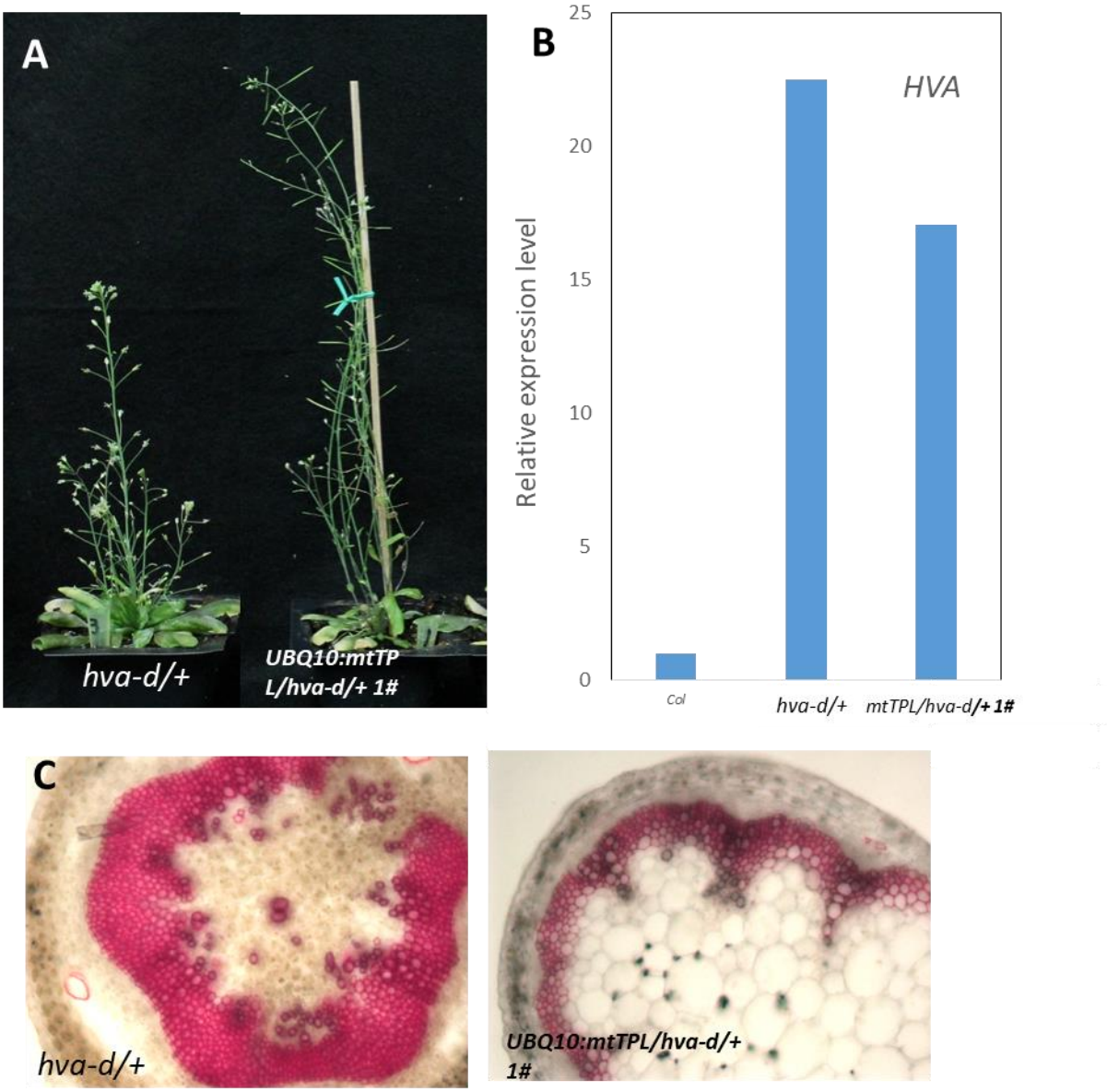

Figure 14: TPL protein is required for HVA function.

(A) Dwarfism growth phenotype was abolished in the 37-day old transgenic plants. The mtTPL(N176H) construct was transformed into *hva-d/+* driven by *UBQ10* promoter. (B) Quantitative RT-PCR showed enhanced expression level of HVA in the transgenic lines similar to hva-d/+ indicating the activation-tagged effect did not change. (C) Cross-section of the transformed hva-d/+ (*UBQ10::mtTPL/hva-d/+ #1*) showed restored vascular organization similar to wild type.

Auxin activity was affected in *hva-d* mutant

The HVA functions as a transcriptional repressor and is responsible for the enhanced vascular development in *hva-d* mutant, but the functional mechanism of HVA in vascular patterning and development is still unknown. Auxin is essential for provascular specification and plays key role in vascular differentiation. After gene expression analysis, quantitative RT-PCR experiment showed that both *PIN1* and *PIN2* were downregulated in *hva-d* mutant background suggesting that polar auxin transportation maybe impaired in *hva-d* mutant (Figure 15). PIN1 and PIN2 are auxin efflux carrier and polar-localized at the basal region of the cells which determine the direction of auxin flow (Peer, Bandyopadhyay et al. 2004). Since previous study reported that mutants of PIN showed increased number of vascular bundles (Turner and Sieburth 2003), we used a weak allele for *PIN1* gene, *pin1-5*, to check the effect of altered auxin transportation on vascular development in inflorescence stems. The mutant *pin1-5* showed determinate inflorescence stems after generating 8 flowers (Figure 16A). Cross-section in the apex of stem showed formation of primary xylem along the stem periphery was enhanced similar to *hva-d/+* (16B to E). We also checked *PIN2* mutant as well, but no altered vascular phenotypes were overserved. Taking all the result together, *PIN1* gene is considered to be a candidate gene which has functions in *hva-d* mutant and controls vascular bundles formation.

We crossed *hva-d/+* with the auxin sensitive reporter *DR5rev: GFP* to detect auxin concentration and distribution. The GFP signals in wild type were restricted mainly in protoxylem regions and were occasionally observed in cambium (Figure 17A to C). In comparison to wild type, strong GFP signals were detected in protoxylem in the *hva-d/+* mutants, indicating enhanced local auxin contribution in mutant stem (Figure 17D to E). We hypothesized that the accumulation of auxin can be caused by the activation of auxin biosynthesis genes, for example *YUCCA* genes. *YUCCA* genes (*YUC1*, *YUC2*, *YUC4*, and *YUC6*) are key auxin biosynthesis genes and are expressed in vascular tissues (Cheng, Dai et al. 2006). Quantitative RT-PCR analysis showed that expression of *YUC2* was increased in *hva-d* mutant background while no change for the other three genes (Figure 18). All the results indicated that auxin homeostasis was affected because auxin polar transportation and auxin distribution were altered in *hva-d* mutant.

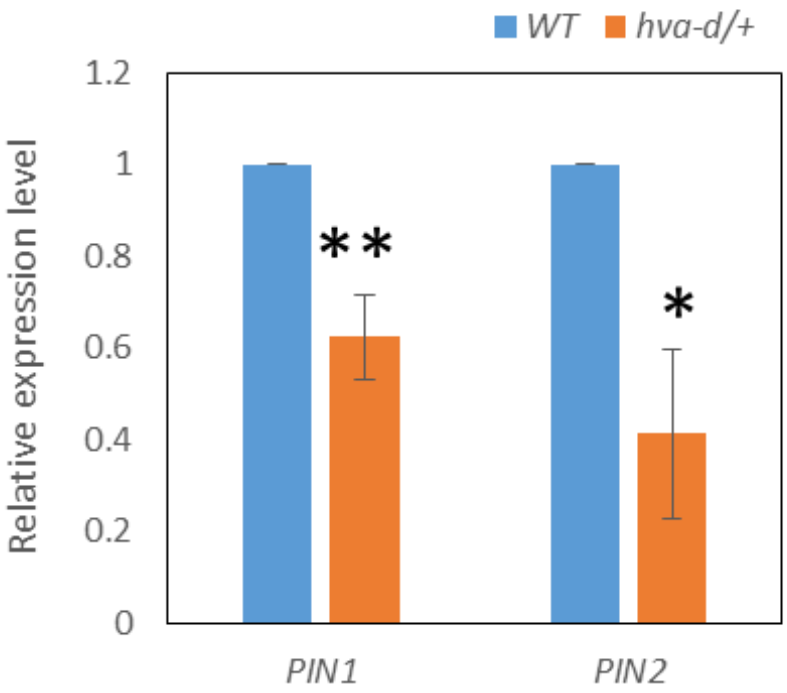

Figure 15: Quantitative RT-PCR analysis showed the expression level of *PIN1* and *PIN2* in *hva-d* mutant background.

The error bars represent SD of three biological replicates. Asterisks indicate a statistically significant difference by Student's t test (**p<0.005, *p<0.01).

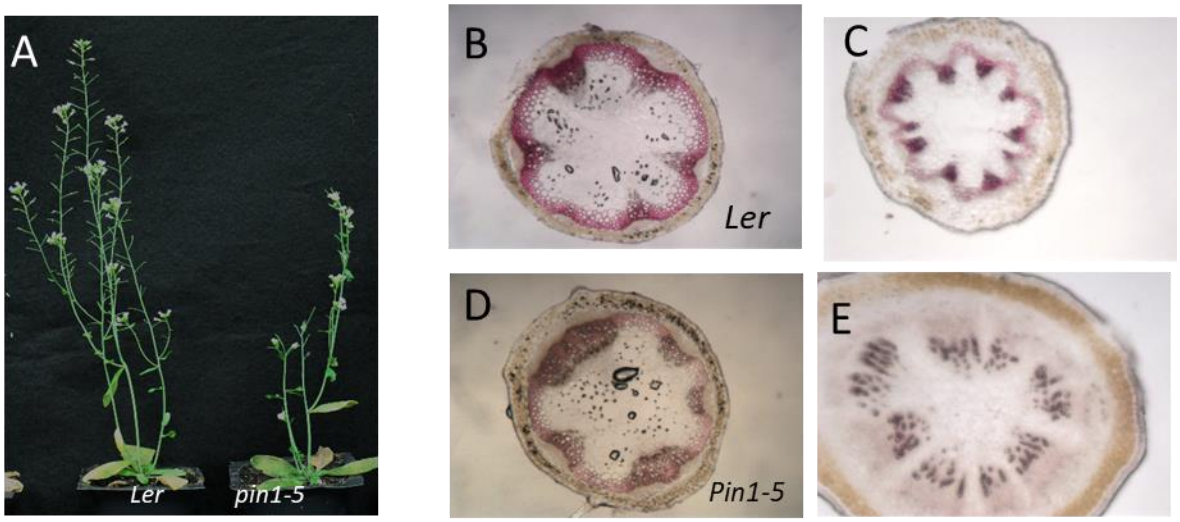

Figure 16: Growth morphology and vascular patterns of 37-day old *pin1-5*.

(A) 37-day old *Landsberg erecta* (*Ler*) on the left and weak allele *pin1-5* mutant on the right. Phloroglucinol staining of the cross-section from *pin1-5* stem basal part (D) and apex region (1cm below the tip) (E) showed enhanced protoxylem formation. (B) and (C) are the cross-section phloroglucinol staining from *Ler* basal part and apex part.

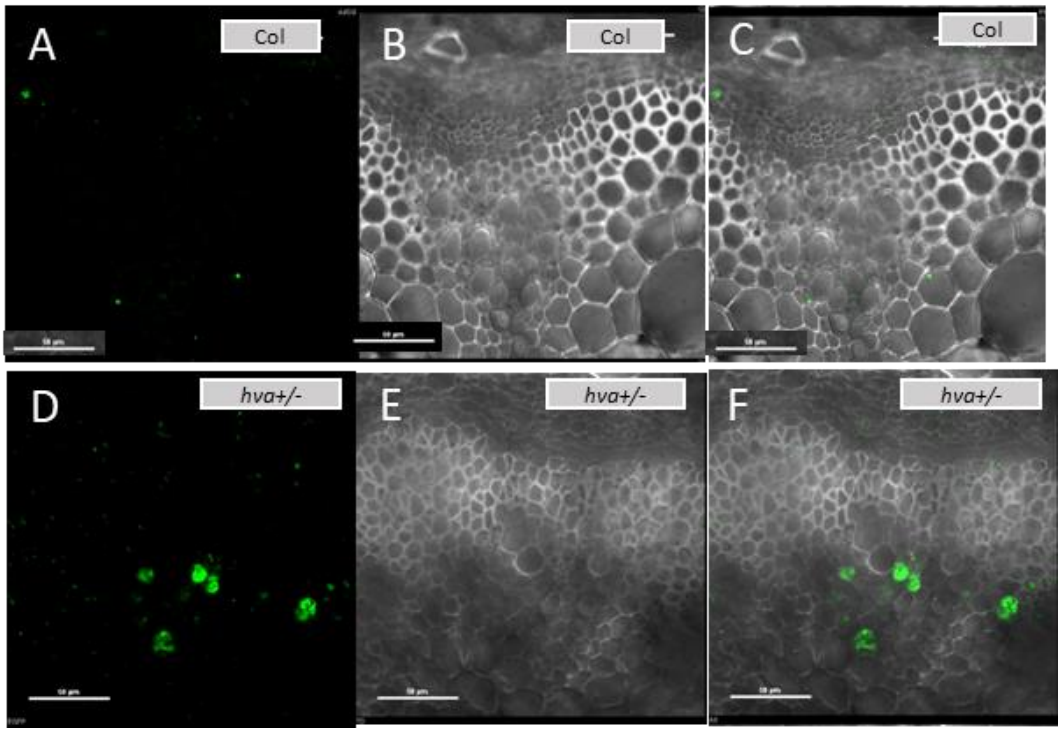

Figure 17: Analysis of *DR5revpro:GFP a*ctivities in the *Arabidopsis* wild type and *hva-d* inflorescence stem.

(A) Confocal images of *DR5rev:GFP* signal in cross-sections samples from WT background in GFP channel. (B) Cross-sections samples of *DR5rev:GFP* signal in WT background in transmitted channel. (C) Confocal images of *DR5rev:GFP* signal in WT background in overlapped channel. (D) Confocal images of *DR5rev:GFP* signal in cross-sections samples from *hva-d/+* mutant in GFP channel. (E) Cross-sections samples of *DR5rev:GFP* signal in *hva-d/+* background in transmitted channel. (F) Confocal images of *DR5rev:GFP* signal in *hva-d/+* background in overlapped channel. All the samples were from 28-day old inflorescence stems basal part. The thickness of cross-section is 100um. Bars, 50 um.

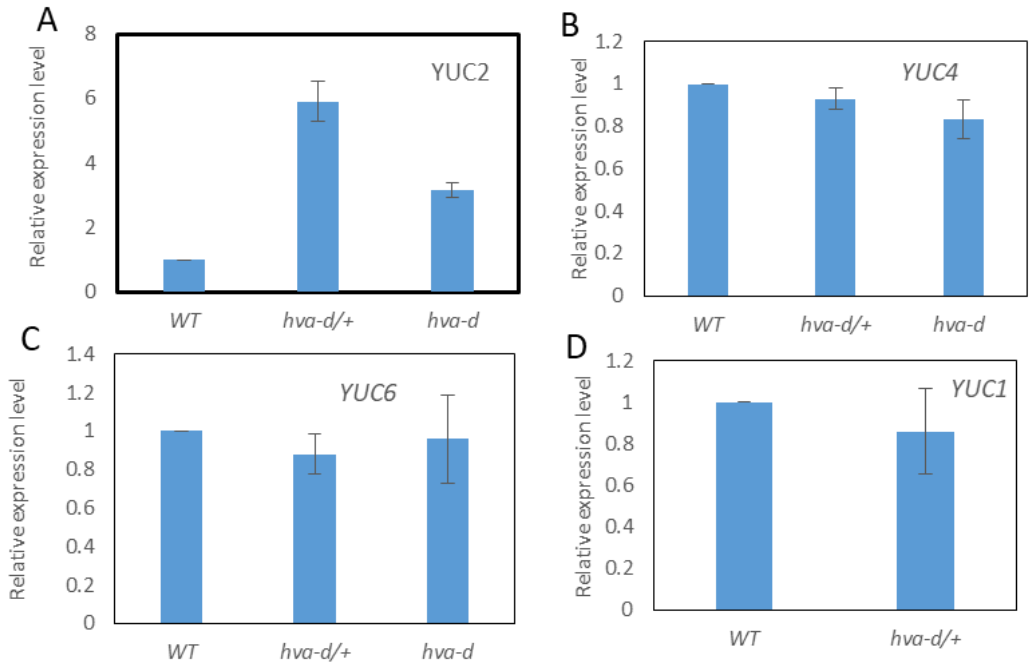

Figure 18: Expression level of *YUC2* gene is activated in *hva-d* mutant background.

(A) Quantitative RT-PCR showed increased expression level of YUC2 genes in *hva-d* mutant. The error bars represent ±SD of three biological replicates. *UBQ5* is used as the reference gene. (B) Quantitative RT-PCR showed expression level of *YUC4* genes in *hva-d* mutant. (C) Quantitative RT-PCR showed increased expression level of *YUC6* genes in *hva-d* mutant. (D) Quantitative RT-PCR showed increased expression level of *YUC1* genes in *hva-d* mutant

HVA protein represses the expression of downstream gene *BP*

KNAT1 (*BP*), a member of class I KNOX family, plays significant roles in meristem maintenance and internode patterning (LongJ 1996). Recent studies showed that *bp* mutant exhibited changes in vascular patterning with altered lignin deposition in stems. The *bp-2* mutant exhibited gaps in the vascular ring and phloem fibers underlying the primary vascular bundles were prematurely lignified (Figure 20E). This vascular phenotype was noticeably similar to the phenotype in *hva-d/+*. Lateral organ boundary genes *BLADE-ON-PETIOLE 1 (BOP1)* and *BOP2* functions downstream of BP in an antagonistic manner, acting as positive regulator in lignin biosynthesis (Ha, Jun et al. 2007, Liebsch, Sunaryo et al. 2014). Quantitative RT-PCR results showed that expression level of *BP* was downregulated in *hva-d/+* mutant, while was dramatically reduced in *hva-d* mutant. As expected, expression of *BOP2* was upregulated when *BP* was repressed (Figure 19A and B). To directly illustrate the regulation of BP expression by *HVA*, we conducted a transient expression experiment using the dual luciferase assay. The effector construct of HVA driven by 35S promoter and a reporter construct, in which the 1.4kb-promoter sequences of *BP* was placed upstream of the firefly luciferase gene, were co-transformed into *Arabidopsis* leaf protoplasts (Figure 19C). In the presence of HVA, the relative expression level of firefly luciferase was reduced more than 30% compared with empty control vector (Figure 19D). Together, results indicated that HVA represses the expression of *BP*, which may partially explain the *hva-d* phenotypes in vascular development.

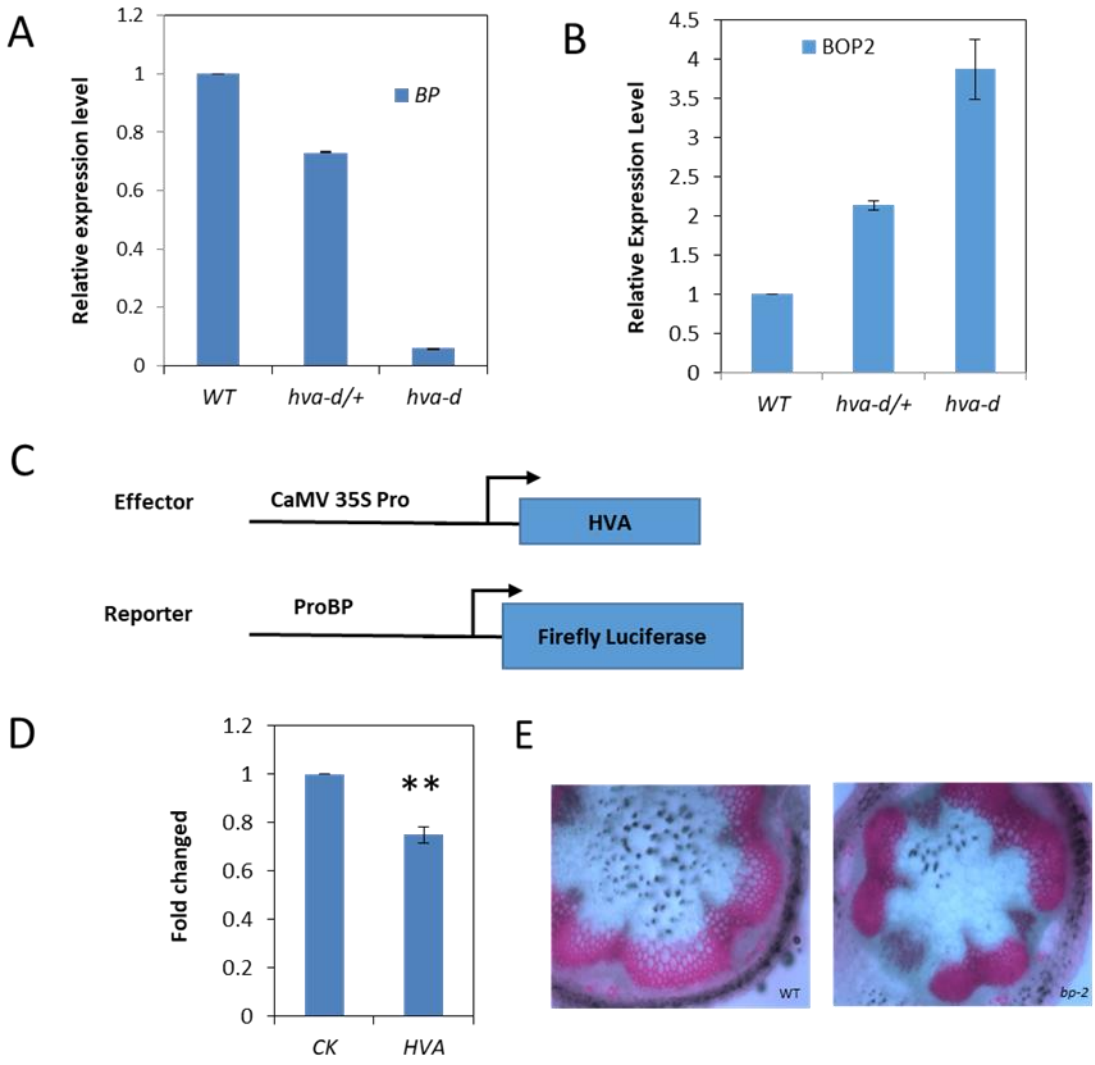

Figure 19: HVA protein represses the expression of downstream transcription factors BP.

(A) Quantitative RT-PCR analysis showed the expression level of *BP* in *hva-d* mutant background. Values are means ±SD of three biological replicates. *UBQ5* is used as the reference gene. (B) Quantitative RT-PCR analysis showed the expression level of *BOP* in *hva-d* mutant background. (C) Effector and reporter constructs used in transient expression assays. (D) Promoter activity of *BP* was repressed by overexpression of *HVA* genes. Error bars represent ± SD from three independent replicates. Asterisks indicate a statistically significant difference compared with wild type by Student's t test ($P < 0.0002$). (E) Cross-sections with phloroglucinol staining from Col and *bp-2* mutant inflorescence stem.

Transcriptome analysis of the *hva-d/+* mutant

To gain an overview of transcriptome change in *hva-d/+* mutant, total RNA was extracted from 35day old wild type and *hva-d/+* stems and analyzed by RNA-Seq. After normalization, approximately 1795 genes (1472 up-regulated and 323 down-regulated) were differentially expressed, more than 2 folds. Because HVA is a transcriptional repressor, we analyzed the 323 downregulated genes. Gene Ontology (GO) Annotations from TAIR categorizes genes into groups based on their predicted or experimentally derived Molecular Function, Biological Process, and Cellular Component (Chad E Niederhuth 2013). The purpose of this project is to work on the correlations between the altered cell wall phenotypes in *hva-d* and the possible transcriptional mechanism that HVA may involves. After analyze the results, there are 105 genes located in the nucleus and 16 genes in the cell wall portion in the Go Cellular Component analysis (Figure 20A). In molecular function analysis, there are 52 genes involved in DNA or RNA binding and 30 genes identified as transcription factors (Fig 20B). Several transcription factors were analyzed to function in vascular organization and picked for further analysis, like WOX14 (vascular cell differentiation) (Denis, Kbiri et al. 2017), LBD15 (xylem differentiation) (Ohashi-Ito, Iwamoto et al. 2018) and WRKY12 (Wang, Avci et al. 2010).

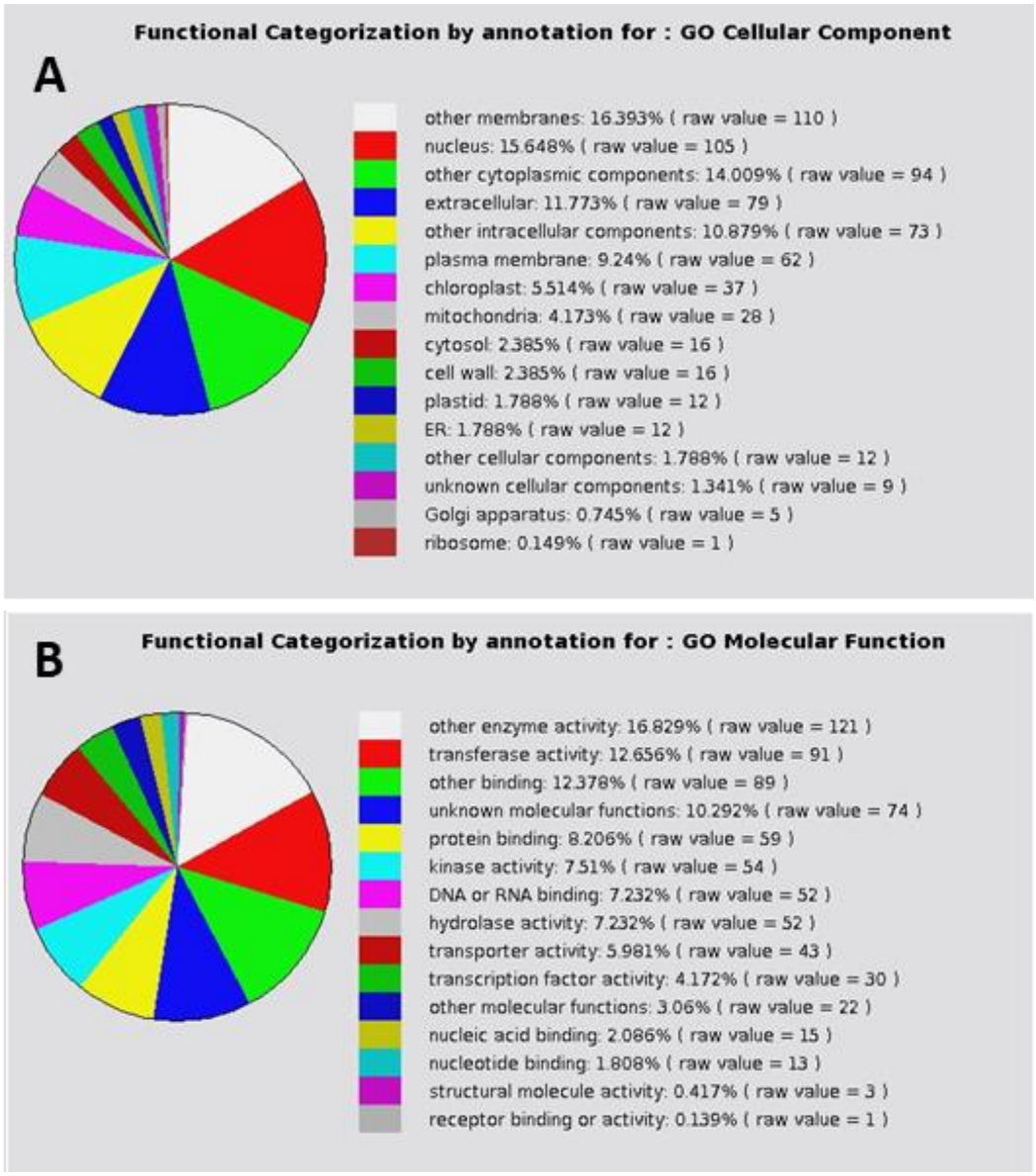

Figure 20: Gene Ontology (GO) analysis of downregulated genes in RNA-seq data for *hva-d* mutants.

(A) Analysis of two-fold downregulated 323 downregulated genes in Go Cellular Component in *hva-d* RNA-seq data. (B) Analysis of the downregulated genes in Go Molecular Function.

Discussions

In this study, a novel and unique activation tagging mutant—*hva-d* was identified. The mutant showed enhanced vascular cambium activity and developed more vascular bundles. A C2H2 Zinc finger transcription factor HVA is responsible for the mutant phenotypes and plays a key role in the regulation of vascular tissue development. In particular, our data suggest that HVA acts as a transcriptional repressor and functions in vascular initiation and cambium differentiation.

Preliminary histochemical analysis phloroglucinol staining showed enhanced formation of protoxylem and ectopic lignification in *hva-d* stem. It suggested that xylem differentiation in *hva-d* mutant was highly activated. We hypothesized that activated xylem differentiation possibly came from enhanced activity of the cambium. In order to examine the vascular activity in the mutant, we used *AtHB8* as a marker for cambial activity and *APL* to monitor phloem developmental dynamic. Beta-glucuronidase (GUS) staining results showed that cambium and phloem activity in *hva-d* mutant were also elevated compared with wild type. There were three reported mutants showed high cambium activity, *cov1* (Parker 2003), *hca* (Pineau, Freydier et al. 2005) and *hca2* (Guo, Qin et al. 2009). The *cov1* and *hca* mutants are recessive alleles derived from EMS mutagenesis and T-DNA insertion, respectively. The activation tagging line *hca2* showed increased interfascicular cambium activity without altering the organization of vascular bundles in stems. Our expression analyses using quantitative RT-PCR showed no expression change for *HCA2* (Figure 21) in the *hva-d* mutant. The phenotypes of previous three mutants showed no effect on vascular bundle number, indicating that this is a novel mutant with unique phenotypes in vascular patterning.

Our results indicated that activation of *HVA* (*AT5G27880*) is responsible for *hva-d* mutant phenotypes. *HVA* gene encodes a putative transcription factor that belongs to C2H2 zinc fingers superfamily comprising 176 members in *Arabidopsis*. Multiple sequence alignment of the most related proteins revealed high similarity between their conserved C2H2 domains and C-terminal conserved ERF-associated amphiphilic repression (EAR) motif. It has been shown that C2H2-type transcription factors play important role in the regulation of plant growth, development, hormone responses, and tolerance to biotic and abiotic stresses (Ciftci-Yilmaz and Mittler 2008,

Kielbowicz-Matuk 2012). It has been reported that EAR motif is crucial for its transcriptional activity, and mediates interaction with the co-repressor TPL. HVA functions as a repressor in the transient expression assay and overexpression of HVAΔEAR showed no phenotypes in vascular patterning. Yeast two hybrid assay and BiFC results proved that HVA protein interacts with TPL. Repression of *TPL* interferes *hva-d* mutant phenotypes demonstrating TPL assists the function of HVA to control plant growth and vascular development. Many studies proved that TPL can interact with a wide variety of downstream genes involved in auxin, jasmonate and BR signaling pathway. But the biological function of interaction between HVA and TPL is unknown. We are still investigating the possible genes or signal pathways downstream of HVA-TPL which can control the pattern of vascular initiation in *hva-d* mutant.

Auxin distribution was enhanced in the protoxylem regions in *hva-d* mutant. And the key auxin biosynthesis gene *YUC2* was activated in the mutant. Auxin is essential for cambium activity. However, auxin level does not alter the number or arrangement of vascular bundles, because overproducing *yacca* mutants did not show obvious vascular pattern changes (Norma Fàbregas 2010). Instead of auxin level, auxin maxima controlled by polar auxin transportation determines vascular bundles formation and spacing. Polar auxin transportation was impaired in *hva-d* mutant since *PIN1* expression was significantly downregulated. Another evidence that PAT can effect vascular pattern came from a weak allele *pin1-5.*The *pin1-5* mutant showed enhanced protoxylem formation in shoot apex which was similar to *hva-d* vascular patterning. The role of Polar Auxin Transportation and *hva-d* mutant phenotype is still unclear. We will transform PIN1 gene to the mutant to check if complementation for the vascular defects can happen or not.

Brassinosteroid (BR) also plays key role in cell expansion and xylem differentiation. A number of BR mutants in *Arabidopsis* and rice showed various vascular differentiation defects (Choe S 1999, Nakamura, Fujioka et al. 2006, Norma Fàbregas 2010). BR was reported to modulate vascular bundle numbers by promoting early procambial cells formation in shoot. So the correlation between BR and *hva-d* mutant phenotypes will also be tested. Furthermore, mutations in CLV result in an increased WUS expression and a larger meristem. The *clv* mutations lead to increased vascular bundle number as a result of the enlarged shoot meristem (Deyoung and Clark 2008). It will be interesting to investigate if there is a correlation between CLV regulatory

pathways and *hva-d* mutant. All these future studies will help to obtain a comprehensive scenario into the function of *HVA* gene in vascular development process.

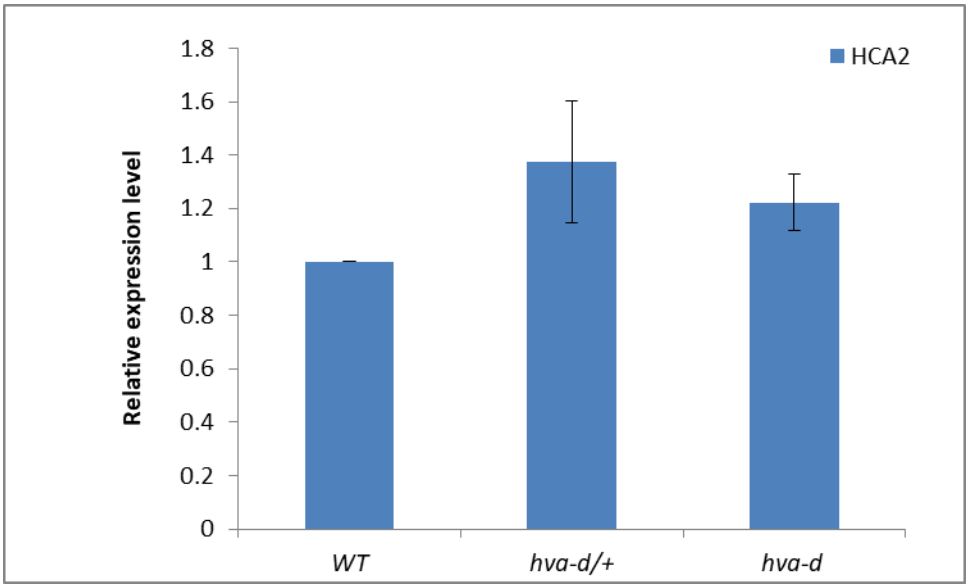

Figure 21: Quantitative RT-PCR showed no altered expression of *HCA2* gene in *hva-d* mutant background.

Values are means ±SD of three biological replicates. *UBQ5* is used as the reference gene.

Materials and methods

Plant material

Arabidopsis thaliana ecotype Col–0, and *Landsberg erecta* (*Ler)* were used in this study as wild-type controls and as the genetic backgrounds. *Nicotiana benthamiana* was used in this study for BiFC. Mutants employed were *pin1-5, pin2* (CS8085). Reporter line *DR5rev:GFP* was ordered from ABRC, *ProAPL:GUS* was received from Dr. Yrjo Helariutta, *ProAtHB8:GUS* was received from Dr. Li-Jia Qu. The *hva-d* mutant was identified from a large-scale mutant screening using UV microscopy. *Arabidopsis* seeds were sterilized and germinated in media (pH 5.7) containing ½ MS salts. Plants were grown in growth chambers under the following conditions: 16 h light/8 h dark; 22°C in the light/20°C in the dark.

Plasmid rescue

The plasmid sequences in pSKI015 flanked by several restriction enzyme sites that can be used for rescue of T-DNA and adjacent plant sequences from transformed plants as describe in (Detlef Weigel 2000). 3µg of genomic DNA, purified with the DNeasy® Plant Mini Kit (Qiagen) and eluted with ddH2O, was digested with KpnI (New England Biolad) for 3 hours. The digested genomic DNA was harvest by phenol-chloroform extraction and was ligated with 1uL of T4 DNA ligase (New England Biolad) in 10µl final volume at 16°C overnight. The ligation system was transformed into *E. coli* by a heat shock. Transformed bacteria were plated onto LB agar media supplemented with 100µg/mL ampicillin. The purified plasmids were send for sequencing to obtain detailed information about the insertion sites by using the left border primers.

Constructs and plant transformation

To produce the HVA overexpression construct, the genomic sequence of HVA was cloned to pENTR/D vector and sequenced. The genomic HVA was ligased into the XmaI and SacI restriction sites of binary vector pBIG-4×35S vector. Plants were transformed by Agrobacterium-mediated transformation. Seeds were selected on plates supplied with 25ug/L kanamycin. Resistant plants were transferred to freshly-prepared soil. To analyze the subcellular localization of HVA, the coding sequences of HVA were cloned as in-frame N-terminal fusions with GFP with CaMV 35S promoter in pK7WGF2. The sequence-confirmed constructs were transformed by GV3101 Agrobacterium cells to wild type plants. After antibiotic selection, 5-day old seedlings were used under Nikon A1R Spectral Confocal.

Real-time PCR

Total RNA from the frozen material was extracted using NucleoSpin® RNA extraction kit (Macherey Nagel). To eliminate the contamination of genomic DNA, total RNA was then treated with DNase for 15 minutes before elution. 2ug of total RNA was reverse transcribed using the Maxima Reverse Transcriptase (Thermo Scientific) in a reaction of 20uL. The cDNA was diluted 5 times and later used as the template for Quantitative RT-PCR. The cDNA samples were used for qRT-PCR with technical duplicates. The 10uL reaction included 2uL of primers (1uM of each primer), 5uL of Universal SYBR® Green Supermix (BioRad), 1uL of diluted cDNA and 2uL of water. The PCR reaction program was set according to the manufacturer's instructions (BioRad). Transcript levels were determined by relative quantification using *Arabidopsis UBQ5* gene as a reference.

Yeast two-hybrid assay

Yeast two-hybrid assays were performed with the GAL4 Two-Hybrid System (Clontech). The complete coding regions of the TPL, HVA and HVAΔEAR proteins were introduced by restriction enzyme digestion into the pGADT7 and pGBKT7 (Clontech). Prey (TPL) was expressed as Gal4-DNA-BD fusion proteins in the pGBKT7 plasmid and transformed into YH2Gold yeast strain; preys (HVA and HVAΔEAR) were expressed as Gal4-AD fusion proteins in pGADT7 vector and transformed into the Y187 strain. Bait- and prey-transformed strains were mated and the resulting diploids were cultured in SD-Leu/-Trp medium. The diploids grew and check protein interactions in SD-Leu/-Trp/-His/X-α-gal medium. 10-fold serial dilutions using distilled water. The interaction between P52 and T proteins was used as a positive control, lam and T were employed as negative controls.

Bimolecular fluorescence complementation assay (BiFC)

For BiFC constructs, the coding sequences of HVA and TPL were amplified and cloned to pENTR/D vector. The sequenced vector were used in an linear recombination (LR) reaction using LR Clonase II (Invitrogen, http://www.invitrogen.com) to insert the coding sequence into the destination vector pUBQ-n-YFP and pUBQ-c-YFP. Plasmids were transformed into the *A. tumefaciens* GV3101 strain and infiltrated into *N. benthamiana* leaves. The p19 protein was used to suppress gene silencing. Three days after infiltration, leaves were observed under Nikon A1R Spectral Confocal.

Histochemical staining

Phloroglucinol-HCl reagent was prepared by mixing 2 volumes of 2% (w/v) phloroglucinol in 95% (v/v) ethanol with 1 volume of concentrated HCl. Cross sections were stained for 1-2

minutes, washed twice with water and photographed immediately. The specimen was obtained from Leica VT1000 S Vibrating Blade Microtome. The microscope used is Nikon Fluorescence Microscope and the photographs were captured by Lumenera's INFINITY ANALYZE Software.

GUS staining

Freshly sectioned stem samples were transferred to staining solution (50 mM NaHPO4 buffer pH 7.2, 2 mM potassium ferricyanide, 2 mM potassium ferrocyanide, 2 mM X-glucuronide). Samples were placed at 37°C overnight. Next day, they were incubated 70% ethanol every two hours until visualization with a microscope.

Dual luciferase assay

Leaves from healthy 30-day-old *Arabidopsis* plants were cut into 0.5–1-mm strips with fresh razor blades. The leaf strips were put into an enzyme solution containing cellulase and macerozyme, then vacuum-infiltrated for 30 min, followed by digestion for 3 h without shaking in the dark. The protoplasts were filtered with nylon mesh, collected, and transformed by PEG-mediated transfection. To construct the effector constructs, coding sequences of HVA was inserted after the 35S promoter of P2GW7. To construct the reporter constructs, 1kb promoters of KNAT1 were cloned to the vector P2GWL7, which included the firefly luciferase reporter gene. Promoter activities are expressed as Firefly LUC/Renilla LUC activities, and normalized to the value obtained from protoplasts transformed with empty effector vector. The luciferase activity was detected by Dual-Luciferase® Reporter Assay System (Promega) and analyzed by GloMax® 96 Microplate Luminometer (Promega).

Transient Repressive Expression Assay

For effector plasmids, the coding sequences of *HVA*, *HVAΔEAR* and *HVAmtEAR* were first cloned into pGBKT7. Then the coding regions of BD fusion were amplified using specific primers and cloned into p2GW7 using LR Clonase II to yield effector plasmids. Transient expression assays were performed with Arabidopsis protoplasts. Each transformation used 5 μg of reporter plasmid and 4 μg of effector plasmid. For normalization of reporter gene activity, 0.5 μg of plasmid pRLC was used as an internal control. The luciferase activity was detected by

Dual-Luciferase® Reporter Assay System (Promega) and analyzed by GloMax® 96 Microplate Luminometer (Promega).

Gene	Sequence	Annotation
AT5G27880 Fw	CACCATGTCTTCTTCAATGTCTTCTGC	Gene Clone
AT5G27880 Re	TCAAAGGGATAAAGATAAATCAATTC	Gene Clone
AT5G27880 Fw XmaI	CACCCCCGGGATGTCTTCTTCAATGTCTTCTGC	Gene Clone
AT5G27880 Re SacI	GAGCTCTCAAAGGGATAAAGATAAATCAATTC	Gene Clone
gAT5G27880 2.4kb XmaI Fw	CACCCCCGGGACAACTGTAGTCAATCACAAGCTGTCTAAGT	Gene Clone
gAT5G27880 2.4kb SacI Re	GAGCTCCATGAATTTCCATTCTTATTGGATCTCC	Gene Clone
gAT5G278890 5.5kb XmaI Fw	CATCCCCCCGGGCACCAGGATTATTAGATGAATTTGAACAAGCC	Gene Clone
gAT5G278890 5.5kb Re	CATCCCGAGCTCTAAACGCTACTACTATTGTACCGCTCCGCAT	Gene Clone
AT5G27880 NdeI Fw	CACCCATATGTCTTCTTCAATGTCTTCTGCA	Gene Clone
AT5G27880 BamH I Re	GGATCCTCAAAGGGATAAAGATAAATCAATTCTC	Gene Clone
TPL NdeI Fw	CACCCATATGTCTTCTCTTAGTAGAGAGCTCGTTTTC	Gene Clone
TPL BamHI Re	GGATCCTCATCTCTGAGGCTGATCAGATG	Gene Clone
AT5G27880 no EAR BamHI Re	GGATCCTCAATCAATTCTCCCGCTTTTAGTTTTT	Gene Clone
AT5G27880 MT EAR BamHI Re	GGATCCTCATGCGGAAGCAGATGCATCAATTCTCCCGCTTTTAGTTTTT	Gene Clone
PrKNAT1 Fw	CACCGATCTAGAGCCCTAGGATTTGA	Gene Clone
PrKNAT1 Re	ACCCAGATGAGTAAAGATTTGAG	Gene Clone
TPL N176H Fw	AGGCTGAGGACTTTGATCCACCAGAGCTTAAATTGGCAA	Gene Clone
TPL N176H Re	TTGCCAATTTAAGCTCTGGTGGATCAAAGTCCTCAGCCT	Gene Clone
At5g27880 I miR-s	gaTATTGGTACTAGTGTTCCCTGtctctcttttgtattcc	Gene Clone
At5g27880 II miR-a	gaCAGGGAACACTAGTACCAATAtcaaagagaatcaatga	Gene Clone
At5g27880 III miR*s	gaCAAGGAACACTAGAACCAATTtcacaggtcgtgatatg	Gene Clone
miR319 Fw	CACCCTGCAAGGCGATTAAGTTGGGTAAC	Gene Clone
miR319 Fw	GCGGATAACAATTTCACACAGGAAACAG	Gene Clone
KNAT1-F1 BP qPCR	CCATTCAGGAAGCAATGGAGTT	RT-PCR
KNAT1-R1 BP qPCR	ACTCTTCCCATCAGGATTGTTGA	RT-PCR
BOP2 real time Fw	CGCCGTTGATCTTGCTCT	RT-PCR
BOP2 real time Re	CCATGCTTGCCAATTGTTT	RT-PCR
AT5G27889 NS Re	AAAAAGCCTCAATGTCTCCCA	RT-PCR
AT5G27880 Real Fw	TCAACCTCTCAAGCCTTAGGTGGT	RT-PCR
AT5G27880 Real Re	CAGCTTCCATCTCCTTCCGCTTTT	RT-PCR
AT5G27889 Real Fw	GGACCGTAGTTGGTTTGATTTG	RT-PCR
AT5G27889 Real Re	CTTCAATCGACAAACCGTCATTTA	RT-PCR
AT5G27890 Real Fw	GTCAATGTATCCGCCGTTGTA	RT-PCR
AT5G27890 Real Re	CTGAAAGTCGCGTCATCCTATC	RT-PCR
PIN1 Real time Fw	TCGTTGCTTCTTATGCCGTT	RT-PCR
PIN1 Real time Re	AGAAGAGTTATGGGCAACGC	RT-PCR
PIN2 Real time Fw	AATGCTGGTTGCTTTGCCTG	RT-PCR
PIN2 Real time Re	CCTTTGGGTCGTATCGCCTT	RT-PCR
YUC2 qRT Fw	CAAGGTGTATCCGGAGTTGA	RT-PCR
YUC2 qRT Re	AATGGCTGCACCAAGCAATC	RT-PCR
qYUC4-Fw	CCGTTCTTGATGTCGGTGCC	RT-PCR
qYUC4-Re	AAGGATTTATTGAAATGAAGATG	RT-PCR
qYUC6-Fw	GGTAGTTAAGCACACGTGTC	RT-PCR
qYUC6-Re	GGCTAGCGTGCCAACGTCGAG	RT-PCR
qYUC1-Fw	CGATGTCGGAGCTATGTCTC	RT-PCR
qYUC1-Re	CTGTACAAGTTTATTACTTCG	RT-PCR

Table 1: Primers used in this study.

Reference

Cano-Delgado, A., J. Y. Lee and T. Demura (2010). "Regulatory mechanisms for specification and patterning of plant vascular tissues." Annu Rev Cell Dev Biol **26**: 605-637.

Cano-Delgado, A., Y. Yin, C. Yu, D. Vafeados, S. Mora-Garcia, J. C. Cheng, K. H. Nam, J. Li and J. Chory (2004). "BRL1 and BRL3 are novel brassinosteroid receptors that function in vascular differentiation in *Arabidopsis*." Development **131**(21): 5341-5351.

Carlsbecker, A. and Y. Helariutta (2005). "Phloem and xylem specification: pieces of the puzzle emerge." Curr Opin Plant Biol **8**(5): 512-517.

Chad E Niederhuth, O. R. P. a. J. C. W. (2013). "Transcriptional profiling of the *Arabidopsis* abscission mutant hae *hsl2* by RNA-Seq." BMC Genomics. **14**(1):37

Cheng, Y., X. Dai and Y. Zhao (2006). "Auxin biosynthesis by the YUCCA flavin monooxygenases controls the formation of floral organs and vascular tissues in *Arabidopsis*." Genes Dev **20**(13): 1790-1799.

Choe S, N. T., Fujioka S, Takatsuto S, Tissier CP, Gregory BD, et al. (1999). "The *Arabidopsis dwf7/ste1* mutant is defective in the *delta7* sterol C-5 desaturation step leading to brassinosteroid biosynthesis." Plant Cell. **11**:207–221

Ciftci-Yilmaz, S. and R. Mittler (2008). "The zinc finger network of plants." Cell Mol Life Sci **65**(7-8): 1150-1160.

Denis, E., N. Kbiri, V. Mary, G. Claisse, E. S. N. Conde, M. Kreis and Y. Deveaux (2017). "WOX14 promotes bioactive gibberellin synthesis and vascular cell differentiation in *Arabidopsis*." Plant J **90**(3): 560-572.

Detlef Weigel, J. H. A., Miguel A. Bla´zquez, Justin O. Borevitz, Sioux K. Christensen, Christian Fankhauser, Cristina Ferra´ndiz, Igor Kardailsky, Elizabeth J. Malancharuvil, Michael M. Neff, Jasmine Thuy Nguyen, Shusei Sato, Zhi-Yong Wang, Yiji Xia, Richard A. Dixon, Maria J. Harrison, Chris J. Lamb, Martin F. Yanofsky, and Joanne Chory (2000). "Activation Tagging in *Arabidopsis*." Plant Physiol. 122: 1003–1013

Deyoung, B. J. and S. E. Clark (2008). "BAM receptors regulate stem cell specification and organ development through complex interactions with CLAVATA signaling." Genetics **180**(2): 895-904.

Dodsworth, S. (2009). "A diverse and intricate signalling network regulates stem cell fate in the shoot apical meristem." Dev Biol **336**(1): 1-9.

Edith Haritatos, R. M., Robert Turgeon (2000). "Minor vein structure and sugar transport in *Arabidopsis thaliana*." Planta. **211**(1):105-111

Elo, A., J. Immanen, K. Nieminen and Y. Helariutta (2009). "Stem cell function during plant vascular development." Semin Cell Dev Biol **20**(9): 1097-1106.

Englbrecht, C. C., H. Schoof and S. Bohm (2004). "Conservation, diversification and expansion of C2H2 zinc finger proteins in the *Arabidopsis thaliana* genome." BMC Genomics **5**(1): 39.

Espinosa-Ruiz, A., C. Martinez, M. de Lucas, N. Fabregas, N. Bosch, A. I. Cano-Delgado and S. Prat (2017). "TOPLESS mediates brassinosteroid control of shoot boundaries and root meristem development in *Arabidopsis thaliana*." Development **144**(9): 1619-1628.

Guo, Y., G. Qin, H. Gu and L. J. Qu (2009). "*Dof5.6/HCA2*, a Dof transcription factor gene, regulates interfascicular cambium formation and vascular tissue development in *Arabidopsis*." Plant Cell **21**(11): 3518-3534.

Ha, C. M., J. H. Jun, H. G. Nam and J. C. Fletcher (2007). "BLADE-ON-PETIOLE 1 and 2 control *Arabidopsis* lateral organ fate through regulation of LOB domain and adaxial-abaxial polarity genes." Plant Cell **19**(6): 1809-1825.

Hall, S. R. T. a. M. (2000). "The gapped xylem mutant identifies a common regulatory step in secondary cell wall deposition." The Plant Journal. **24**(4):477-488

Hannele Tuominen, L. P., Siegfried Fink, and Bjorn Sundberg (1997). "A Radial Concentration Gradient of Indole-3-Acetic Acid is Related to Secondary Xylem Development in Hybrid Aspen." Plant Physiol. **115**: 577-585

HeidiSzemenyei, M., JeffA.Long (2008). "TOPLESS Mediates Auxin-Dependent Transcriptional Repression During *Arabidopsis* Embryogenesis " Science. **319**(5868):1384-1386

Jouannet, V., K. Brackmann and T. Greb (2015). "(Pro)cambium formation and proliferation: two sides of the same coin?" Curr Opin Plant Biol **23**: 54-60.

Jürgens, D. W. a. G. (2002). "Stem cells that make stems." Nature. **415**(6873): 751–754

Kagale, S. and K. Rozwadowski (2014). "EAR motif-mediated transcriptional repression in plants." Epigenetics **6**(2): 141-146.

Kielbowicz-Matuk, A. (2012). "Involvement of plant C(2)H(2)-type zinc finger transcription factors in stress responses." Plant Sci **185-186**: 78-85.
Kondo, Y., T. Tamaki and H. Fukuda (2014). "Regulation of xylem cell fate." Front Plant Sci **5**: 315.
Liebsch, D., W. Sunaryo, M. Holmlund, M. Norberg, J. Zhang, H. C. Hall, H. Helizon, X. Jin, Y. Helariutta, O. Nilsson, A. Polle and U. Fischer (2014). "Class I KNOX transcription factors promote differentiation of cambial derivatives into xylem fibers in the Arabidopsis hypocotyl." Development **141**(22): 4311-4319.
LongJ, M. E., MedfordJ,Barton M. (1996). "A memberof the KNOTTED class of homeodomainproteins encoded by the STM gene of Arabidopsis." Nature. **379**(6560):66-69
MacDaniels, A. J. E. a. (1947). "An Introduction To Plant Anatomy." New York, NY: MacGraw-Hill Book Company, Inc.
Mansfield, S. G. and L. G. Briarty (1991). "Early embryogenesis in Arabidopsis thaliana. II. The developing embryo." Canadian journal of botany. **69**(3): 461-476.
Marta Iban˜ es, N. F. b., Joanne Choryc, and Ana I. Can˜ o-Delgado (2010). "Brassinosteroid signaling and auxin transport are required to establish the periodic pattern of Arabidopsis shoot vascular bundles." Proceedings of the National Academy of Sciences, 106 (32) 13630-13635
Miyashima, S., J. Sebastian, J. Y. Lee and Y. Helariutta (2013). "Stem cell function during plant vascular development." EMBO J **32(**2): 178-193.
Nakamura, A., S. Fujioka, H. Sunohara, N. Kamiya, Z. Hong, Y. Inukai, K. Miura, S. Takatsuto, S. Yoshida, M. Ueguchi-Tanaka, Y. Hasegawa, H. Kitano and M. Matsuoka (2006). "The role of OsBRI1 and its homologous genes, OsBRL1 and OsBRL3, in rice." Plant Physiol **140**(2): 580-590.
Norma Fàbregas, M. I., and Ana I. Caño-Delgado (2010). "A systems biology approach to dissect the contribution of brassinosteroid and auxin hormones to vascular patterning in the shoot of Arabidopsis thaliana." Plant Signal Behav. **5(**7): 903–906
Ohashi-Ito, K. and H. Fukuda (2014). "Xylem." Curr Biol **24(**24): R1149.
Ohashi-Ito, K., K. Iwamoto and H. Fukuda (2018). "LOB DOMAIN-CONTAINING PROTEIN 15 Positively Regulates Expression of VND7, a Master Regulator of Tracheary Elements." Plant Cell Physiol **59(**5): 989-996.

Ohta, M., Matsui, K., Hiratsu, K., Shinshi, H. and Ohme-Takagi, M. (2001). "Repression Domains of Class II ERF Transcriptional Repressors Share an Essential Motif for Active Repression." Plant Cell. **13**(8):1959-1968

Osmont, K. S. and C. S. Hardtke (2008). "The topless plant developmental phenotype explained!" Genome Biol **9**(4): 219.

Parker, G. (2003). "Isolation of COV1, a gene involved in the regulation of vascular patterning in the stem of Arabidopsis." Development **130**(10): 2139-2148.

Pauwels, L., G. F. Barbero, J. Geerinck, S. Tilleman, W. Grunewald, A. C. Perez, J. M. Chico, R. V. Bossche, J. Sewell, E. Gil, G. Garcia-Casado, E. Witters, D. Inze, J. A. Long, G. De Jaeger, R. Solano and A. Goossens (2010). "NINJA connects the co-repressor TOPLESS to jasmonate signalling." Nature **464**(7289): 788-791.

Pineau, C., A. Freydier, P. Ranocha, A. Jauneau, S. Turner, G. Lemonnier, J. P. Renou, P. Tarkowski, G. Sandberg, L. Jouanin, B. Sundberg, A. M. Boudet, D. Goffner and M. Pichon (2005). "*hca*: an Arabidopsis mutant exhibiting unusual cambial activity and altered vascular patterning." Plant J **44**(2): 271-289.

Ruzicka, K., R. Ursache, J. Hejatko and Y. Helariutta (2015). "Xylem development - from the cradle to the grave." New Phytol **207**(3): 519-535.

Scheres, B. (2007). "Stem-cell niches: nursery rhymes across kingdoms." Nat Rev Mol Cell Biol **8**(5): 345-354.

Schuetz, M., R. Smith and B. Ellis (2013). "Xylem tissue specification, patterning, and differentiation mechanisms." J Exp Bot **64**(1): 11-31.

Spicer, R. and A. Groover (2010). "Evolution of development of vascular cambia and secondary growth." New Phytol **186**(3): 577-592.

ten Hove, C. A., K. J. Lu and D. Weijers (2015). "Building a plant: cell fate specification in the early Arabidopsis embryo." Development **142**(3): 420-430.

Turner, S. and L. E. Sieburth (2003). "Vascular patterning." Arabidopsis Book **2**: e0073.

Ulrike Brand, J. C. F., Martin Hobe, Elliot M. Meyerowitz, Ru¨diger Simon (2000). "Dependence of Stem Cell Fate in Arabidopsis on a Feedback Loop Regulated by CLV3 Activity." Science. **289**(5479):617-619

Wang, H., U. Avci, J. Nakashima, M. G. Hahn, F. Chen and R. A. Dixon (2010). "Mutation of WRKY transcription factors initiates pith secondary wall formation and increases stem biomass

in dicotyledonous plants." Proceedings of the National Academy of Sciences, **107**(51): 22338-22343.

Ye, Z. H. (2002). "Vascular tissue differentiation and pattern formation in plants." Annu Rev Plant Biol **53**: 183-202.

Zhenghua Ye, J. E. V. (1994). "Expression of an auxin- and cytokinin-regulated gene in cambial region in *Zinnia*." Proceedings of the National Academy of Sciences, **91** (14) 6539-6543.

Zhong, R. and Z. H. Ye (2015). "Secondary cell walls: biosynthesis, patterned deposition and transcriptional regulation." Plant Cell Physiol **56**(2): 195-214.

Chapter 2 Activation of *miR165b* represses *AtHB15* expression and induces pith secondary wall development in *Arabidopsis*

Abstract

Secondary cell-wall thickening takes place in sclerenchyma cells, but not in surrounding parenchyma cells. The molecular mechanism of switching on and off secondary wall synthesis in various cell types is still elusive. Here, we identified a dominant mutant *stp–2d* showing secondary wall thickening in pith cells (STP). Immunohistochemistry assays confirmed accumulation of secondary cell walls in the pith cells of the *stp–2d* mutant. Activation of microRNA 165b (*miR165b*) expression is responsible for the STP phenotype, as demonstrated by transgenic over-expression experiments. The expression of three class III HD–ZIP transcription factor genes, including *AtHB15*, was repressed in the *stp–2d* mutant. Transgenic overexpression of a mutant form of *AtHB15* that is resistant to *miR165*-mediated cleavage reversed the *stp–2d* mutant phenotype to wild-type, indicating that *AtHB15* represses secondary wall development in pith. Characterization of two *athb15* mutant alleles further confirmed that functional AtHB15 is necessary for retaining primary walls in parenchyma pith cells. Expression analyses of cell-wall synthetic genes and wall-related transcription factors indicated that a transcriptional pathway is involved in AtHB15 function. These results provide insight into the molecular mechanism of secondary cell-wall development.

Introduction

Plant cells may develop two categories of cell walls, primary walls and secondary walls, depending on cell types and developmental stages (Carpita and Gibeaut, 1993; Zhong and Ye, 2007a). In stem tissues, sclerenchyma cells develop secondarily thickened walls, while epidermis, cortex and pith cells develop thin primary walls (Demura and Fukuda, 2007). Secondary cell walls are important for plants, providing mechanical strength and facilitating water and nutrient transport (Wang and Dixon, 2012). Secondary cell walls also provide fibers and timber for human use, and serve as a major source of renewable biomass feedstock for biofuel production (Carroll and Somerville, 2009; Pauly and Keegstra, 2010). Ectopic accumulation of secondary walls in ground tissues increases biomass density (Wang et al., 2010; Hines, 2011), but how plant cells turn secondary wall development on and off in different cell types is still poorly understood. Secondary cell walls are mainly composed of cellulose, hemicelluloses and lignin. The synthesis of these three components is highly coordinated and regulated by transcriptional networks (Demura and Fukuda, 2007; Zhong and Ye, 2007a; Wang and Dixon, 2012). Several closely related NAM, ATAF1/2 and CUC2 domain transcription factors (NACs) act as the first layer of master regulators of secondary wall biosynthesis; these are NST1 (NAC secondary wall thickening promoting factor 1), NST2 and NST3/ SND1 (secondary wall-associated NAC domain protein 1) (Mitsuda et al., 2005, 2007; Zhong et al., 2006). Interestingly, the function of NAC master regulators is conserved in various plant species (Zhao et al., 2010; Wang et al., 2011; Lin et al., 2013; Valdivia et al., 2013; Grover et al., 2014). MYB domain transcription factors also serve as master regulators, but many operate downstream of the NACs (Zhong et al., 2007; Ko et al., 2009; McCarthy et al., 2009; Zhou et al., 2009; Bhargava et al., 2010). Further downstream of the regulatory pathway are many other

transcription factors that may directly interact with biosynthetic genes of cellulose, lignin and xylan (Zhong et al., 2008; Ko et al., 2009; Bhargava et al., 2010). The aforementioned transcription factors form hierarchical and non-hierarchical regulatory networks to coordinate the biosynthesis of secondary walls (Demura and Fukuda, 2007; Wang and Dixon, 2012; Zhong and Ye, 2014).

The NAC master regulators of secondary wall development are further regulated by upstream factors. In *Arabidopsis*, mutation of *MYB26* resulted in male sterility due to defects in anther dehiscence (Steiner-Lange et al., 2003). Functional analysis indicated that MYB26 is a positive regulator of *NST1* and *NST2*, activating endothecium secondary wall formation (Yang et al., 2007). Negative regulation has also been reported to control NAC master regulators. Loss of function of *WRKY12* resulted in secondary cell-wall thickening in pith cells (Wang et al., 2010). WRKY12 negatively regulates the expression of *NST2* and the zinc-finger transcription factors encoded by *AtC3H14* and *AtC3H14L*, and represses cell-wall biosynthetic genes in pith cells (Ko et al., 2009; Wang et al., 2010; Kim et al., 2014). Orthologs of *WRKY12* were found to have similar functions in wall development in monocotyledonous grass species (Yu et al., 2013). Thus the NAC master regulators play a critical role in switching on and off secondary wall biosynthesis.

Five class III homeodomain leucine zipper (HD–ZIP) transcription factors, encoded by *AtHB15/CORONA (CNA)*, *PHABULOSA (PHB)*, *PHAVOLUTA (PHV)*, *REVOLUTA/INTERFASCICULAR FIBRELESS (REV/IFL)* and *AtHB8*, play critical roles in xylem tissue formation, as well as in organ polarity and meristem formation (Emery et al., 2003; Prigge et al., 2005; Schuetz et al., 2013). *AtHB15* and its *Zinnia elegans* counterpart *ZeHB13* are expressed in procambium and regulate early vascular development (Ohashi-Ito and Fukuda,

2003). The expression of *ATHB8/ZeHB10* coincides with the location of tracheary element precursors, and affects vascular cell differentiation (Baima et al., 2001; Ohashi-Ito et al., 2005). *REV/ZeHB12* promotes the development of procambium and xylem parenchyma cells (Emery et al., 2003; Zhong and Ye, 2004; Ohashi-Ito et al., 2005). A triple loss-of-function mutant (*rev phb phv*) showed an amphicribral radial pattern of tissue development/differentiation, where the phloem surrounds the xylem (Emery et al., 2003), while *phb phv* can shows an extra amphivasal bundle in the pith, where the xylem surrounds the phloem (Prigge et al., 2005). These results indicate that the five class III HD–ZIP factors have overlapping but sometimes antagonistic functions in xylem differentiation.

The class III HD–ZIP genes are post-transcriptionally regulated by the microRNAs *miR165* and *miR166* (Kim et al., 2005; Williams et al., 2005; Zhou et al., 2007; Carlsbecker et al., 2010). Activation tagging of *miR166a* resulted in mRNA cleavage of *PHB*, *PHV* and *AtHB15*, and hence enlargement of the shoot apical meristem and enhancement of vascular cell differentiation (Kim et al., 2005). Similar phenotypes were also observed in a *miR166g* activation-tagged mutant (Williams et al., 2005). There are two *miR165* genes in the *Arabidopsis* genome, *miR165a* and *miR165b*. To date, no activation-tagged mutant of *miR165* has been described. Transgenic over-expression of *miR165a* caused an approximately five-fold reduction in expression of all five class III HD–ZIP genes (Zhou et al., 2007). The phenotypes of the *miR165a* over-expression lines include loss of the shoot apical meristem, altered organ polarity and impaired interfascicular fiber development.

Here, we report that activation tagging of *miR165b* results in secondary cell-wall development in the pith cells. We found that activation of *miR165b* reduced the transcript levels of *PHB*, *PHV* and *AtHB15*, but *AtHB8* and *REV* expression were not significantly changed. Transgenic analysis

and knockout mutant characterization confirmed that *AtHB15* is mainly responsible for the pith secondary wall development. Expression analyses indicated that the secondary wall-related transcriptional network was affected by *AtHB15*. These results provide evidence that *miR165b* plays important roles in the regulation of pith cell-wall identity.

Results

Identification of the *stp–2d* mutant in *Arabidopsis*

Mutant plants with secondary wall thickening in pith cells (STP) have been reported in *Medicago truncatula* (*mtstp1*) and in *Arabidopsis* (Wang et al., 2010; Wang and Dixon, 2012). These plants accumulate more biomass per plant than the wild-type, and provide research models for optimizing biomass feedstocks (Hines, 2011). To identify novel regulators of pith cell wall development, we screened an activation-tagged population in *Arabidopsis* using UV microscopy. Cross-sections of stem tissues were prepared from 5-week-old mutant plants using a vibrotome, and observed under a fluorescence microscope. Secondarily thickened cell walls are lignified and show blue autofluorescence under UV light. A semi-dominant mutant showing the STP phenotype was identified by screening of 10,419 mutant plants, and we named this mutant *stp–2d*. Pith cells of heterozygous (*stp–2d/+*) mutant plants started lignifying from peripheral regions next to the fascicular and interfascicular fibers, and the lignified zone gradually extended further toward the pith center as plants got older. Examination of cross-sections from the stem base of 6-week-old plants showed that all pith cells were parenchyma cells in wild type plants (Figure 22a), but the pith cell walls were lignified in the heterozygous and homozygous *stp* plants (Figure 22b,c). An extra amphivasal vascular bundle was observed in the pith region of the

homozygous plants, but not in the heterozygous plants. Phloroglucinol staining confirmed the ectopic lignification phenotypes observed by UV microscopy (Figure 22d–f).

Plant growth was negatively affected in the mutant lines. Three-week-old mutant plants, especially the homozygotes, were noticeably smaller than the wild-type (Figure 22g–i). The mutant leaves were small with short petioles (Figure 22h, i). Mature mutant plants were dwarf, and developed shorter and fewer siliques compared to the wild-type (Figure 22j). The stem diameter was significantly smaller in the mutant lines compared to the wild-type (Figure 22a–f).

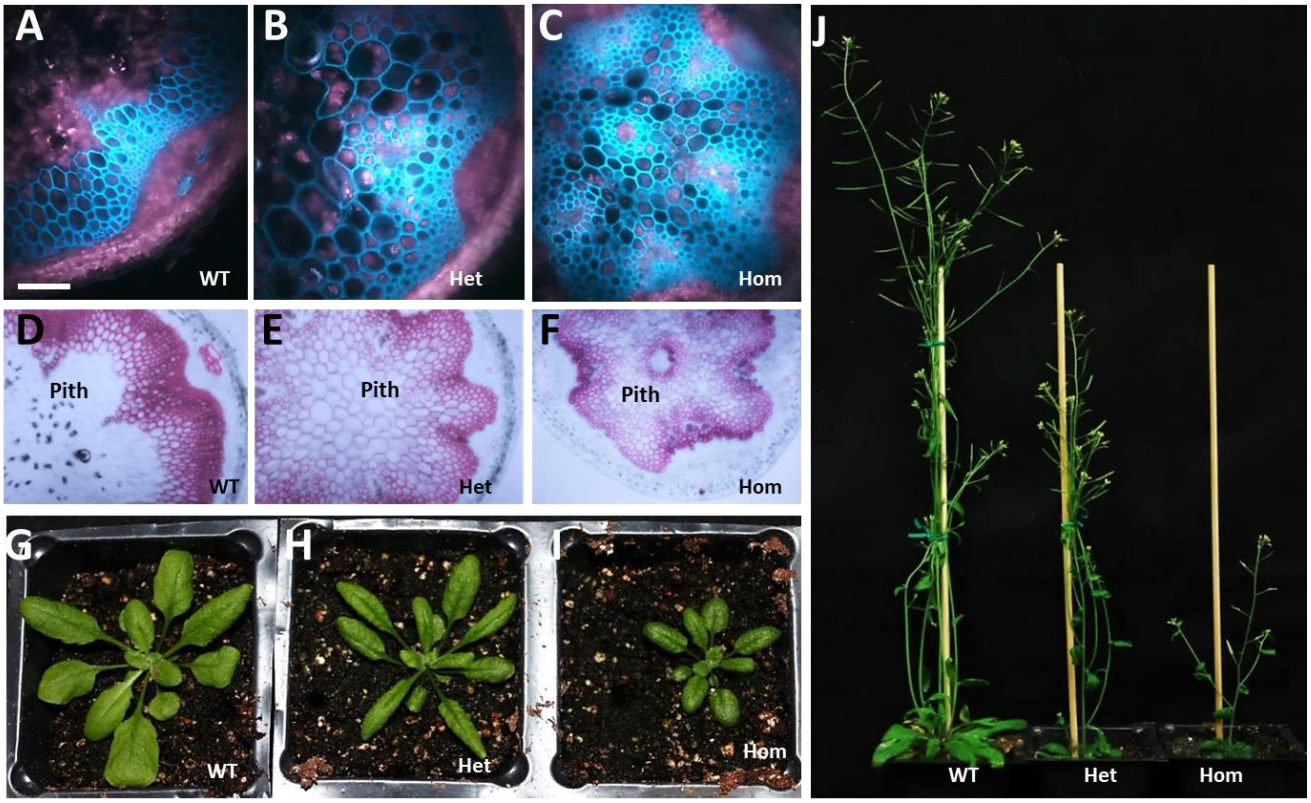

Figure 22. Identification of the *stp–2d* mutant showed ectopic lignification in pith and growth defect.

(a–f) Characterization of stem cross-sections by UV microscopy (a–c) and phloroglucinol staining (d–f), showing that pith cells are lignified in *stp–2d* mutant plants. An amphivasal bundle was observed in the pith region of the homozygous *stp–2d* mutant (c) and (f). Scale bars = 100 um. (g–j) Growth of 21-day-old plants (g–i) and 35-day-old plants (j). The heterozygous (Het) and homozygous (Hom) mutant plants are smaller in size and shorter in height compared to the wild-type plants (WT).

Lignin is one of the three major components of secondary cell walls. To determine whether the ectopically lignified pith cells of *stp–2d* mutants also accumulated cellulose and xylan (the main hemicellulose in *Arabidopsis*), we characterized the stem cross-sections using histochemical approaches. To characterize cellulose accumulation, we performed Calcofluor-white staining and histochemistry using a carbohydrate-binding module (CBM3a) that binds crystalline cellulose. The pith cells of *stp–2d* mutant plants accumulated cellulose in a pattern that was indistinguishable from the fiber cells of the vascular bundles and interfascicular tissues (Figure 23a, b, white arrows). The accumulation of xylan in the mutant pith cells was demonstrated by an immunohistochemical approach using a xylan-specific monoclonal antibody CCRC–M149 (Pattathil et al., 2010) that recognizes the unmodified xylan backbone (Schmidt et al., 2015) (Figure 23c). The results confirmed significant xylan accumulation in pith cells of the *stp–2d* mutant. We localized pectic polysaccharides using CCRC– M38, a monoclonal antibody that binds to de-esterified homogalacturonan (Pattathil et al., 2010), which is abundant in parenchyma cells. The results indicate that pith cells of the mutant lines show lower binding intensity compared to those of the wild-type, in which pith cells are equally as well stained as the parenchyma epidermal and cortical cells (Figure 23d). To investigate whether the pith cell walls are secondarily thickened in the mutant lines, we characterized the pith walls by transmission electric microscopy. The results clearly show wall thickening in the heterozygous and homozygous *stp–2d* mutant lines (Figure 24). These results indicate that pith cells of the *stp–2d* mutant plants develop secondary cell walls similar to the sclerenchyma cells in the fascicular and interfascicular tissues.

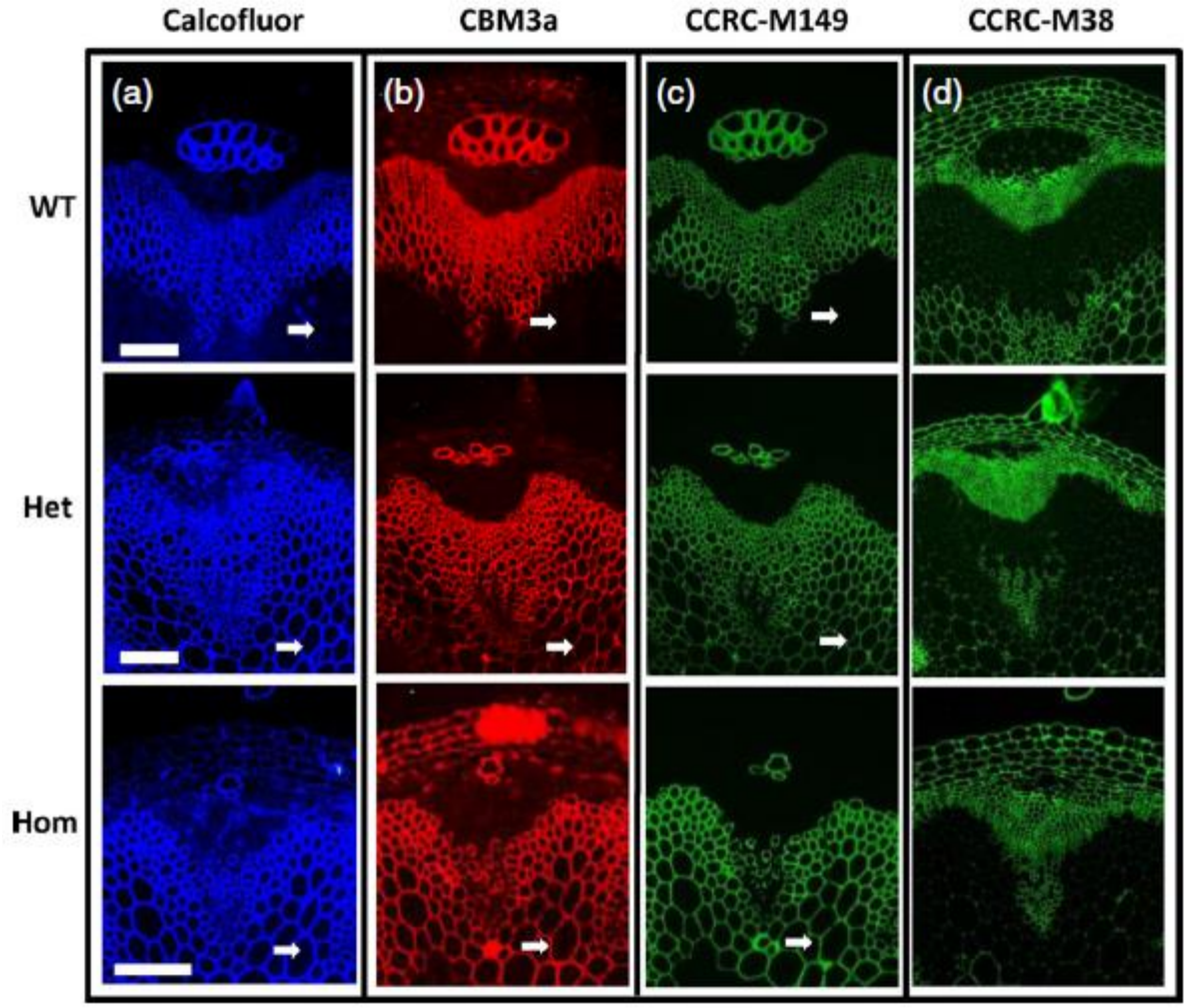

Figure 23. Cellulose and xylan accumulation in the pith cells of *stp–2d* mutant.

(a,b) Detection of cellulose by Calcofluor-white staining (a) and labeling with CBM3a, a carbohydrate-binding module that binds crystalline cellulose (b). (c) Detection of xylan by immunohistochemistry using monoclonal antibody CCRC–M149. (d) Detection of de-esterified homogalacturonan, a pectic polysaccharide typically found in primary cell walls, using CCRC–M38. The pith cells of the *stp–2d* mutant accumulate cellulose and xylan similar to the fascicular and interfascicular fibers, indicating secondary cell-wall development. White arrows indicate pith cells that show positive signals for cellulose or xylan in the mutant line, but not in the wild-type plants. Scale bars = 100 um; these apply to all images.

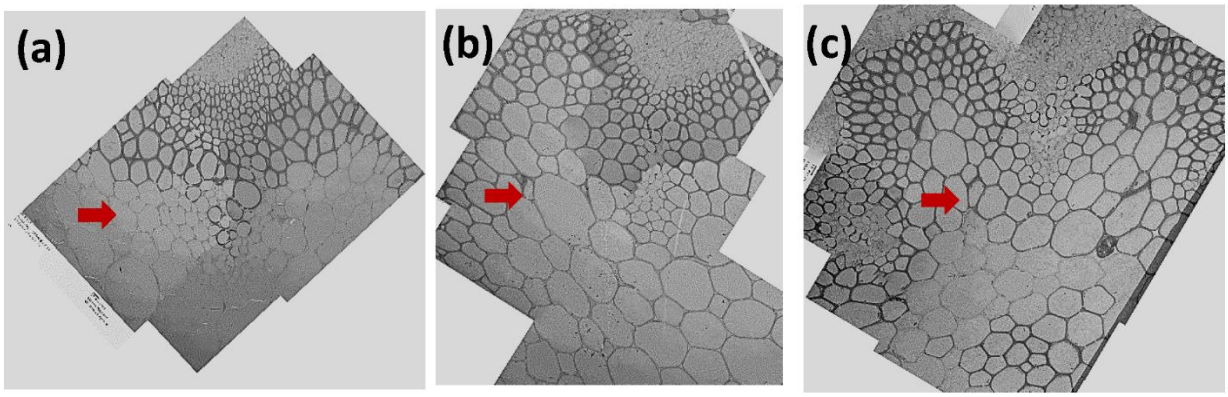

Figure 24. Transmission electron microscopy (TEM) analysis indicates that the pith cells of *stp-2d* mutants are secondarily thickened.

(a) to (c) TEM images of cross sections of wild type (a) heterozygotous *stp-2d/+* (b) and *stp-2d* (c) showing secondary thickening of pith cell walls in the mutant lines. Red arrows indicate pith cells. All images are taken at the same magnification.

The STP phenotype in the *stp–2d* mutant results from activation of *miR165b*

The *stp–2d* mutant was identified from an activation-tagged mutant population and showed a semi-dominant phenotype, indicating that the mutant phenotype may be caused by a T–DNA insertion harboring an activation tag. To identify the T–DNA insertion locus, we performed TAIL-PCR and subsequent sequencing. The results indicated that a T–DNA was located 1219 bp upstream of the *miR165b* gene on chromosome 4 (Figure 25a). To investigate whether the T–DNA insertion co-segregates with the STP phenotype, we determined the genotypes of individuals from a segregating population. PCR-based genotyping indicated that the segregation ratio of wild-type, heterozygous and homozygous mutants was 60:145:78 (P = 0.29) in a population of 283 plants, which fits Mendelian ratios and suggest that this T–DNA insertion may be responsible for the *stp–2d* phenotype. Activation tagging of the microRNAs *miR166a* and *miR166g* located on chromosomes 2 and 5, respectively, has been reported previously (Kim et al., 2005; Williams et al., 2005). The mature microRNA sequence of *miR166a* and *miR166g* is the same, and differs from that of *miR165a/b* only at the 17th nucleotide (U instead of C). Phenotypes of the *miR166* activation-tagged mutants included fasciated inflorescence stems and enlarged shoot apical meristems, which were not observed in the *stp–2d* mutant lines. The phenotype common to all three lines was the presence of ectopic amphivasal vascular bundle(s) in the pith region. Activation tagging of *miR165b* resulted in a previously undescribed phenotype of secondary cell-wall development in pith cells.

To determine whether expression of *miR165b* was increased because of activation tagging, we performed a Northern blot analysis. RNA samples prepared from seedlings and stem tissues were used for this experiment. We found that mature *miR165b* was significantly up-regulated in heterozygous and homozygous mutant plants (Figure 25b). Real-time RT–PCR analysis further

confirmed that expression of the *pre-miR165b* transcripts was highly upregulated in the mutant lines compared to the wildtype (Figure 26). This result also indicated that real-time RT–PCR may be used as an accurate estimation of the expression level of mature *miR165b*. The *miR165/166* microRNAs have been implicated in xylem development, indicating that *miR165b* may control the pith phenotype in the mutant plants.

Class III HD–ZIP transcription factors are known to be post-transcriptionally regulated by *miR165/166* members (McConnell et al., 2001; Zhong and Ye, 2004; Kim et al., 2005; Williams et al., 2005; Carlsbecker et al., 2010; Miyashima et al., 2011). Therefore, we performed real-time RT– PCR analyses to determine whether the transcript level of these HD–ZIP genes was affected in *stp–2d* mutants. As shown in Figure 25(c), the expression of *ATHB15*, *PHB* and *PHV* was significantly down-regulated, while that of *REV* was only slightly lower than in the wild-type, and *ATHB8* expression was not affected. These results confirm that activation of *miR165b* negatively regulates three class III HD–ZIP transcription factors.

To characterize the expression of *miR165b* in various tissues of wild-type plants, we performed a real-time RT–PCR analysis. We found that *miR165b* is highly expressed in roots, leaves and young stems, but expression is low in flowers, siliques and old stems (Figure 25d). The expression of *miR165b* in root tissues was consistent with previous research using a promoter:GUS line (Jung and Park, 2007). Because *miR165/166* and class III HD–ZIP genes are important for root development (Carlsbecker et al., 2010), we reasoned that activation of *miR165b* in the *stp–2d* mutant may affect root growth. To check this hypothesis, we characterized root growth of seedlings growing on vertical plates. The root length of 7-day-old *stp–2d* mutant seedlings was significantly longer than that of wild-type roots (Figure 25e, f). Longer roots were observed in *phb phv* double mutant plants (Dello Ioio et al., 2012). Therefore,

the enhanced root growth of *stp–2d* may be due to down-regulated expression of *PHB* and *PHV* genes. These results indicate that activation tagging of *miR165b* affects both stem and root development in *Arabidopsis*.

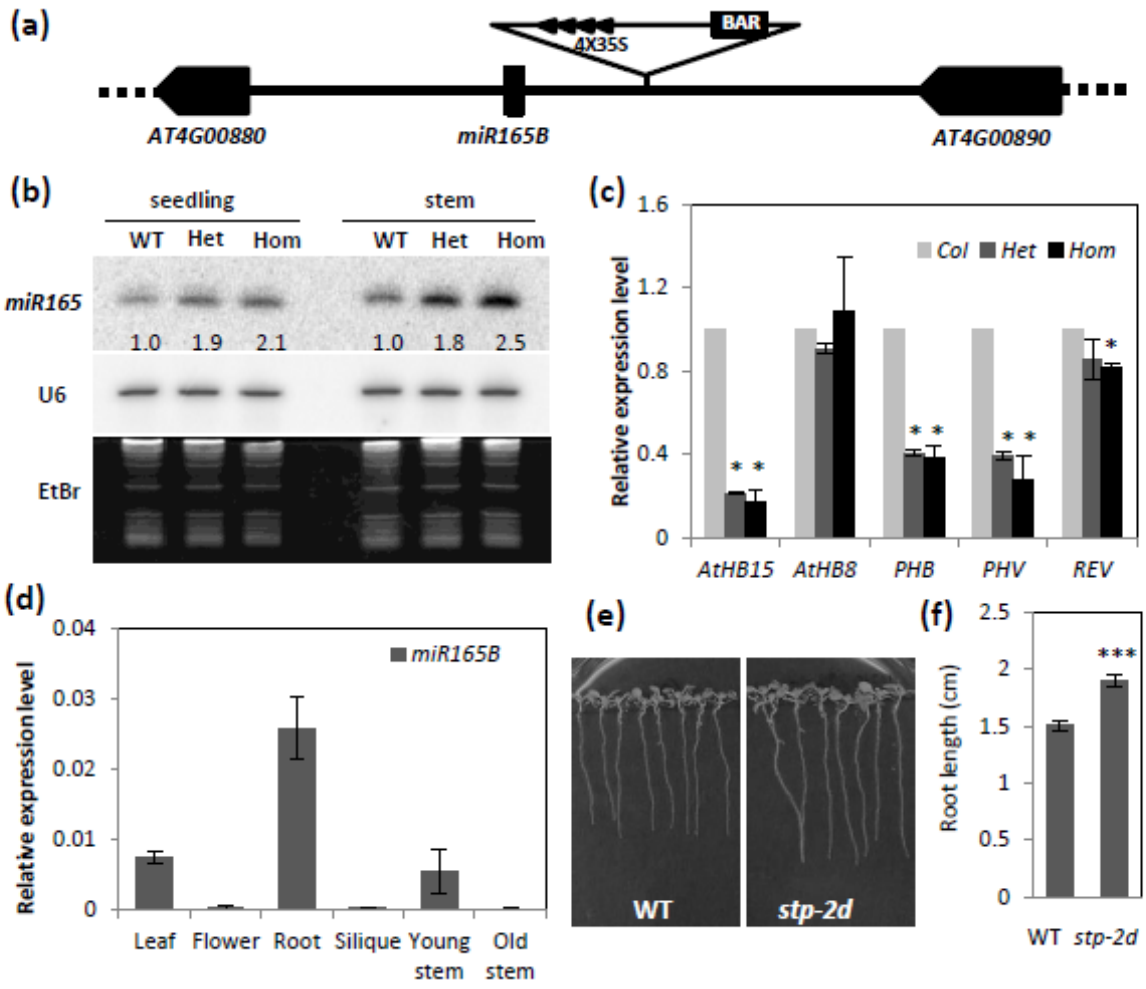

Figure 25. Activation of *miR165b* represses the expression of three HD–ZIP genes in the *stp–2d* mutant.

(a) Schematic diagram showing the activation tag insertion close to the *miR165* genomic sequence. The triangle indicates the T–DNA, with the 4×35S activation tag on the right border and *BAR* (Basta resistant gene) on the left border. The blocks indicate genes, and lines indicate intergenic regions. (b) Northern blot analysis of mature *miR165* accumulation in seedlings and stem tissues in the wild-type (WT), heterozygotes (Het) and homozygotes (Hom). Numbers under the *miR165* gel blot indicate the fold changes compared to wild-type. Expression of the U6 small nuclear RNA gene was used for normalization. (c) Expression of *AtHB15*, *PHABULOSA* (*PHB*, *ATHB9*) and *PHAVOLUTA* (*PHV*, *ATHB14*) is repressed in the *stp–2d* mutant. Values are means ±SD of three biological replicates. Asterisks (*) indicate a statistically significant

difference by Student's t test ($P < 0.5$). (d) Real-time RT–PCR analysis of the expression abundance of *pre-miR165b* in various tissues of wild-type plants. Young stem represents top half of inflorescence stem, and old stem represents bottom part of stem. The number represented in Y axis were calculated from delta Ct. Values are means ±SD of three biological replicates. (e) Root growth of wild-type and *stp-2d* seedlings on half-strength MS medium. (f) Root length measurement for WT and the *stp-2d* mutant. Values are means ±SE for $\geqslant$ 30 seedlings of both genotypes. Asterisks (***) indicate a statistically extremely significant difference by Student's t test ($P < 0.0001$).

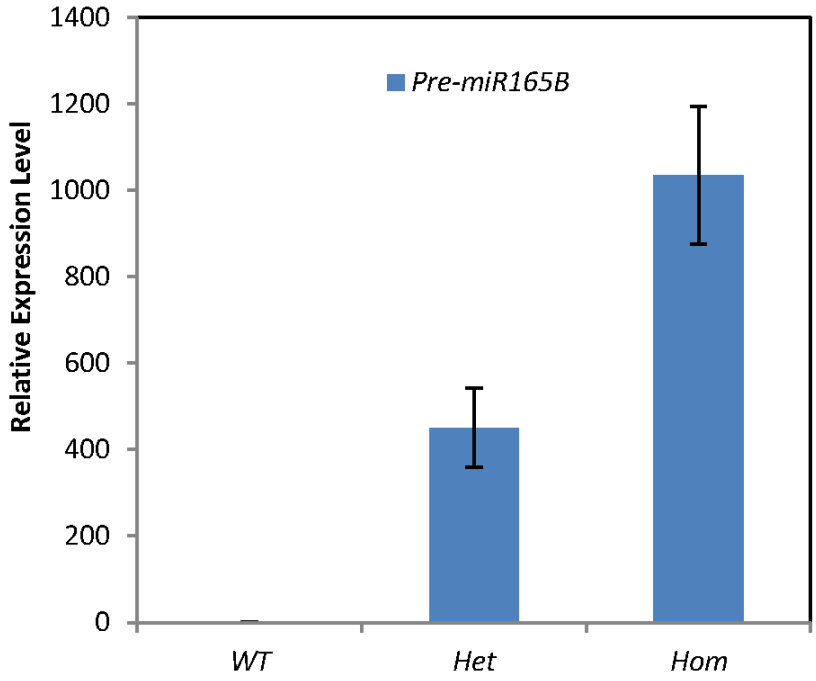

Figure 26. Real-time PCR analysis showed over-expression of *pre-miR165b* in the *stp-2d* mutant stem tissues compared with wild type.

Expression of an ubiquitin (*UBQ5*) gene was used as reference. Values are means ±SD of three biological replicates.

Over-expression of *miR165b* mimics the *stp–2d* phenotype

To further investigate whether activation of *miR165b* is responsible for the STP phenotype in the *stp–2d* mutant, we performed transgenic analyses. We over-expressed *miR165b* in the wild-type background driven by a CaMV 35S promoter. A 0.7 kb DNA fragment including the stem-loop sequence of *miR165b*, together with 250 bp sequences upstream and downstream of *miR165b*, was cloned by PCR using high-fidelity polymerase. The cloned fragment was sub-cloned into binary vector pK2GW7, and transformed into Agrobacterium for plant transformation. Two independent transgenic lines were selected for detailed characterization. We first examined stem cross-sections from transgenic lines using phloroglucinol staining. The pith cells were significantly more lignified compared to the wild-type, suggesting ectopic secondary thickening of pith walls in these lines (Figure 27a). We confirmed the over-expression of *miR165b* using real-time RT– PCR analysis (Figure 27b). The over-expression lines were dwarf compared with wild-type plants (Figure 27c). These results indicate that over-expression of *miR165b* driven by the 35S promoter mimicked the STP phenotype of the *stp–2d* mutant. Because *AtHB15* is repressed in the *stp–2d* mutant line, we reasoned that over-expression of *miR165b* should also affect *AtHB15* transcript levels. Indeed, real-time RT–PCR analysis confirmed that expression of *AtHB15* was significantly repressed in the three independent *miR165b* over-expression lines (Figure 27d). We also observed that some over-expression plants showed curly, wavy and sometimes very tiny leaves (Figure 28), which were not observed in the *stp–2d* mutants, indicating that the effects of over-expression of *miR165b* driven by the 35S promoter were somehow different from those of activation tagging.

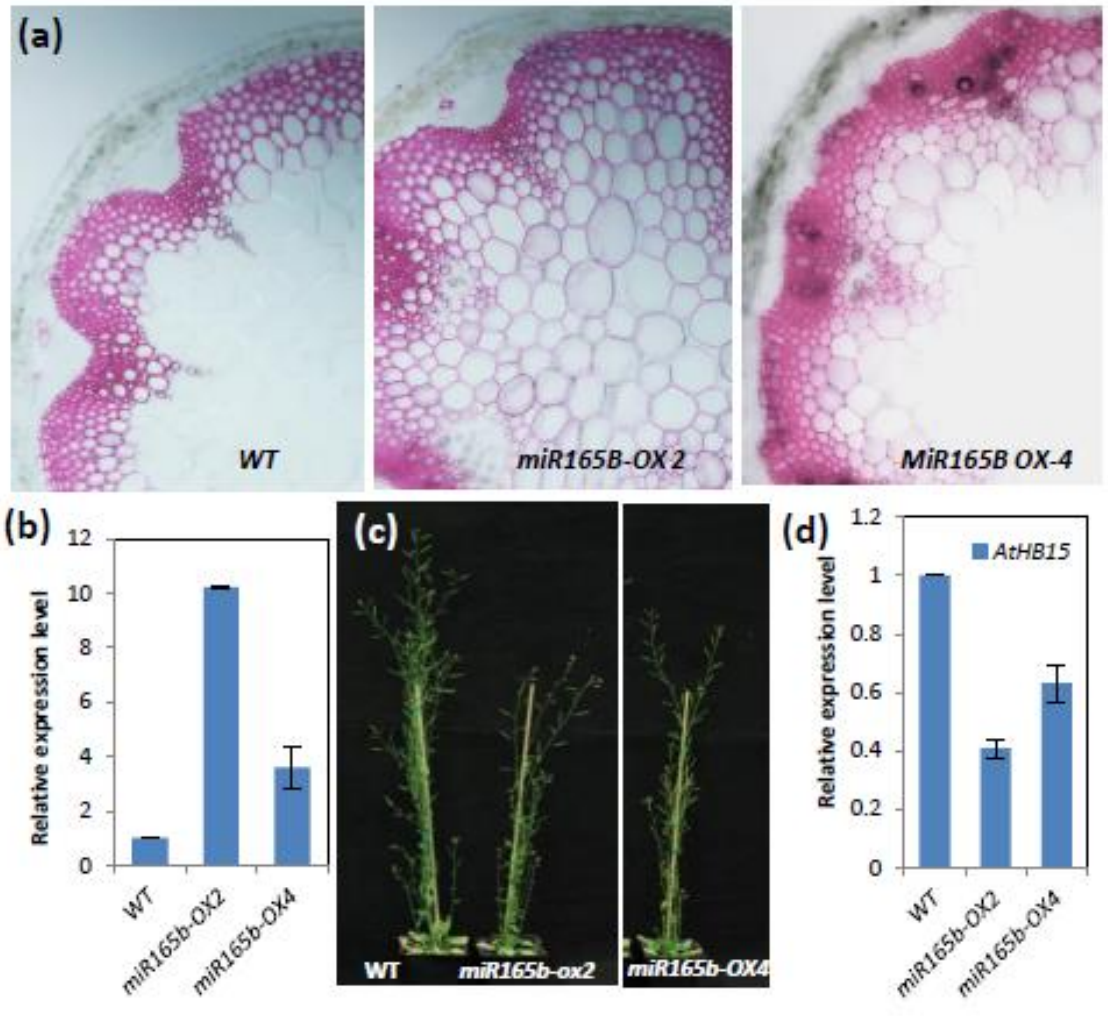

Figure 27. Over-expression of *miR165b* under the control of the CaMV 35S promoter results in secondary wall thickening in pith cells.

(a) Phloroglucinol staining of stem cross-sections showing lignification of pith cells in the *miR165b* over-expression lines. (b) Real-time RT–PCR analysis of *miR165b* expression in two independent *35S::miR165b* transgenic lines. Values are means ±SD of three biological replicates. (c) The growth phenotype of *miR165b* over-expressing plants. The transgenic lines are dwarf compared to the wild-type plants. (d) Real-time analysis of the expression of *AtHB15* in the *miR165b* over-expression lines. Values are means ±SD of three biological replicates.

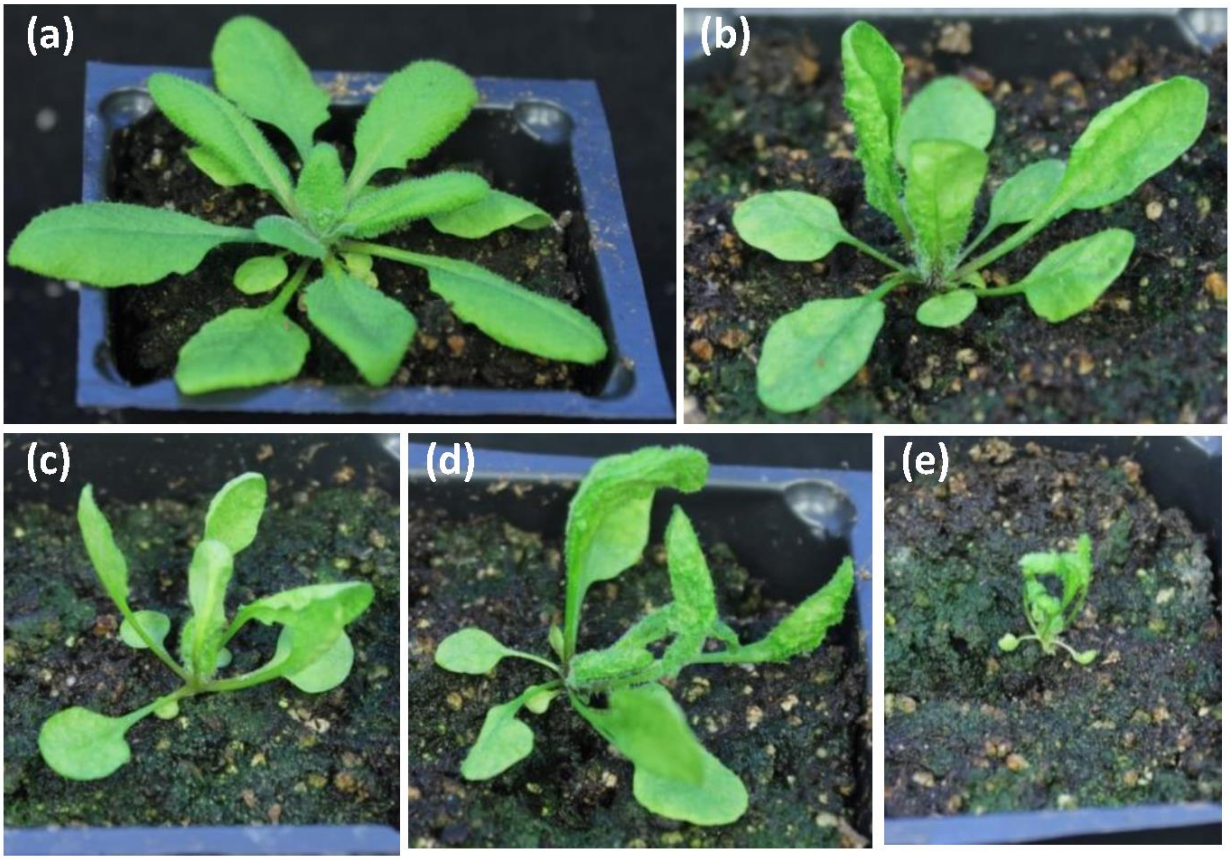

Figure 28. Overexpression of *miR165b* results in curled leaf phenotypes.

(a) two-week-old wild type plants. (b) to (e) Transgenic plants overexpressing *miR165b* showing curled leaf phenotypes with varied severity.

Over-expression of mutated *AtHB15* reverts the *stp–2d* phenotype to wild-type

The transcript levels of *AtHB15*, *PHB* and *PHV* were all lower in the *stp–2d* stem tissue compared to wild-type, with the *AtHB15* transcript level being reduced the most (Figure 25c). Expression analysis using real-time RT–PCR indicated that *ATHB15* is highly expressed in stem tissues, to a level almost three times higher than expression in root tissues (Figure 29a). Although *PHB* and *PHV* were also expressed in stem tissues (Figure 30), their expression levels were much lower than those of *ATHB15*. We reasoned that *ATHB15* may play a major role in controlling the STP phenotype in the *stp–2d* mutant. To test our hypothesis, we mutated the microRNA binding site on the *AtHB15* cDNA (*mATHB15*) using base substitutions that did not change the amino acid coding (Figure 29b). These mutations are known to be resistant to miR166a cleavage (Kim et al., 2005). The *mATHB15* over-expression construct driven by a 35S promoter was transformed into the *stp–2d* background. Sixty-six positive transgenic T0 plants were selected, grown in soil and used for phenotype analyses. A large proportion of the transgenic plants (37 plants) grew normally without any visible growth phenotypes, but some plants showed fasciated stems, curled leaves or downward pedicels (Figure 31). The curled leaf and downward pedicel phenotypes were reported previously in *AtHB15* gain-of-function mutants (Ochando et al., 2006, 2008). Transgenic over-expression of *mAtHB15* in the wild-type background did not result in these phenotypes (Kim et al., 2005), indicating that the *stp–2d* background is partially responsible for the observed phenotypes. We focused our analyses on the transgenic plants that showed no obvious growth phenotype. We first confirmed the expression of *mAtHB15* by real-time RT–PCR analysis (Figure 29c). The expression level of *mAtHB1*5 was much higher compared to the transgenic background *stp–2d* mutant, but was similar to that

observed in wild-type plants. Examination of stem cross-sections and phloroglucinol staining confirmed that the STP phenotype reverted to wild-type traits (Figure 29d). These results indicate that repression of *AtHB15* expression by *miR165b* is mainly responsible for the STP phenotype in the *stp–2d* mutant plants.

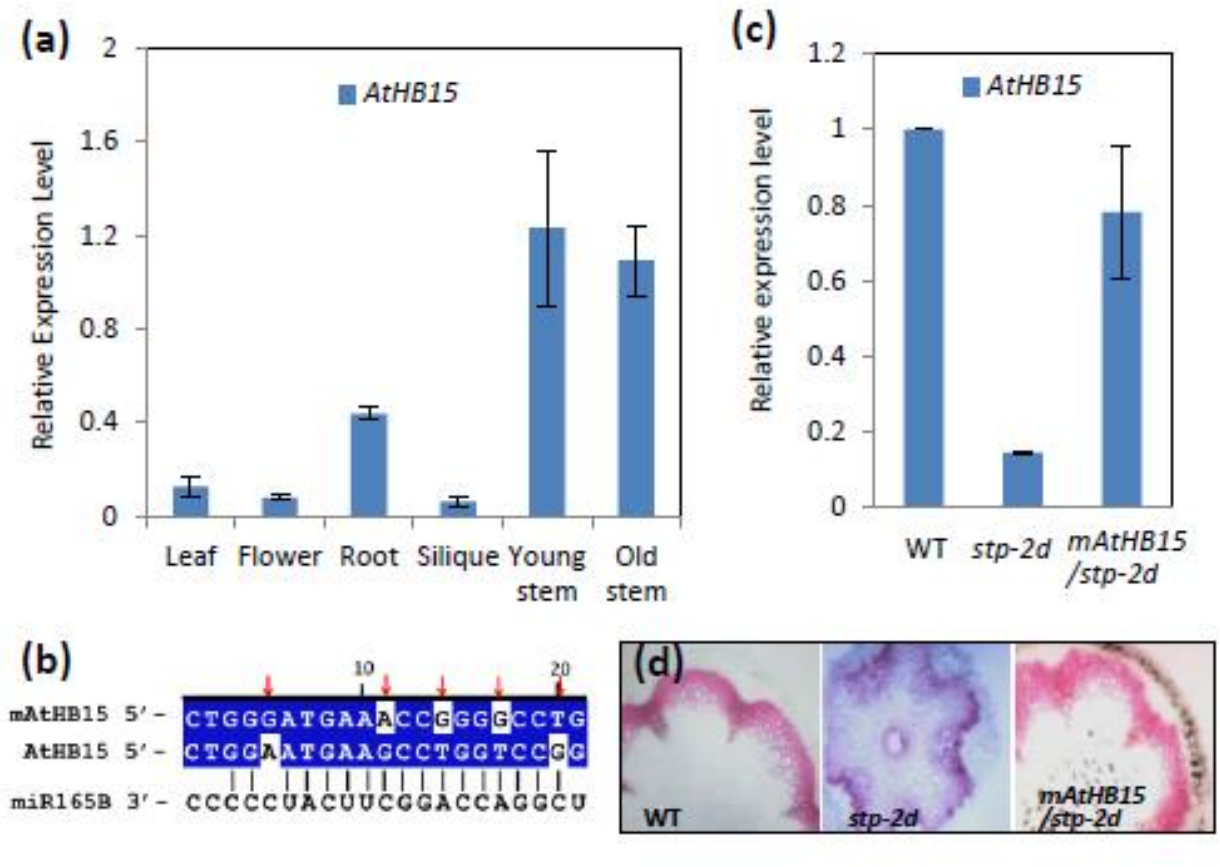

Figure 29. Over-expression of mutated *ATHB15* (*mATHB15*) reverts the *stp–2d* mutant phenotype to wild-type.

(a) Expression pattern of *ATHB15* in various tissues of wild-type plants. The number represented in Y axis were calculated from delta Ct. Values are means ± SD of three biological replicates. (b) Sequence alignment showing mutations of the *ATHB15* cDNA (*mATHB15*) that result in resistance to *miR165b*-mediated cleavage. Arrows indicate the positions of mutated nucleotides. (c) Expression of the *mAtHB15* in the *stp–2d* mutant plants was determined by real-time PCR. Expression of an ubiquitin (*UBQ5*) gene was used as reference. Values are means ±SD of three biological replicates. (d) Phloroglucinol staining of stem cross-sections showing that over-expression of *mATHB15* reverts the *stp–2d* mutant phenotype to wild-type.

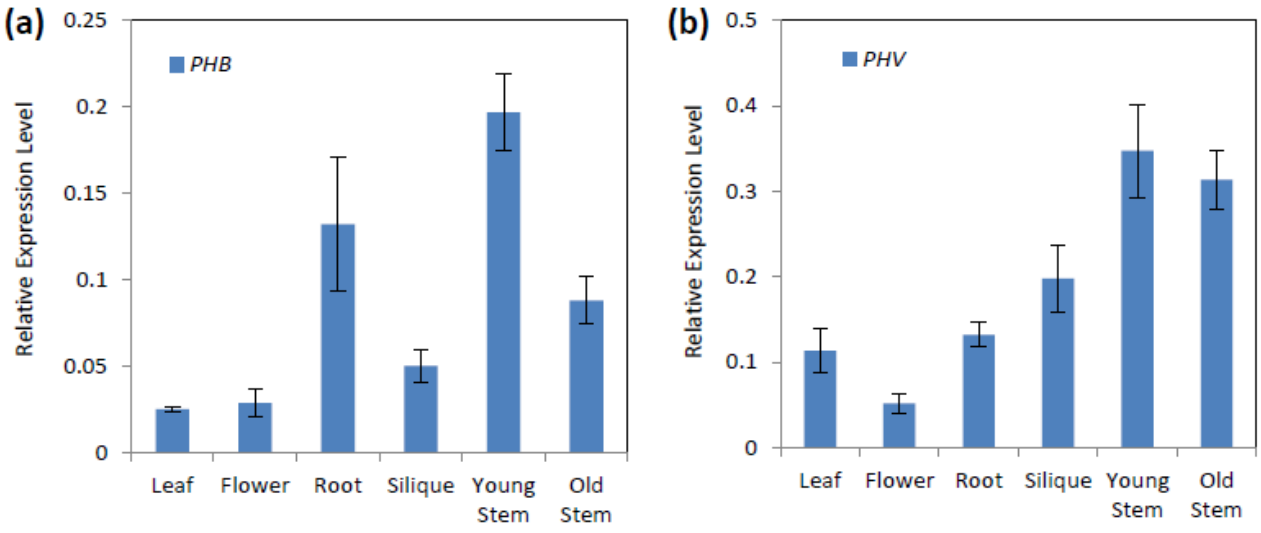

Figure 30. The expression pattern of *PHB* (a) and *PHV* (b) in different tissues.

The number represented in Y axis were calculated from delta Ct. Values are means ± SD of three biological replicates.

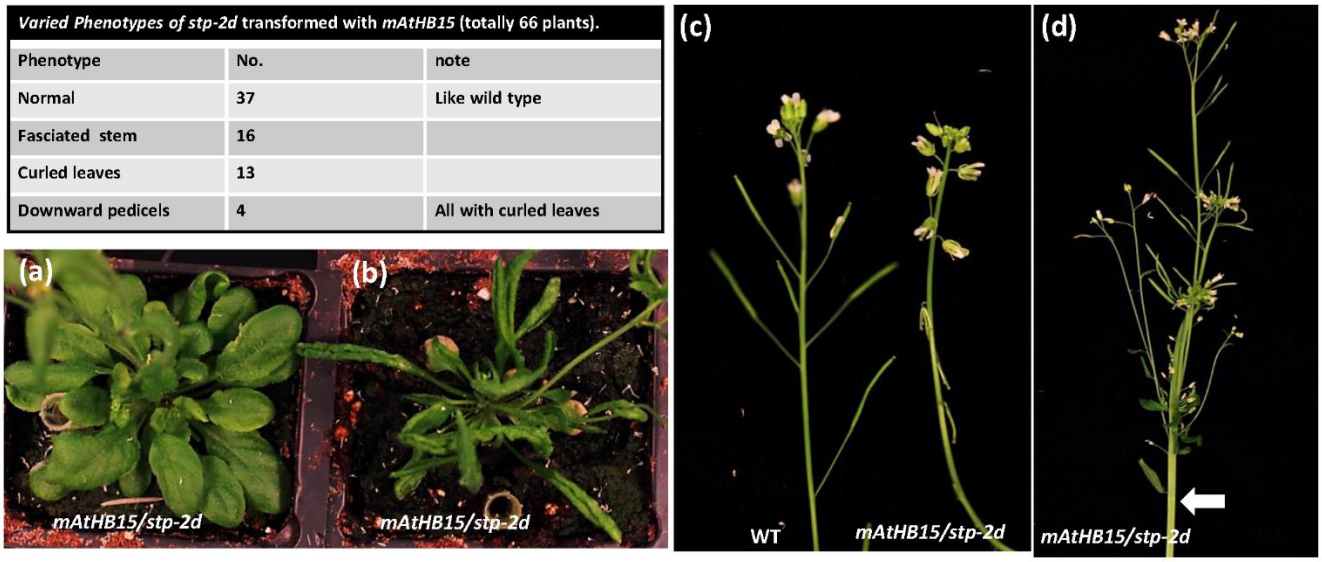

Figure 31. Overexpression of *mAtHB15* in the *stp-2d* mutant results in defects in leaves, stems and pedicels.

Four categories of phenotypes and plant numbers in each category were shown in the upper left table. (a) and (b) Rosette leaves of transgenic stp-2d plants with normal (a) or curled up leaf blade (b) . (c) Downward pedicels were observed in some mAtHB15/*stp-2d* transgenic lines (right). (d) Fasciated stems (white arrow) phenotype in some mAtHB15/*stp-2d* transgenic lines.

Ectopic secondary cell-wall development in the pith cells of *athb15* mutant plants

Over-expression of *mATHB15* in *stp–2d* plants reversed the STP phenotype, indicating that *ATHB15* functions as a negative regulator of secondary wall development in pith cells. We hypothesized that mutation of the *ATHB15* gene may de-repress secondary wall development in pith cells. Although *ATHB15* has been implicated in the development of vascular tissues and interfascicular fibers (Kim et al., 2005; Cassan-Wang et al., 2013), detailed analysis of *athb15* knockout mutants is still lacking. We obtained two T–DNA insertional *athb15* mutant alleles from the Arabidopsis Biological Resource Center (https://abrc.osu.edu/). The T–DNA insertion in line CS862347 was located 223 bp in front of the start codon in the 5' UTR. The second line, SALK_017186C, had a T–DNA insertion located in the first intron (Figure 32a). Gene expression analyses using RT– PCR indicated that no full-length *ATHB15* transcripts were present in either line (Figure 32b). However, weak partial transcripts were detected using primers covering the 3' rear region of the *AtHB15* coding sequence. The level of partial transcripts in SALK_017186 was about twice as high as in the CS862347 line, although the levels were both lower than in the wild-type. As expected, UV microscopy and phloroglucinol staining indicated that the pith cells were ectopically lignified in both lines (Figure 32c). The plant height of these two lines was similar to that of wildtype controls (Figure 32d), indicating that mutation of *ATHB15* has no significant effect on plant growth. The two insertion lines CS862347 and SALK_07186C were renamed as *athb15–1* and *athb15–2*, respectively. The *athb15–1* line was selected for further analysis.

To assess pith cell-wall development in the *athb15–1* mutant, we performed histochemical analysis of stem cross-sections. Both Calcofluor-white staining and histochemistry using CBM3a indicated that the mutant pith cells accumulate cellulose, similar to fiber cells (Figure 33a, b).

Xylan accumulation was detected in the *athb15–1* mutant using the xylan-directed monoclonal antibody CCRC–M149 (Figure 33c). Immunohistochemical analysis using CCRC-M38 confirmed that, in terms of their homogalacturonan content, the *athb15–1* pith cell walls are more similar to vascular bundles and interfascicular fibers than to ground tissues (Figure 33d). These results confirm that mutation of *AtHB15* results in secondary cell-wall development in pith cells that is similar to that observed in the *stp–2d* mutant lines.

To characterize the cell-wall composition of *stp–2d* and *athb15* mutant plants, we analyzed the monosaccharide composition, as well as lignin content and monomer composition, in the stem tissues (Figure 34). We used heterozygous *stp–2d* mutant plants for cell-wall composition analyses because the growth of homozygous *stp–2d* mutants was severely retarded (Figure 22). According to the glycosyl composition analyses, the cell walls of the heterozygous *stp-2d* mutants were largely similar to the walls of wild-type plants (Figure 34a). In contrast, cell walls from *athb15-1* mutants exhibited differences in sugar composition compared to control plants. A significant increase in xylose content was detected in the *athb15-1* mutants, suggesting enhanced xylan content. On the other hand, a significant reduction in galacturonic acid and galactose contents was observed in the *athb15-1* plants, suggesting reduced proportions of pectic components (Figure 34b). Total lignin content was measured in *stp–2d* and *athb15–1* mutant lines using the acetyl bromide method (Figure 34c, d). The total lignin content of *stp–2d* heterozygous plants was significantly decreased, suggesting that overall secondary growth was affected despite the ectopic lignification in the pith cells of the mutants. The lignin content of the *athb15–1* mutant was not significantly different from that of control plants. Consistent with the acetyl bromide results, fewer guaiacyl (G) and syringyl (S) monomers, the main measurable monolignol components, were detected in the *stp–2d* plants (Figure 34e). Interestingly, the S/G

ratio increased in the *stp–2d* heterozygous mutants (0.51) compared to control plants (0.29). In contrast, *athb15–1* mutant plants showed a higher lignin content (G plus S), with a similar S/G ratio to that of control plants (Figure 34f). The glycosyl residue composition analyses and lignin measurements indicated a significant difference between *stp–2d* and *athb15–1* mutant plants. We reasoned that mutations of multiple class III HD–ZIP members in the *stp–2d* mutant plants result in retarded growth, which may in turn be responsible for the observed differences in cell wall composition.

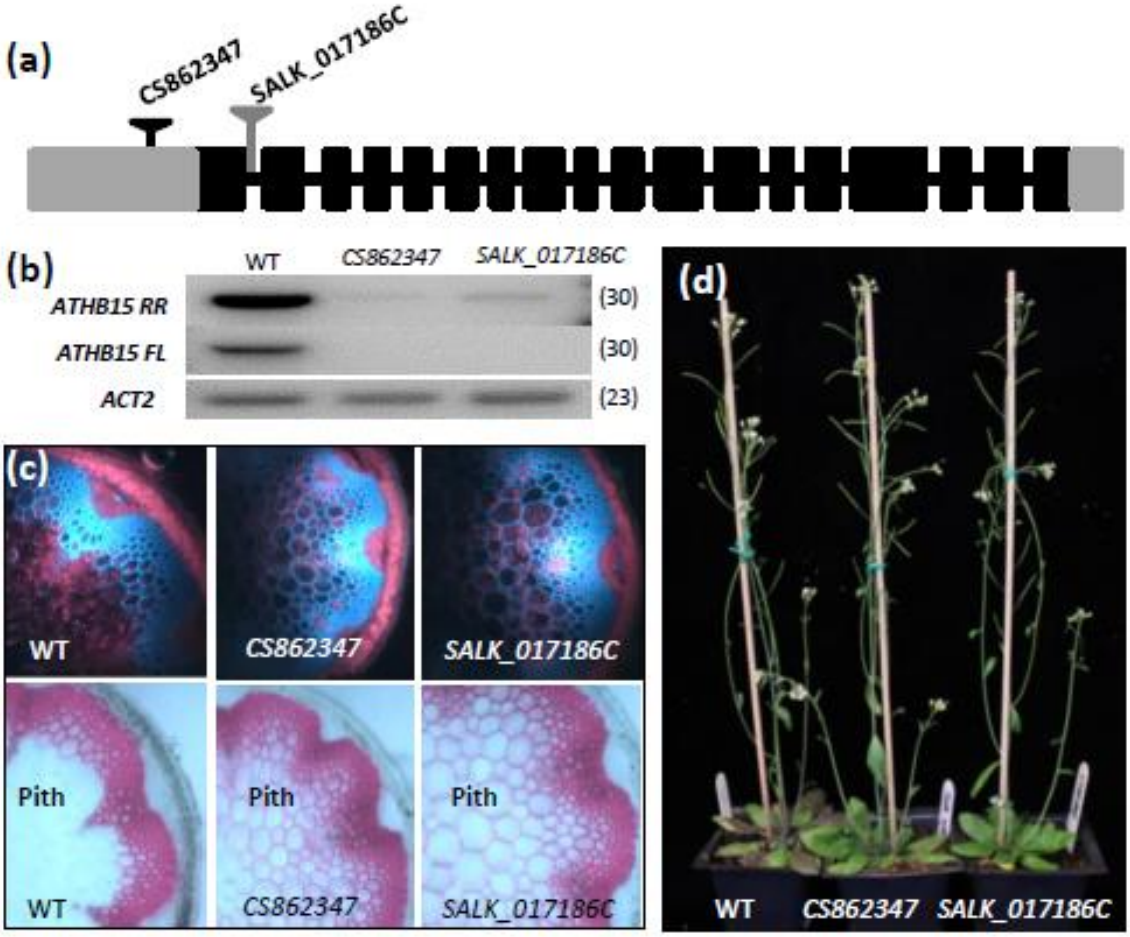

Figure 32. Mutations of *ATHB15* result in secondary wall thickening in pith.

(a) Schematic diagram showing the genomic structure of *ATHB15* and the positions of two T–DNA insertions. (b) RT–PCR analysis showing the absence of *ATHB15* full-length transcripts (FL) in both alleles, and a reduced abundance of the rear region of the gene (RR). Expression of *Actin2* (*ACT2*) was used as an expression control. The numbers on the right indicate the number of cycles used for PCR amplification. (c) Lignification of the pith cells in the two *athb15* mutant alleles as determined by UV microscopy (upper panels) and phloroglucinol staining (lower panels). (d) The morphology and development of the two mutant lines are normal compared to wild-type plants.

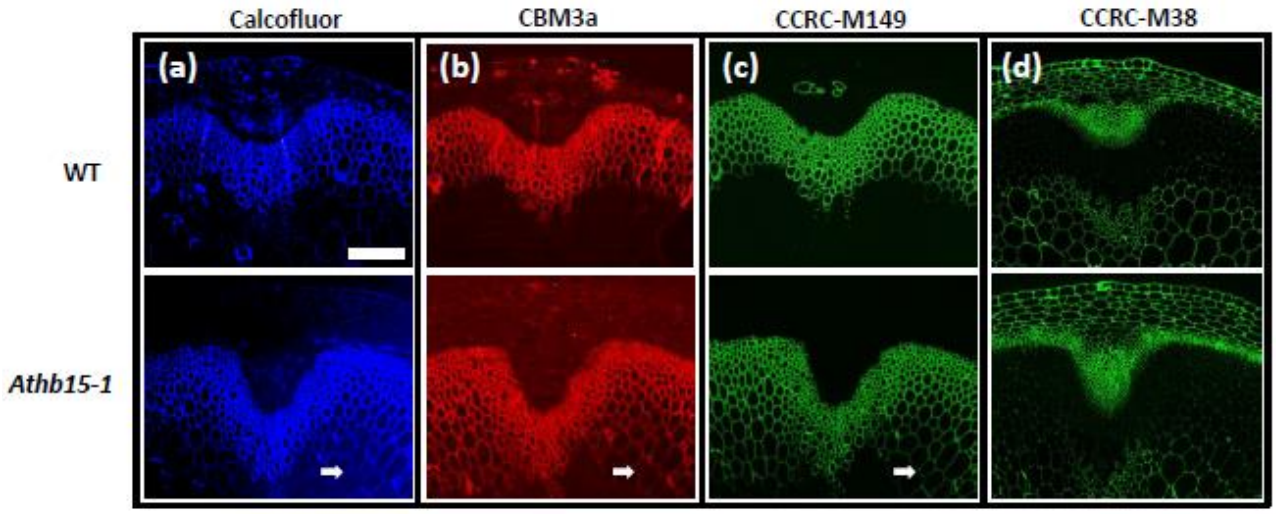

Figure 33. Cellulose and xylan accumulation in the pith cells of the *athb15–1* mutant.

(a,b) Detection of cellulose by Calcofluor-white staining (a) and labeling with cellulose-binding module CBM3a. (b) in the wild-type and *athb15–1* mutant. (c) Immunohistochemical detection of xylan using the monoclonal antibody CCRC–M149. (d) Detection of de-esterified homogalacturonan typically present in primary cell walls using CCRC–M38. The *athb15–1* mutant plants accumulate cellulose and xylan in pith cells, similar to the fiber cells in the fascicular and interfascicular region. White arrows indicate pith cells showing positive signals for cellulose or xylan in the mutant line, but not in wild-type plants. Scale bar = 100 lm; this applies to all images.

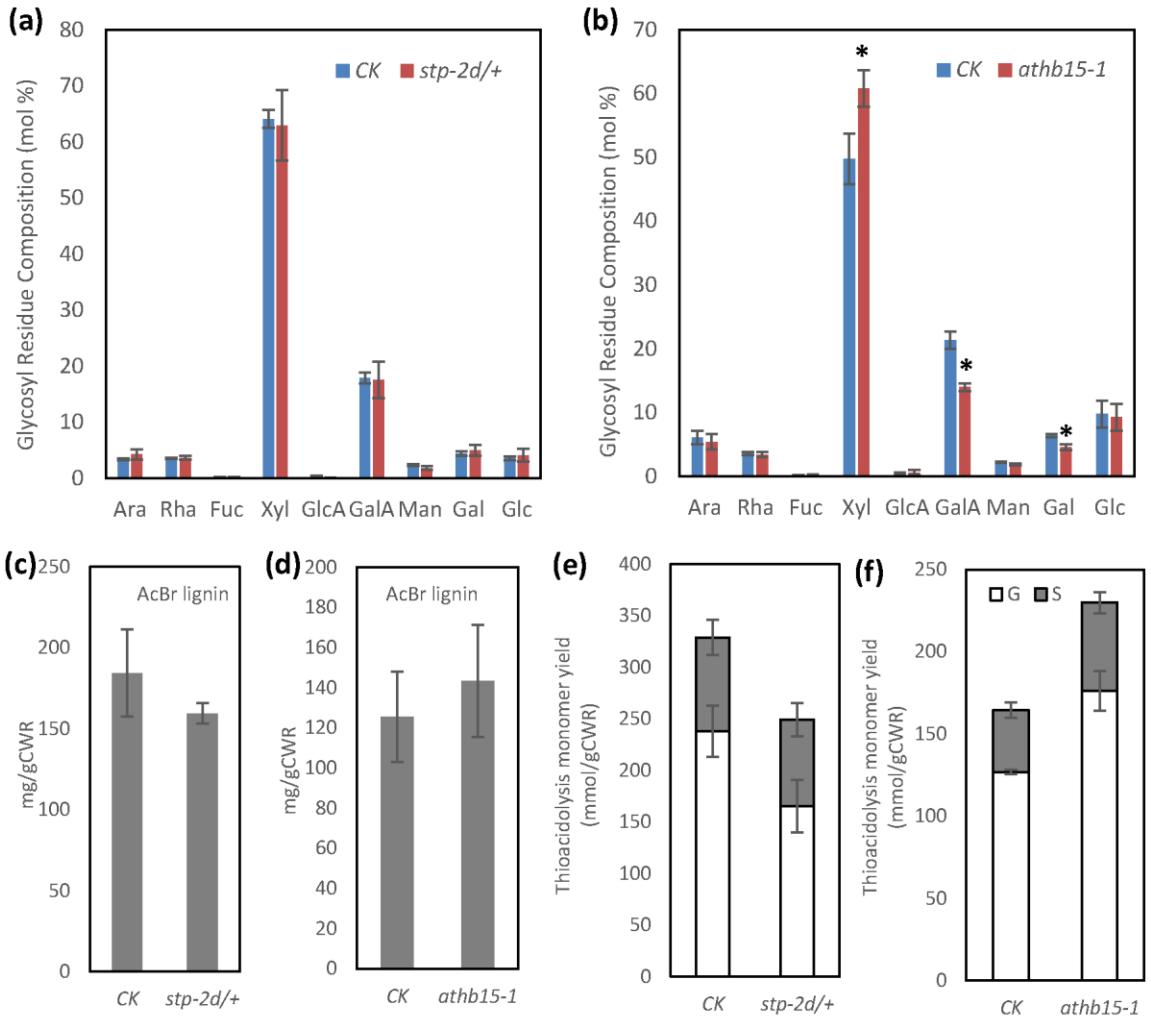

Figure 34. Analysis of cell wall compositions in the mutant lines.

(A) and (B), Glycosyl residue composition analysis of *stp-2d* (A) and *athb15-1* (B) mutants. The glycosyl residue composition of cell walls determined by GC-MS of trimethylsilyl (TMS) derivatives. Glycosyl residues are abbreviated as arabinose (Ara), rhamnose (Rha), fucose (Fuc), xylose (Xyl), galacturonic acid (GalA), mannose (Man), galactose (Gal), and glucose (Glc). * denotes significant difference ($p<0.5$, student t test). (C) and (D) Acetyl bromide (AcBr) lignin levels in the *stp-2d* (C) and *athb15-1* (D) mutants. (E) and (F), Yields of guiacyl (G) and syringyl (S) monomers in the *stp-2d* (E) and *athb15-1* (F) mutants. The amount of p-hydroxyphenylmonolignol is beyond detection limit.

Secondary wall-related transcriptional pathways were affected in the *athb15* mutant

To understand the genes and pathways that potentially function downstream of *ATHB15* to regulate secondary wall development in pith cells, we performed real-time RT– PCR analyses using RNA prepared from stem tissues. We first examined the expression of secondary wall biosynthetic genes. As shown in Figure 29, the expression levels for four lignin synthetic genes [Phenylalanine Ammonia Lyase 4 (*PAL4*), Caffeoyl CoA O-Methyl Transferase (*CCoAOMT*), Cinnamoyl CoA Reductase 1 (*CCR1*) and *CCR2*], two cellulose synthetic genes [Cellulose synthase A catalytic subunit 7 (*CesA7*) and *CesA8*] and two xylan synthetic genes [Fragile Fiber 8 (*FRA8*) and Irregular Xylem 9 (*IRX9*)]) were all up-regulated in the *athb15–1* mutant (Figure 35a). Secondary cell walls are known to be collaboratively regulated by transcriptional networks. If the genes responsible for the synthesis of secondary wall major components are activated, we reasoned that the upstream transcription factors may also be up-regulated in the *athb15–1* mutant. We then examined the expression of the master regulator genes *SND1*, *NST2* and *AtC3H14*. The expression of these three transcription factors was up-regulated as expected (Figure 35b–d). In a previous report, we found that *NST2* and *AtC3H14* were negatively regulated by AtWRKY12 (Wang et al., 2010). We then investigated whether the expression of *AtWRKY12* was affected by AtHB15. Real-time PCR results indicated that expression of *AtWRKY12* was also up-regulated in the *athb15–1* mutant line (Figure 35e). Because both *AtHB15* and *AtWRKY12* are negative regulators of secondary cell-wall synthesis, the upregulation of *AtWRKY12* may indicate a feedback regulation in pith wall development. Taken together, our results indicate that *AtHB15* represses secondary cell-wall development in pith cells by regulating transcriptional pathways.

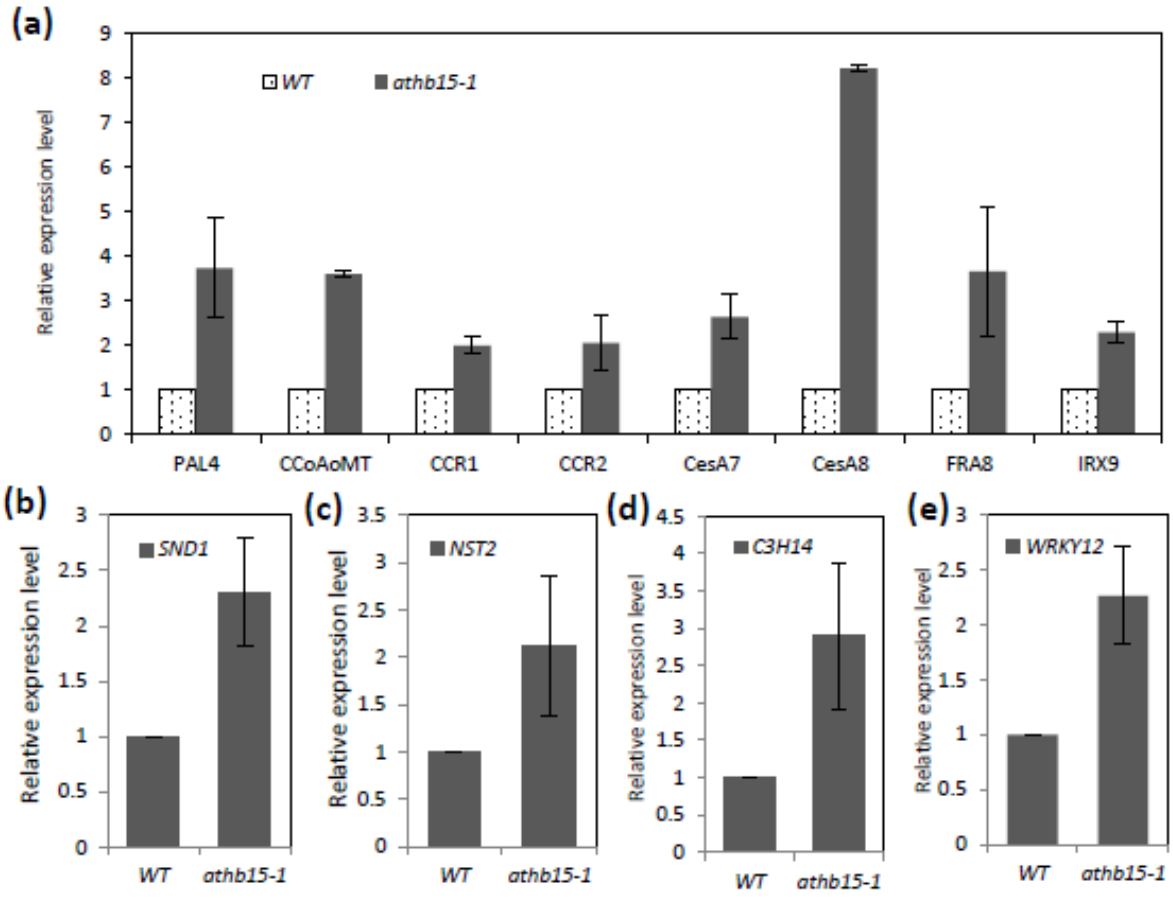

Figure 35. Genes responsible for secondary wall biosynthesis are activated in the *athb15–1* mutant.

(a) Real-time RT–PCR analysis showing activation of the lignin biosynthetic genes *PAL4*, *CCoAOMT*, *CCR1* and *CCR2*, the cellulose synthetic genes *CesA7* and *CesA8*, and the xylan synthetic genes *FRA8* and *IRX9*. (b–e) Expression of transcription factor genes *SND1* (b), *NST2* (c), *C3H14* (d) and *WRKY12* (e) is up-regulated in the *athb15–1* mutant. Values are means ±SD of three biological replicates.

Discussion

The *miR156/166* genes encode 21-nt microRNAs that target the START domain of class III HD–ZIP transcription factors (McConnell et al., 2001; Kidner and Martienssen, 2004; Kim et al., 2005). Among the six *miR166* genes and two *miR165* genes, activation tagging of *miR166a* and *miR166g* has been described previously (Reinhart et al., 2002; Rhoades et al., 2002; Kim et al., 2005; Williams et al., 2005). Here, we describe activation tagging of *miR165b*. Activation tagging of *miR166a* and *miR166g* showed similar phenotypes, including fasciated stems, enlarged meristems and extra amphivasal vascular bundles in the stem center (Kim et al., 2005; Williams et al., 2005). Activation tagging of *miR165b* showed very different phenotypes compared to those for the two *miR166* genes. The only phenotype in common was that one or more amphivasal bundle(s) were observed in the homozygous *stp–2d* mutant plants. At the gene regulation level, activation tagging of these three microRNAs showed similar effects on mRNA cleavage of three of the class III HD–ZIP genes: *AtHB15*, *PHB* and *PHV*. Similar post-transcriptional regulation of target gene(s) by *miR165/166* is expected, because the cleavage sites for *miR165* and *miR166* on HD–ZIP mRNAs are the same and have been experimentally confirmed (Tang et al., 2003; Zhong and Ye, 2004; Kim et al., 2005). Previous reports indicated that individual *miR166/165* genes exhibited distinct expression patterns in different plant tissues, and were dynamically controlled (Jung and Park, 2007). Therefore, the different phenotypes of activation-tagged *miR165/166* mutants may result from their distinct expression patterns, rather than their cleavage preference for target genes.

Over-expression of *miR165a* has been reported to cause loss of shoot apical meristem, alteration of organ polarity, inhibition of vascular development, and aberrant differentiation of interfascicular fibers (Zhou et al., 2007). Gene expression analyses indicated that over-expression

of *miR165a* affected all five class III HD–ZIP transcription factors, in contrast to the results for the three available activation-tagging mutants, *miR166a*, *miR166g* and *miR165b* (Kim et al., 2005; Williams et al., 2005; Zhou et al., 2007). On the other hand, over-expression of an antisense *miR165a* resulted in extra amphivasal vascular bundles in the pith regions, as observed in the three activation-tagging mutants (Kim et al., 2005; Williams et al., 2005; Zhong and Ye, 2007b). The discrepancy in phenotypes between over-expression of *miR165a* and activation tagging of *miR165/166* may be explained by the antagonistic functions of class III HD–ZIP members. The functions of *AtHB15* and *REV* in vascular development may be very different. The triple loss-of-function mutant, *rev phb phv*, showed amphicribral bundles, while *phb phv cna* (*athb15*) developed amphivasal bundles in the pith (Emery et al., 2003; Prigge et al., 2005). Thus the functions of various *miR165/ 166* members in regulating class III HD–ZIP genes are worthy of further investigation.

Activation tagging of *miR165b* in the *stp–2d* mutant caused an STP phenotype. Gene expression analyses and characterization of the *athb15* mutants indicated that suppression of *AtHB15* expression was mainly responsible for the STP phenotype. The *AtHB15* gene is known to be expressed in procambium, and regulates early vascular development (Ohashi-Ito and Fukuda, 2003). There are also indications that *AtHB15* regulates xylem differentiation. Mutation of *AtHB15* by an antisense transgene or a T–DNA insertion resulted in an expanded interfascicular fiber region due to enhanced cambium activity (Kim et al., 2005; Cassan-Wang et al., 2013). Here, we found that *AtHB15* negatively regulates secondary cell-wall development in pith cells. In accordance with its function in pith cells, expression of *AtHB15* was detected in pith cells around the protoxylem using a promoter:GUS reporter line (Fisher and Turner 2007). The functional mechanism of AtHB15 in cell-wall development was assessed with gene expression

analyses. *AtHB15* represses pith secondary cell-wall development by modulating the expression of the NAC master regulators *SND1* and *NST2,* and subsequently secondary wall biosynthetic genes (Figure 29). We detected up-regulation of *AtWRKY12* in the *athb15* mutant. This result is somewhat unexpected because both genes are negative regulators of secondary wall development. We reasoned that the up-regulation of *AtWRKY12* may serve as a negative feedback mechanism to offset the secondary wall development in pith cells. Our results also indicate that *AtHB15* may have much broader functions than *AtWRKY12* in pith wall development. In a previous study, the *AtHB15* gene was not among those genes affected in *atwrky12* mutant lines (Wang et al., 2010). Furthermore, *AtWRKY12* specifically regulates *NST2* but not other genes encoding NAC domain transcription factors (Wang et al., 2010; Wang and Dixon, 2012). Taken together, this research highlights an uncharacterized function of *miR165* in regulating secondary wall development through the class III HD–ZIP transcription factor *AtHB15*.

Materials and methods

Plant material

Arabidopsis thaliana ecotype Col–0, and *athb15* mutant lines, CS862347 and SALK_07186C, were used in this research. The *stp–2d* mutant was identified from a large-scale mutant screening using UV microscopy. *Arabidopsis* growth and treatment were performed as described previously (Wang et al., 2010). Plants were grown in growth chambers under the following conditions: 16 h light/8 h dark; 22°C in the light/20°C in the dark; relative humidity 70-80%.

Phenotypic characterization

The activation-tagged mutant population was created by transformation of wild-type *Arabidopsis* plants using activation-tagging vector pSKI015 as described previously (Weigel et al., 2000). Identification of mutants with defects in vascular development was performed using stem cross-sections and UV microscopy. In brief, cross-sections (100 um) of the stem were cut just above the rosette leaves using an RM2255 microtome (Leica, www.leicamicrosystems.com/). Stem sections were placed on glass slides and observed using a Micophot-FX microscope (Nikon, www.nikon.com/). Micrographs were taken using an INFINITY3 color camera (Scientific Imaging Company, www.scientificimagingcompany. com/) using identical settings of objective lens and exposure time. Mutants identified from the UV microscopy screening were further characterized in detail using growth phenotype analysis and histobiochemical staining of cell walls.

Phloroglucinol staining

Phloroglucinol HCl reagent was prepared by mixing two volumes of 2% w/v phloroglucinol in 95% v/v ethanol with one volume of concentrated HCl. Cross-sections were stained for 1-2 min,

washed twice on slides by adding then removing a few drops of water using a pipette, and photographed immediately. The staining and washing steps were performed at room temperature. All photographs were taken within 30 min after staining as previously described (Guo et al., 2001).

Immunohistochemistry

Fixation, tissue processing and immunolocalization of stem samples were performed as described previously (Avci et al., 2012). All images obtained using a given antibody or by histochemistry using CBM3a were captured after the same duration of exposure using a Nikon Eclipse 80i epifluorescence microscope equipped with a DS-Ri1 camera and NIS Elements basic research software.

Gene cloning

The gene responsible for the *stp–2d* mutant phenotype was cloned using as described previously (Liu et al., 1995). DNA fragments were cut from the agarose gel, purified using a DNA purification kit (Qiagen, www.qiagen.com), and sent for sequencing at the Biotech Center at the University of Connecticut. The precise insertion site of the T–DNA containing the activation tag was determined based on the sequencing results. Further genotyping assays and genetic analyses confirmed that the activation tag is responsible for the mutant phenotype. Primers used for gene cloning are provided in Table S1.

Constructs

To over-express *miR165b*, the genomic sequence of the *miR165b* was cloned using high-fidelity polymerase, and inserted into the TOPO–D vector (Invitrogen, www.lifetechnologies.com/). The primers used for cloning *miR165b* are MIR165B Fw (50-

caccACAAGACTAGGGTTTCGGAATGAC-30, cacc were added to facilitate TOPO cloning) and MIR165B Re (50-TAAAATATGCTATTACAA TCCGACGTTAG CAA-30). To create a plasmid expressing the clone the *mATHB15* cDNA, we first cloned full-length *AtHB15* into the TOPO–D vector using primers AtHB15 Fw (50-CACCGAATTCATGG CAATGTCTTGCAAGGATGGTAAGTTG-30) and AtHB15 Re (50-GGA TCCTCACACAAAGGACCAATTGATGAACACAAAGCA-30). Then we designed a pair of complementary primers containing the mutated nucleotides, i.e. mATHb15 Fw (50-CAGATGCCTGGGATGAAACCG GGGCCTGATTCCATT-30) and mAtHB15 Re (50-AATGGAATCAGGC CCCGGTTTCATCCCAGGCATCTG-30). Combining the AtHB15 Fw and AtHB15 Re primers, we amplified the m*AtHB15* after two rounds of PCR reactions, and inserted the PCR product into the TOPO–D vector. Both constructs, expressing *miR165b* or *mAtHB15*, were confirmed by sequencing, and sub-cloned into destination vector pK2GW7 (Laboratory of Plant Systems Biology, Ghent University, Belgium) by LR reaction according to manufacturer's instructions (LR recombinase, Invitrogen).

Plant transformation

The floral dipping method was used for *Arabidopsis* transformation (Clough and Bent, 1998). Seeds collected from the transformed *Arabidopsis* plants were plated on half-strength MS (Murashige and Skoog) medium supplied with appropriate antibiotics. Resistant plants that survived on the selective plate were transferred to soil for further analysis.

Gene expression analysis

Plant tissues were collected from stems of 35-day-old plants or whole seedlings, flash frozen in liquid nitrogen, and stored at -80°C. Total RNAs were isolated using a RNA isolation kit (Qiagen). RNA samples were treated with RNase-free DNase (Qiagen) to eliminate

contamination from genomic DNA. Three micrograms of total RNA was reverse-transcribed using a Superscript III RT kit (Invitrogen) in a 20 ul reaction system. The cDNA was diluted 10 times, and used as the template for RT–PCR or quantitative RT– PCR as previously described (Wang et al., 2010). Briefly, the PCR amplification was performed on an ABI 7900HT real-time PCR machine using SYBR Green qPCR master mix (Life Technologies, www.lifetechnologies.com/). For each reaction, 1ul diluted cDNA sample was used in a 10ul reaction system. The PCR reaction program was set according to the manufacturer's instructions (Life Technologies). Primers used for real-time RT–PCR are listed in Table S1.

Glycosyl composition analysis

Glycosyl composition analyses were performed using GC/MS of per-O-trimethylsilyl derivatives of the monosaccharide methyl glycosides as described previously (Merkle and Poppe 1994). In brief, samples were placed into test tubes and 20 ug of inositol was added. Methyl glycosides were then prepared from the dry samples by methanolysis in 1 M HCl in methanol at 80°C for 18 h, followed by re-N–acetylation with pyridine and acetic anhydride in methanol (for detection of amino sugars). Samples were then perO–trimethylsilylated by treatment with Tri–Sil (Pierce, www.lifetechnologies.com/us/en/home/brands/thermo-scientific/pierce-protein-biology) at 80°C for 30 min. GC/MS analysis of the per-Otrimethylsilyl methyl glycosides was performed on an Agilent 7890A gas chromatograph interfaced with a 5975C MSD system (Agilent, www.agilent.com), using a Supelco Equity–1 fused-silica capillary column (Sigma, www.sigmaaldrich.com).

Determination of lignin content and composition

Total lignin content and lignin composition of the stem materials were determined using the acetyl bromide and thioacidolysis methods, respectively. The methods for determining lignin content and composition have been described previously (Wang et al., 2010).

pSKI LB1	ATACGACGGATCGTAATTTGTC
pSKI LB2	TAATAACGCTGCGGACATCTAC
pSKI LB3	TTGACCATCATACTCATTGCTG
DG1	WGCNAGTNAGWANAAG
DG2	AWGCANGNCWGANATA
DG3	NGTCGASWGANAWGAA
DG4	WGTGNAGWANCANAGA
DG5	STTGNTASTNCTNTGC
DG6	NTCGASTWTSGWGTT
DG7	AGWGNAGWANCAWAGG
SALK_017186C LP	GCATATAAAGCAGCTCAACGG
SALK_017186C RP	TAACAATGTTCCTTGCTTGGG
SAIL_274_B07 LP	TGTGACACTTGCTTCTGCAAC
SAIL_274_B07 RP	TCAATGAGAGCTCGAAGAAGG
AtSND1 QF	GCCCGGTCGACCAAAGTT
AtSND1 QR	CTCTTGAACGGGAGAGAAATCG
AtC3H14 QF1	CGCGGCGTCTACTGTTACAG
AtC3H14 QR1	GGAGGCGGCGATGAGTTTA
NST2 QF	CAACTGCCACGTCAGCAAAG
NST2 QR	AAGCGGCCCAGCTAGTGA
CCR1 QF1	GCTCTTAAGGCGGCGATTG
CCR1 QR1	ACAGGAGAAGCCGTGTGAAAG
CCR2 QF	TGAACCCTAACCGTGACACTCAAGC
CCR2 QR	GCCAACATCTTCCCGTAGCAATACC
PAL4 QF1	CCTCCGGTGACCTTGTTCCT
PAL4 QR1	AGTTGGGACGGCCAGTGA
CCoAOMT QF	ACAAGAAACTCTCGGCTGATCAG
CCoAOMT QR	TCGCCAAGCGCAGCTT
CesA7 QF	TTGTTGCAGGCATCTCAGATG
CesA7 QR	GCAGTTGATGCCACACTTGGA
CesA8 QF	TGAGCTTTACATTGTCAAATG
CesA8 QR	GCAATCGATCAAAAGACAGTT
FRA8 QF	GACTTGTTGAATCGGTGGCTC
FRA8 QR	GAAAGAGTTTGACCTTCTAAC
PHB-real-new-PF	CCAGCAGGACTCCTTTCTAT
PHB-real-new-PR	TGCGCGAAATAGCGACTATG
PHV-real-new-PF	CCAGCTAATCTTCTCTCGAT
PHV-real-new-PR	TGCGTGAAACAGCTACGATA
REV-real-new-PF	CCTGCTGGATTGCTCTCAAT
REV-real-new-PR	GAAATGGCAAAGATGCCAACCG
pre-miR165b-F	TGTTGTTTGGATCGAGGATATCA
pre-miR165b-R	TACCATGTGGCATGTATGTATATATATGTA

Table 2: Primers used in this research.

Reference

Avci, U., Pattathil, S. and Hahn, M.G. (2012) Immunological approaches to plant cell wall and biomass characterization: immunolocalization of glycan epitopes. Methods Mol. Biol. 908, 73 – 82.

Baima, S., Possenti, M., Matteucci, A., Wisman, E., Altamura, M.M., Ruberti, I. and Morelli, G. (2001) The *Arabidopsis* ATHB-8 HD–zip protein acts as a differentiation-promoting transcription factor of the vascular meristems. Plant Physiol. 126, 643–655.

Bhargava, A., Mansfield, S.D., Hall, H.C., Douglas, C.J. and Ellis, B.E. (2010) *MYB75* functions in regulation of secondary cell wall formation in the *Arabidopsis* inflorescence stem. Plant Physiol. 154, 1428–1438.

Carlsbecker, A., Lee, J.Y., Roberts, C.J. et al. (2010) Cell signalling by *microRNA165/6* directs gene dose-dependent root cell fate. Nature, 465, 316–321.

Carpita, N.C. and Gibeaut, D.M. (1993) Structural models of primary cell walls in flowering plants: consistency of molecular structure with the physical properties of the walls during growth. Plant J. 3, 1–30.

Carroll, A. and Somerville, C. (2009) Cellulosic biofuels. Annu. Rev. Plant Biol. 60, 165–182.
Cassan-Wang, H., Goue, N., Saidi, M.N., Legay, S., Sivadon, P., Goffner, D. and Grima-Pettenati, J. (2013) Identification of novel transcription factors regulating secondary cell wall formation in *Arabidopsis*. Front. Plant Sci. 4, 189.

Clough, S.J. and Bent, A.F. (1998) Floral dip: a simplified method for Agrobacterium-mediated transformation of *Arabidopsis thaliana*. Plant J. 16, 735–743.

Dello Ioio, R., Galinha, C., Fletcher, A.G. et al. (2012) A PHABULOSA/cytokinin feedback loop controls root growth in *Arabidopsis*. Curr. Biol. 22, 1699–1704.

Demura, T. and Fukuda, H. (2007) Transcriptional regulation in wood formation. Trends Plant Sci. 12, 64 –70.

Emery, J.F., Floyd, S.K., Alvarez, J., Eshed, Y., Hawker, N.P., Izhaki, A., Baum, S.F. and Bowman, J.L. (2003) Radial patterning of *Arabidopsis* shoots by class III HD–ZIP and *KANADI* genes. Curr. Biol. 13, 1768– 1774.

Fisher, K. and Turner, S. (2007) PXY, a receptor-like kinase essential for maintaining polarity during plant vascular-tissue development. Curr. Biol. 17, 1061–1066.

Grover, A., Singh, S., Pandey, P., Patade, V.Y., Gupta, S.M. and Nasim, M. (2014) Overexpression of *NAC* gene from *Lepidium latifolium L.* enhances biomass, shortens life cycle and induces cold stress tolerance in tobacco: potential for engineering fourth generation biofuel crops. Mol. Biol. Rep. 41, 7479–7489.

Guo, D., Chen, F., Inoue, K., Blount, J.W. and Dixon, R.A. (2001) Downregulation of caffeic acid 3-O–methyltransferase and caffeoyl CoA 3-O–methyltransferase in transgenic *alfalfa*. impacts on lignin structure and implications for the biosynthesis of G and S lignin. Plant Cell, 13, 73 –88.

Hines, J.P. (2011) Boosting biofuels. Science, 311, 11. Jung, J.H. and Park, C.M. (2007) *MIR166/165* genes exhibit dynamic expression patterns in regulating shoot apical meristem and floral development in Arabidopsis. Planta, 225, 1327–1338.

Kidner, C.A. and Martienssen, R.A. (2004) Spatially restricted microRNA directs leaf polarity through *ARGONAUTE1*. Nature, 428, 81 –84.

Kim, J., Jung, J.H., Reyes, J.L. et al. (2005) microRNA-directed cleavage of *ATHB15* mRNA regulates vascular development in *Arabidopsis* inflorescence stems. Plant J. 42, 84 –94.

Kim, W.C., Kim, J.Y., Ko, J.H., Kang, H., Kim, J. and Han, K.H. (2014) AtC3H14, a plant-specific tandem CCCH zinc-finger protein, binds to its target mRNAs in a sequence-specific manner and affects cell elongation in *Arabidopsis thaliana*. Plant J. 80, 772–784.

Ko, J.H., Kim, W.C. and Han, K.H. (2009) Ectopic expression of *MYB46* identifies transcriptional regulatory genes involved in secondary wall biosynthesis in *Arabidopsis*. Plant J. 60, 649–665.

Lin, Y.C., Li, W., Sun, Y.H., Kumari, S., Wei, H., Li, Q., Tunlaya-Anukit, S., Sederoff, R.R. and Chiang, V.L. (2013) *SND1* transcription factor-directed quantitative functional hierarchical genetic regulatory network in wood formation in *Populus trichocarpa*. Plant Cell, 25, 4324–4341. Liu, Y.G., Mitsukawa, N., Oosumi, T. and Whittier, R.F. (1995) Efficient isolation and mapping of *Arabidopsis thaliana* T-DNA insert junctions by thermal asymmetric interlaced PCR. Plant J. 8, 457–463.

McCarthy, R.L., Zhong, R. and Ye, Z.H. (2009) MYB83 is a direct target of *SND1* and acts redundantly with *MYB46* in the regulation of secondary cell wall biosynthesis in *Arabidopsis*. Plant Cell Physiol. 50, 1950–1964.

McConnell, J.R., Emery, J., Eshed, Y., Bao, N., Bowman, J. and Barton, M.K. (2001) Role of *PHABULOSA* and *PHAVOLUTA* in determining radial patterning in shoots. Nature, 411, 709–713.

Merkle, R.K. and Poppe, I. (1994) Carbohydrate composition analysis of glycoconjugates by gas-liquid chromatography/mass spectrometry. Methods Enzymol, 230, 1 –15.

Mitsuda, N., Seki, M., Shinozaki, K. and Ohme-Takagi, M. (2005) The NAC transcription factors NST1 and NST2 of *Arabidopsis* regulate secondary wall thickenings and are required for anther dehiscence. Plant Cell, 17, 2993–3006.

Mitsuda, N., Iwase, A., Yamamoto, H., Yoshida, M., Seki, M., Shinozaki, K. and Ohme-Takagi, M. (2007) NAC transcription factors, NST1 and NST3, are key regulators of the formation of secondary walls in woody tissues of *Arabidopsis*. Plant Cell, 19, 270–280.

Miyashima, S., Koi, S., Hashimoto, T. and Nakajima, K. (2011) Non-cellautonomous *microRNA165* acts in a dose-dependent manner to regulate multiple differentiation status in the *Arabidopsis* root. Development, 138, 2303–2313.

Ochando, I., Jover-Gil, S., Ripoll, J.J., Candela, H., Vera, A., Ponce, M.R., Martinez-Laborda, A. and Micol, J.L. (2006) Mutations in the microRNA complementarity site of the *INCURVATA4* gene perturb meristem function and adaxialize lateral organs in *Arabidopsis*. Plant Physiol. 141, 607–619.

Ochando, I., Gonzalez-Reig, S., Ripoll, J.J., Vera, A. and Martinez-Laborda, A. (2008) Alteration of the shoot radial pattern in *Arabidopsis thaliana* by a gain-of-function allele of the class III HD–Zip gene *INCURVATA4*. Int. J. Dev. Biol. 52, 953–961.

Ohashi-Ito, K. and Fukuda, H. (2003) HD–zip III homeobox genes that include a novel member, *ZeHB-13* (*Zinnia*)/*ATHB-15* (*Arabidopsis*), are involved in procambium and xylem cell differentiation. Plant Cell Physiol. 44, 1350–1358.

Ohashi-Ito, K., Kubo, M., Demura, T. and Fukuda, H. (2005) Class III homeodomain leucine-zipper proteins regulate xylem cell differentiation. Plant Cell Physiol. 46, 1646–1656.

Pattathil, S., Avci, U., Baldwin, D. et al. (2010) A comprehensive toolkit of plant cell wall glycan-directed monoclonal antibodies. Plant Physiol. 153, 514–525.

Pauly, M. and Keegstra, K. (2010) Plant cell wall polymers as precursors for biofuels. Curr. Opin. Plant Biol. 13, 305–312.

Prigge, M.J., Otsuga, D., Alonso, J.M., Ecker, J.R., Drews, G.N. and Clark, S.E. (2005) Class III homeodomain-leucine zipper gene family members have overlapping, antagonistic, and distinct roles in *Arabidopsis* development. Plant Cell, 17, 61 –76.

Reinhart, B.J., Weinstein, E.G., Rhoades, M.W., Bartel, B. and Bartel, D.P. (2002) MicroRNAs in plants. Genes Dev. 16, 1616–1626.

Rhoades, M.W., Reinhart, B.J., Lim, L.P., Burge, C.B., Bartel, B. and Bartel, D.P. (2002) Prediction of plant microRNA targets. Cell, 110, 513–520.

Schmidt, D., Schuhmacher, F., Geissner, A., Seeberger, P.H. and Pfrengle, F. (2015) Automated synthesis of arabinoxylan-oligosaccharides enables characterization of antibodies that recognize plant cell wall glycans. Chemistry, 21, 5709–5713.

Schuetz, M., Smith, R. and Ellis, B. (2013) Xylem tissue specification, patterning, and differentiation mechanisms. J. Exp. Bot. 64, 11–31.

Steiner-Lange, S., Unte, U.S., Eckstein, L., Yang, C., Wilson, Z.A., Schmelzer, E., Dekker, K. and Saedler, H. (2003) Disruption of *Arabidopsis thaliana MYB26* results in male sterility due to non-dehiscent anthers. Plant J. 34, 519–528.

Tang, G., Reinhart, B.J., Bartel, D.P. and Zamore, P.D. (2003) A biochemical framework for RNA silencing in plants. Genes Dev. 17, 49 –63.

Valdivia, E.R., Herrera, M.T., Gianzo, C., Fidalgo, J., Revilla, G., Zarra, I. and Sampedro, J. (2013) Regulation of secondary wall synthesis and cell death by NAC transcription factors in the monocot *Brachypodium distachyon*. J. Exp. Bot. 64, 1333–1343.

Wang, H.Z. and Dixon, R.A. (2012) On-off switches for secondary cell wall biosynthesis. Mol. Plant, 5, 297–303.

Wang, H., Avci, U., Nakashima, J., Hahn, M.G., Chen, F. and Dixon, R.A. (2010) Mutation of WRKY transcription factors initiates pith secondary wall formation and increases stem biomass in dicotyledonous plants. Proc. Natl Acad. Sci. USA, 107, 22338–22343.

Wang, H., Zhao, Q., Chen, F., Wang, M. and Dixon, R.A. (2011) NAC domain function and transcriptional control of a secondary cell wall master switch. Plant J. 68, 1104–1114.

Weigel, D., Ahn, J.H., Blazquez, M.A. et al. (2000) Activation tagging in *Arabidopsis*. Plant Physiol. 122, 1003–1013.

Williams, L., Grigg, S.P., Xie, M., Christensen, S. and Fletcher, J.C. (2005) Regulation of Arabidopsis shoot apical meristem and lateral organ formation by microRNA *miR166g* and its AtHD–ZIP target genes. Development, 132, 3657–3668.

Yang, C., Xu, Z., Song, J., Conner, K., Vizcay Barrena, G. and Wilson, Z.A. (2007) *Arabidopsis MYB26*/*MALE STERILE35* regulates secondary thickening in the endothecium and is essential for anther dehiscence. Plant Cell, 19, 534–548.

Yu, Y., Hu, R., Wang, H., Cao, Y., He, G., Fu, C. and Zhou, G. (2013) *MlWRKY12*, a novel Miscanthus transcription factor, participates in pith secondary cell wall formation and promotes flowering. Plant Sci. 212, 1–9.

Zhao, Q., Gallego-Giraldo, L., Wang, H., Zeng, Y., Ding, S.Y., Chen, F. and Dixon, R.A. (2010) An NAC transcription factor orchestrates multiple features of cell wall development in *Medicago truncatula*. Plant J. 63, 100– 114.

Zhong, R. and Ye, Z.H. (2004) *Amphivasal vascular bundle 1*, a gain-offunction mutation of the *IFL1/REV* gene, is associated with alterations in the polarity of leaves, stems and carpels. Plant Cell Physiol. 45, 369–385.

Zhong, R. and Ye, Z.H. (2007a) Regulation of cell wall biosynthesis. Curr. Opin. Plant Biol. 10, 564–572.

Zhong, R. and Ye, Z.H. (2007b) Regulation of HD–ZIP III genes by *microRNA 165*. Plant Signal. Behav. 2, 351–353.

Zhong, R. and Ye, Z.H. (2014) Complexity of the transcriptional network controlling secondary wall biosynthesis. Plant Sci. 229, 193–207.

Zhong, R., Demura, T. and Ye, Z.H. (2006) SND1, a NAC domain transcription factor, is a key regulator of secondary wall synthesis in fibers of *Arabidopsis*. Plant Cell, 18, 3158–3170.

Zhong, R., Richardson, E.A. and Ye, Z.H. (2007) The MYB46 transcription factor is a direct target of *SND1* and regulates secondary wall biosynthesis in *Arabidopsis*. Plant Cell, 19, 2776–2792.

Zhong, R., Lee, C., Zhou, J., McCarthy, R.L. and Ye, Z.H. (2008) A battery of transcription factors involved in the regulation of secondary cell wall biosynthesis in *Arabidopsis*. Plant Cell, 20, 2763–2782.

Zhou, G.K., Kubo, M., Zhong, R., Demura, T. and Ye, Z.H. (2007) Overexpression of *miR165* affects apical meristem formation, organ polarity establishment and vascular development in *Arabidopsis*. Plant Cell Physiol. 48, 391–404.

Zhou, J., Lee, C., Zhong, R. and Ye, Z.H. (2009) MYB58 and MYB63 are transcriptional activators of the lignin biosynthetic pathway during secondary cell wall formation in *Arabidopsis*. Plant Cell, 21, 248–266.